Piezoelectric Coefficients of Gallium Arsenide, Gallium Nitride and Aluminium Nitride

Supasarote MUENSIT

B.Sc. (Physics), Prince of Songkhla University, Hatyai
M.Sc.(Physics), Chulalongkorn University, Bangkok
Thailand

A thesis submitted for the degree of Doctor of Philosophy.
This work was carried out within the Semiconductor Science and Technology Laboratories (SSTL) of Macquarie University's School of Mathematics, Physics, Computing and Electronics. Sydney, NSW, AUSTRALIA

1998.

Copyright in relation to this Thesis

Table of Contents

Declaration

Acknowledgements

Abstract

List of Symbols

Chapter One : Introduction 1-1

1.1 Background and Thesis Outline 1-1

1.2 Fundamentals of Piezoelectricity 1-3

1.2.1 Brief history 1-3

1.2.2 Piezoelectric coefficients 1-5

1.2.3 Piezoelectric constitutive equations 1-8

1.2.4 Piezoelectric effects on the elastic and dielectric constants 1-8

1.2.5 The piezoelectric tensor and transformation laws 1-10

1.3 Piezoelectric Contribution to Semiconducting Properties 1-14

1.4 Piezoelectric Coefficient Measurements : Conventional Methods 1-17

1.4.1 Static and quasi-static methods 1-17

1.4.2 Resonance methods 1-19

1.5 Piezoelectric Coefficient Measurement in Thin Films 1-20

1.6 Measuring the Piezoelectric Coefficients in Semiconductors 1-22

Chapter Two : A Michelson Interferometer for Measurement of Piezoelectric Coefficients 2-1

2.1 Introduction 2-1

2.2 Principle of the Michelson Interferometer 2-2

2.3 Setting up the Michelson Interferometer 2-4

2.3.1 Experimental setup 2-4
2.3.2 Electronic stabilizer 2-6
2.3.3 Drive voltage harmonic content 2-8
2.3.4 Detector response 2-9
2.4 Measurement of Electric Field Induced Strains 2-11
2.5 Initial System Calibration 2-14
2.6 Effects of Resonance 2-17
2.7 Noise Limitation and Interferometer Resolution 2-20
2.7.1 Theoretical noise level 2-20
2.7.2 Signal-to-noise ratio and theoretical detection limit 2-22
2.7.3 Noise measurement 2-24
2.7.4 Interferometer resolution 2-26
2.8 Determination of the Piezoelectric Coefficient Sign 2-27
2.9 Conclusions 2-29
Chapter Three : The Piezoelectric Coefficient of Gallium Arsenide 3-1
3.1 Introduction 3-1
3.2 Review of Previous Work 3-2
3.3 Crystal Structure and [111] Plane 3-6
3.4 Crystal Symmetry and the Piezoelectric Tensor 3-8
3.4.1 Effect of crystal symmetry on the piezoelectric tensor 3-8
3.4.2 Transformed piezoelectric coefficient 3-10
3.5 Measurement of the d_{14} Coefficient 3-12
3.5.1 Sample preparation 3-12
3.5.2 Electrode material 3-12
3.5.3 Effect of electrode dimensions 3-14

3.5.4 The sign of the d_{14} coefficient 3-16

3.6 Conclusions 3-16

Chapter Four : Extensional Piezoelectric Coefficients of Gallium Nitrides and Aluminium Nitride 4-1

4.1 Introduction 4-1

4.1.1 Review of previous work 4-2

4.1.2 Applications of piezoelectric effect of GaN and AlN 4-3

4.2 Crystal Structure and the Piezoelectric Coefficients 4-5

4.3 Experimental Techniques 4-6

4.3.1 Sample preparation 4-6

4.3.1.1 GaN films 4-6

4.3.1.2 AlN films 4-7

4.3.2 Measurement of the d_{33} and d_{31} coefficients 4-8

4.3.3 Resistivity measurement 4-9

4.4 Experimental Results 4-10

4.4.1 Film resistivity 4-10

4.4.2 Bending effects 4-11

4.4.3 The d_{33} and d_{31} coefficients 4-14

4.4.4 Substrate clamping 4-19

4.4.5 Piezoelectric coefficients of zincblende GaN and AlN 4-22

4.4.6 Direction of the 3 axis 4-22

4.5 Conclusions 4-23

Chapter Five : Shear Piezoelectric Coefficients of Gallium Nitride and Aluminium Nitride 5-1

5.1 Introduction 5-1

5.2 A Method for Measuring Shear Coefficients 5-3

5.2.1 Measurement of shear strain 5-3

5.2.2 Application of the field 5-5

5.3 Experimental Techniques 5-7

5.3.1 Sample preparation 5-7

5.3.2 Determination of the d_{15} coefficient 5-8

5.4 Experimental Results 5-8

5.4.1 AlN 5-8

5.4.2 GaN 5-12

5.4.2.1 GaN with SiC substrate 5-12

5.4.2.2 GaN with sapphire substrate 5-12

5.5 Discussion 5-15

5.5.1 The d_{15} coefficient of AlN 5-16

5.5.2 The d_{15} coefficient of GaN 5-16

5.6 Conclusions 5-17

Chapter Six : Electrostriction in Gallium Nitride, Aluminium Nitride and Gallium Arsenide 6-1

6.1 Introduction 6-1

6.2 Background 6-2

6.2.1 Fundamental relations 6-2

6.2.2 Crystal symmetry and electrostrictive coefficients 6-6

6.3 Electrostriction Measurements 6-7

6.4 Other Quadratic Effects 6-9

6.4.1 Maxwell stress 6-9

6.4.2 Thermal expansion 6-9

6.5 Experimental Techniques 6-10
6.5.1 Sample preparation 6-10
6.5.2 Interferometer setup 6-11
6.5.3 Dielectric measurement 6-11
6.6 Experimental Results 6-12
6.6.1 Dielectric constant 6-12
6.6.2 Results for GaN and AlN 6-12
6.6.3 Results for GaAs 6-17
6.7 Discussion 6-19
6.7.1 Maxwell stress effect contribution 6-19
6.7.2 Thermal expansion contribution 6-20
6.7.3 Size of electrostriction for GaN and AlN 6-22
6.8 Conclusions 6-23
Chapter Seven : Summary and Prognosis 7-1
7.1 Main Conclusions 7-1
7.2 Prognosis for Future Work 7-4

Appendix A-1
Table A.1 A-1
Table A.2 A-2
References R-1
Publications by the Author

Declaration

This thesis is submitted in accordance with the regulations for the degree of Doctor of Philosophy of Macquarie University. It reports the work carried out within the Semiconductor Science and Technology Laboratories Of Macquarie University's School of Mathematics, Physics, Computing and Electronics between July 1995 and August 1998. I declare that to the best of my knowledge the research work described herein is original, except where otherwise indicated and acknowledged. I further declare that this thesis has not, either in whole or in part, been submitted for a higher degree to any other University.

S. Muensit

S. Muensit

September, 1998.

Acknowledgements

I am in debted to my parents who have cared for my two girls, and to my husband for his patience throughout my time in Australia.

I would like to thank my supervisor, Dr. Ian. L. Guy, for his invaluable guidance and care, without which I would not have been able to complete my study. I also wish to thank Prof. Trevor. L. Tansley, the Director of the SSTL, for his generous support , both academic and personal.

The following people who have kindly contributed their samples for my investigations are gratefully acknowledged : Dr. B. Zhou, Dr. Xin Li and Dr. K. S. A. Butcher, the members of the SSTL in the past, and Dr. J. P. David, Department of Electronic and Electrical Engineering, University of Sheffield, England. I am also grateful to Dr. Ewa Goldys for providing the commercial GaN samples and Bernadette Davies for GaN etching. I would also like to thank Rajeev Katti, Lou Guirin, and Douglas. J. Wilson, for their helping hands and invaluable suggestions. Without them my study would have taken considerably longer

It is my pleasure to thank Dr. Marie Wintrebert, my friend in the Electronics Department, also Ms. Krystyna Tomsia and my friends within the SSTL, in particular Graeme Nott, Helen Zuo, and Albinur Limbong.

To all these people and others who have contributed with ideas and discussion over the last three years, I extend my sincere thanks.

Finally, I would like to acknowledge the support of Royal Thai Government (RTG) through the Annual RTG Scholarship, and the support of Macquarie University through the Research Grant Scheme and the reduction of the 1998 tuition fee.

Abstract

The present work represents the first use of the interferometric technique for determining the magnitude and sign of the piezoelectric coefficients of III-V compound semiconductors, in particular gallium arsenide (GaAs), gallium nitride (GaN), and aluminium nitride (AlN). The interferometer arrangement used in the present work was a Michelson interferometer, with the capability of achieving a resolution of 10^{-13} m.

The samples used were of two types. The first were commercial wafers, with single crystal orientation. Both GaAs and GaN were obtained in this form. The second type of sample was polycrystalline thin films, grown in the semiconductor research laboratories at Macquarie University. GaN and AlN samples of this type were obtained.

The d_{14} coefficient of GaAs was measured by first measuring the d_{33} value of a [111] oriented sample. This was then transformed to give the d_{14} coefficient of the usual [001] oriented crystal. The value obtained for d_{14} was (-2.7±0.1) pmV^{-1}. This compares well with the most recent reported measurements of -2.69 pmV^{-1}. The significance of the measurement is that this represents the first time this coefficient has been measured using the inverse piezoelectric effect.

For AlN and GaN samples, the present work also represents the first time their piezoelectric coefficients have been measured by interferometry. For GaN, this work presents the first reported measurements of the piezoelectric coefficients, and some of these results have recently been published by the (Muensit and Guy, 1998). The d_{33} and d_{31} coefficients for GaN were found to be (3.4 ± 0.1) pmV^{-1} and (−1.7 ± 0.1) pmV^{-1} respectively. Since these values were

measured on a single crystal wafer and have been corrected for substrate clamping, the values should be a good measure of the true piezoelectric coefficients for bulk GaN.

For AlN, the d_{33} and d_{31} coefficients were found to be (5.1 ± 0.2) pmV^{-1}, and (–2.6 ± 0.1) pmV^{-1} respectively. Since these figures are measured on a polycrystalline sample it is quite probable that the values for bulk AlN would be somewhat higher.

The piezoelectric measurements indicate that the positive c axis in the nitride films points away from the substrate. The piezoelectric measurements provide a simple means for identifying the positive c axis direction.

The interferometric technique has also been used to measure the shear piezoelectric coefficient d_{15} for AlN and GaN. This work represents the first application of this technique to measure this particular coefficient. The d_{15} coefficients for AlN and GaN were found to be (–3.6 ± 0.1) pmV^{-1} and (–3.1 ± 0.1) pmV^{-1} respectively. The value for AlN agrees reasonably well with the only reported value available in the literature of -4.08 pmV^{-1}. The value of this coefficient for GaN has not previously been measured.

Some initial investigations into the phenomenon of electrostriction in the compound semiconductors were also performed. It appears that these materials have both a piezoelectric response and a significant electrostrictive response. For the polycrystalline GaN and AlN, the values of the M_{33} coefficients are of the order of 10^{-18} m^2V^{-2}. The commercial single crystal GaN and GaAs wafers display an asymmetric response which cannot be explained.

List of Symbols

A	area
C	capacitance
c	specific heat, elastic stiffness
D	electric displacement
d	piezoelectric strain coefficient
g	piezoelectric strain coefficient
E	electric field
e	piezoelectric stress coefficient
h	piezoelectric stress coefficient
F	force
f	frequency
h	Planck constant
I	light intensity
i	current
k	Boltzmann constant, oscillator constant
l	length
M	electrostrictive coefficient
m	mass, electrostrictive coefficient
P	electric polarization
Q	electrostrictive coefficient
q	electron charge, electrostrictive coefficient
R	resistance
S	strain

s	elastic compliance
T	stress, temperature
t	thickness, time
V	voltage
X, x	mechanical displacement
Ω	ohm
α	coefficient of thermal expansion
β	impermittivity, shear angle
χ	dielectric stiffness
ε	dielectric constant (relative permittivity)
ε_o	permittivity of free space
η	dielectric susceptibility
λ	wavelength
ρ	resistivity
ρ_m	density
ω	angular frequency

1

Introduction

1.1 Background and Thesis Outline

The term *piezoelectricity* refers to the phenomenon, present in some crystalline materials, whereby mechanical stress gives rise to the generation of charge on the crystal surfaces. The magnitude of the effect is described by defining various piezoelectric coefficients, whose nature is described in this chapter. Piezoelectric coefficients can be measured using either the direct piezoelectric effect, in which the charges generated by a known mechanical stress are measured, or the inverse piezoelectric effect, in which the electrically induced strains are measured. Probably the most common approach is use the direct effect (Arlt and Quadflieg, 1968, and references therein; Bottom, 1970, and references therein; Yu et al., 1997). Measurements based on the inverse effect appear to be less common (Zhang et al., 1988). It is the aim of the present work to utilize the inverse effect to measure the piezoelectricity in compound semiconductors. The

mechanical strain is measured using an optical interferometer, with the sample positioned in one of the interferometer arms. This arrangement has been used successfully for measuring the piezoelectric coefficients of ferroelectric ceramic materials and is claimed to be capable of achieving resolutions as low as to 10^{-14} m (Kwaaitaal et al., 1980 ; Li et al., 1995).

It is well known that a strong piezoelectric effect exists in some semiconducting materials (Hutson, 1960 ; Jaffe et al., 1960) but it is only in relatively recent times that there has been increased interest in this area. This interest has been stimulated by two factors. Firstly, because of the interaction between the piezoelectric effect and the semiconducting properties (Li and Ni, 1996; Wan et al., 1995; Bykhovski et al., 1993) and secondly, because of the possibility of making use of the piezoelectric effect in deliberately strained structures to produce devices with desirable properties (Sánchez-Rojas et al., 1994 ; Pabla et al., 1994 ; Grey et al., 1995 ; Bykhovski et al., 1995). The measurement of the piezoelectric coefficients in semiconductors is thus of interest from both an engineering and a basic science viewpoint.

This work represents the first use of the interferometric technique for determining the magnitude and sign of the piezoelectric coefficients of III-V compound semiconductors, in particular gallium arsenide (GaAs), gallium nitride (GaN) and aluminium nitride (AlN).

Reports of measurements of piezoelectric coefficients of these materials are surprisingly scarce and it is possible that the difficulties encountered in obtaining suitable samples are a part of the reason for this. In the present case samples were obtained from two types of source. The first were commercial wafers, with single crystal orientation. Both GaAs and GaN were obtained in this form. The second type of sample was polycrystalline

thin films, grown in research laboratories. GaN and AlN samples of this type were obtained.

The remainder of this chapter is devoted to setting the background, by describing the meaning of the various coefficients and some of the issues which arise in their measurement.

Chapter 2 describes the interferometric method and gives a detailed description of the interferometer used here. Limitations of the method, and of the particular equipment used in this case, are also discussed.

Chapter 3 describes the measurement of the piezoelectric cofficient (d_{14}) of GaAs, while chapter 4 describes the measurements for the extensional piezoelectric coefficients (d_{33} and d_{31}) of GaN and AlN.

Measurement of the shear coefficient (d_{15}) in GaN and AlN was attempted during the course of this work. The method used and the results obtained are presented in chapter 5.

Closely related to piezoelectricity is the phenomenon of electrostriction. This appears never to have been measured in the compound semiconductors prior to this work. Some initial measurements are presented in chapter 6.

Chapter 7 concludes by drawing together the various threads initiated in earlier chapters and identifying areas which arose during the course of the investigation and which merit further attention.

1.2 Fundamentals of Piezoelectricity

1.2.1 Brief history

The piezoelectric effect was first discovered in 1880 by the Curie brothers, Pierre and Jacques (Cady, 1964, p2 ; Mason, 1950, p2). They found that some crystals (tourmaline, quartz, topaz, cane sugar, and

Rochelle salt) when compressed in particular directions, produced charges which were proportional to the pressure, and which disappeared when the pressure was removed. This was the direct piezoelectric effect. The existence of an inverse piezoelectric effect was mathematically deduced from fundamental thermodynamic principles by Lippmann in 1881, and the Curies verified this prediction experimentally in the same year.

During the years following the discovery of the piezoelectric effect, several well known researchers, including Lord Kelvin, Pockels and Duhem developed theories of piezoelectricity. The state of piezoelectric knowledge up to the beginning of World War I was summarized by Voigt in his monumental 'Lehrbuch der Kristallphysik', published in Berlin in 1910. In Voigt's publication, the crystal classes in which the piezoelectric effect exists were identified, and the particular coefficients for each class were also described (Mason, 1950, p2).

At that time, piezoelectricity was essentially a curiosity, with no practical applications. During the First World War, in France, Langevin conceived the idea of activating the quartz plates electrically to serve as emitters, and later also as receivers, of high frequency sound waves. By emitting a high frequency pulse underwater and timing the return echo of this pulse, a means of measuring the depth of the ocean was achieved and gained a lot of attention (Mason, 1950, p2). Since that time, the development of piezoelectric applications has increased enormously and the range of applications appears never ending.

Piezoelectric materials have been used in a wide range of applications, for example, microphones, loudspeakers, accelerometers, ultrasonic transducers, bender element actuators, and phonograph pick-ups.

More recent applications include nondestructive testing, medical imaging and the scanning tunneling microscopes making use of piezoelectric positioners.

The most common piezoelectric application is probably as the control element in electronic oscillators and filters. Every television set, computer and most clocks have at least one piezoelectric crystal, most commonly quartz.

1.2.2 Piezoelectric coefficients

As indicated in the previous sections, piezoelectricity refers to the generation of electrical effects by mechanical distortion and vice versa. Cady (1964, p4) defined piezoelectricity as "electric polarization produced by mechanical strain in crystals belonging to certain classes, the polarization being proportional to the strain and changing sign with it". This statement represents the *direct piezoelectric effect,* while another closely related definition, "a piezoelectric crystal becomes strained, when electrically polarized" represents the *inverse piezoelectric effect.*

Piezoelectricity is a fundamental property of all crystals which lack sufficient symmetry. Of the 32 crystal classes 20 show such a lack, while crystals in the remaining 12 classes are of too high a degree of symmetry to show piezoelectric properties. The asymmetry in piezoelectric crystals means that certain elastic deformations of the crystals are associated with the displacement of positively charged ions relative to negative ones. This relative movement leads to an electric dipole moment in each the unit cell in the crystal. Polarization, which is the electric dipole moment per unit volume, is proportional to the strain. Fig. 1.1 shows a schematic representation of the way in which the effect arises in quartz.

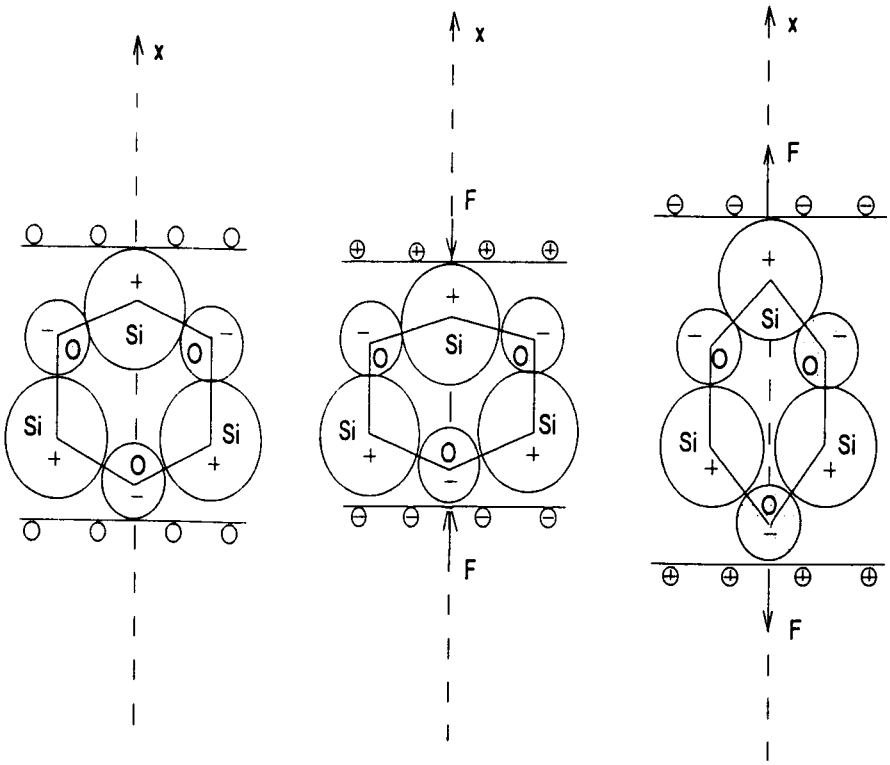

Fig.1.1 A simple representation of the piezoelectric effect in quartz (after Kuttruff, 1991, p86).

The piezoelectric coefficients relate mechanical and electrical variables, as for example

$$D = dT \tag{1.1a}$$

where the coefficient d relates the electric displacement D to the mechanical stress T. Thermodynamics can be used to show that the coefficient for the inverse effect is equal to that for the direct effect (Nye, 1985, p115). Thus the coefficient d also gives the strain in terms of the field:

$$S = dE \tag{1.1b}$$

Piezoelectricity is a coupling between the mechanical and electrical systems. The mechanical variables may be either stress or strain, while either the electrical displacement or the field can be used as the electrical variable.

This leads to the necessity of defining four different piezoelectric coefficients. These are: *d* and *g*, which are termed the piezoelectric strain coefficients, and *e* and *h*, the piezoelectric stress coefficients. These coefficients are defined by the following equations (IEEE Standard on Piezoelectricity, 1988) :

$$d = \left(\frac{\partial D}{\partial T}\right)_E = \left(\frac{\partial S}{\partial E}\right)_T \tag{1.2a}$$

$$e = \left(\frac{\partial D}{\partial S}\right)_E = \left(\frac{\partial T}{\partial E}\right)_S \tag{1.2b}$$

$$g = \left(\frac{\partial E}{\partial T}\right)_D = \left(\frac{\partial S}{\partial D}\right)_T \tag{1.2c}$$

$$h = \left(\frac{\partial E}{\partial S}\right)_D = \left(\frac{\partial T}{\partial D}\right)_S \tag{1.2d}$$

It can be seen from equations (1.2) that each coefficient has two forms, one corresponding to the direct effect and one to the inverse effect.

Not all four coefficients are independent and the following relations exist between them (Ikeda, 1990, p17):

$$d = \varepsilon g = es \tag{1.3a}$$

$$e = \varepsilon h = dc \tag{1.3b}$$

$$g = \beta d = hs \tag{1.3c}$$

$$h = \beta e = gc \tag{1.3d}$$

where s and *c* are the elastic compliance and stiffness, while ε and β the electrical permittivity and impermittivity respectively.

1.2.3 Piezoelectric constitutive equations

Sets of constitutive relations can be derived from the relevant thermodynamic functions such as the Helmholz free energy and the Gibbs free energy (Ikeda, 1990, p16). These equations are derived assuming that the interaction between mechanical and electrical systems is reversible and isothermal.

The constitutive equations are listed in table 1.1. These equations have been expressed in a simplified form by omitting tensor notation and the necessary mechanical and electrical conditions. These matters are introduced in subsequent sections.

Table 1.1 Piezoelectric constitutive equations.

Independent variables	Fundamental equations	
	Direct effect	Inverse effect
(S,E)	$D = eS + \varepsilon E$	$T = cS - eE$
(T,D)	$E = -gT + \beta D$	$S = sT + gD$
(S,D)	$E = -hS + \beta D$	$T = cS - hD$
(T,E)	$D = dT + \varepsilon E$	$S = sT + dE$

1.2.4 Piezoelectric effects on the elastic and dielectric constants

The fundamental material parameters required for describing piezoelectric properties are the dielectric, elastic and piezoelectric coefficients. As indicated in previous sections, piezoelectricity refers to a coupling between the mechanical and electrical systems. In piezoelectric materials, the mechanical properties are affected by electrical conditions and vice versa.

When a mechanical stress is applied to a piezoelectric material, the resulting strain is determined not only by the stress, but also by the electrical

conditions. An *electrically clamped state* is defined when the polarization is constant, and an *electrically free state* when the surrounding medium has infinite dielectric susceptibility. An isolated (i.e., remote from all conductors) piezoelectric material would be in the first state, while the electric field would be held constant in the second state. The mechanical properties, described by the stiffness or the compliance, are dependent on which set of conditions apply. To indicate the conditions under which the elasticity or stiffness have been measured, a superscript is usually added to the symbol. Thus the symbols c^E and s^E represent the stiffness and compliance under the conditions of a constant field, while c^D and s^D refer to values measured with constant displacement.

Measurements of velocities of plane waves propagating along certain symmetry directions can be used to determine the stiffness of the crystal. Conventional ultrasonic pulse-echo techniques are the most common methods for measuring such velocities with relatively high accuracy (IEEE Standard on Piezoelectricity, 1988, p49).

When measuring the dielectric properties of a piezoelectric material, then the mechanical conditions need to be specified. Two conditions are usually used, either a *clamped* (constant strain) state or a *free* (constant stress) state. In the clamped state, the surfaces of the piezoelectric material are firmly attached to a surrounding medium of infinite rigidity, so that all strains are zero. In the free state the surrounding medium must have infinite compliance. The piezoelectric medium is then free from external stress, and the piezoelectric strain can assume its full theoretical value. As with the mechanical conditions, the dielectric constants have a superscript added to indicate the conditions under which they have been measured. The

permittivities, measured under constant stress or strain, are denoted ε^T or ε^S respectively.

In practice, the free permittivity can be obtained by measuring the capacitance at frequencies well below mechanical resonance, while the clamped permittivity is obtained from capacitance measurements made well above the mechanical resonance.

1.2.5 The piezoelectric tensor and transformation laws

The dielectric, elastic and piezoelectric coefficients are tensors and a knowledge of the values of all tensor components is necessary for a complete understanding of the material behaviour.

As an illustration, equation (1.1b), when written in full tensor notation would become:

$$S_{jk} = d_{ijk} E_i \tag{1.4}$$

Since this equation is of major importance in the work described in this thesis, it will be used for illustrative purposes here.

In equation (1.4) each of the subscripts can have values ranging from 1 to 3. In addition, the summation convention is assumed. In this convention, any subscript which is repeated in a term indicates that that term is to be summed over the possible values of the subscript.

The piezoelectric coefficient d_{ijk} is a third rank tensor and thus should have 27 components. However d_{ijk} is symmetric in j and k and this reduces the number of independant elements to 18. Crystal symmetry reduces this number even further. The number of nonzero piezoelectric coefficients for the different crystal classes is listed in an appendix (Table A.1).

The piezoelectric coefficients are related to a set of cartesian axes. These axes in turn are related to the conventional crystal axes in a standard

manner (Nye, 1985). On occasion it may become convenient to rotate to a different set of axes, and this is done by following normal transformation rules.

If a set of axes, denoted by x is rotated to a new system x', then coordinates in the old system transform to the new system by the transformation (Nye, 1985, p9) :

$$x'_i = a_{ij} x_j \ , \qquad i,j = 1,2,3 \tag{1.5}$$

where a_{ij} represents the cosine of the angle between the old x_j axis and the new x'_i. The various a_{ij} are illustrated in Fig.1.2.

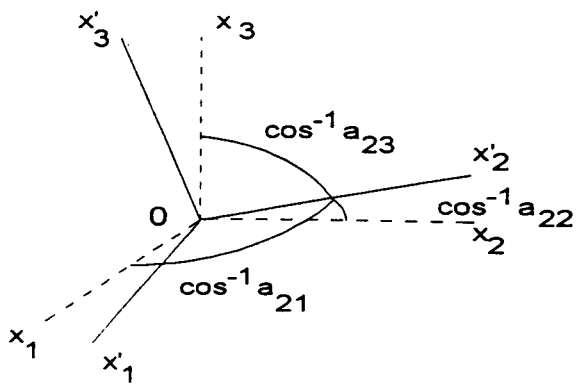

Fig.1.2 Transformation of axes and the a_{ij}.

For a third rank tensor, the tensor components will be changed by a rotation of the axes. If the third rank tensor X_{ijk} becomes X'_{ijk} in the new coordinate system, then the transformation is given by (Nye, 1985, p111):

$$X'_{ijk} = a_{il} a_{jm} a_{kn} X_{lmn} \tag{1.6}$$

Since the piezoelectric tensor is third rank, it will transform in the manner shown by equation (1.6), the piezoelectric tensor elements in the original coordinate system d_{ijk} transforming to d'_{ijk} , where :

$$d'_{ijk} = a_{il}a_{jm}a_{kn}d_{lmn} \tag{1.7}$$

Such transformations become significant for crystals which are grown on non-conventional growth planes.

Tensor components can be written in a more compact notation known as matrix notation (Nye, 1985, p113). This notation relies on the symmetry of the tensor components. For the second rank tensors stress, strain and permittivity, the tensors are symmetric in the two subscripts. For the third rank piezoelectric coefficients the symmetry is in the last two subscripts. For the fourth rank elastic constants, the subscripts can be collected in pairs and the symmetry occurs within each pairing. The paired subscripts can thus only have 6 values. This fact is exploited by replacing the paired subscripts, whose values can run from 1 to 3, by one subscript whose value can run from 1 to 6. The convention used for replacing the 2 tensor subscripts by 1 matrix subscript is:

tensor notation	11	22	33	23 or 32	13 or 31	12 or 21
matrix notation	1	2	3	4	5	6

The stress and elastic stiffness are transformed simply using the above notation. For example T_{13} becomes T_5 and c_{1213} becomes c_{65}. In order to keep the constitutive equations simple, there are additional requirements imposed on the strain, compliance and the piezoelectric *d* and *g* tensors. These are (IEEE Standard on Piezoelectricity, 1988):

$$S_j = S_{pq} \qquad \text{when } p = q\ ,\ j = 1,2,3 \qquad (1.8a)$$

$$S_j = 2S_{pq} \qquad \text{when } p \neq q,\ j = 4,5,6 \qquad (1.8b)$$

$$d_{ip} = d_{ijk} \qquad \text{when } j = k,\ p = 1,2,3 \qquad (1.8c)$$

$$d_{ip} = 2d_{ijk} \qquad \text{when } j \neq k,\ p = 4,5,6 \qquad (1.8d)$$

$$s^E_{jk} = s^E_{pqmn} \qquad \text{when } p = q \text{ and } m = n,\ j,k = 1,2,3 \qquad (1.8e)$$

$$s^E_{jk} = 2s^E_{pqmn} \qquad \text{when } p = q \text{ and } m \neq n,\ j = 1,2,3,\ k = 4,5,6 \qquad (1.8f)$$

$$s^E_{jk} = 4s^E_{pqmn} \qquad \text{when } p \neq q \text{ and } m \neq n,\ j,k = 4,5,6 \qquad (1.8g)$$

If this system were not followed, then the factors 2 and 4, appearing in equations (1.8), would appear in the constitutive equations.

The advantage of the matrix notation is that it becomes possible to write tensors up to rank 4 as a two dimensional array. The physical significance of the subscripts for stress and strain is illustrated in Fig.1.3. The numbers 1, 2, and 3 represent directions along the x_1, x_2 and x_3 axes, while 4, 5, and 6 represent shears about x_1, x_2 and x_3 respectively.

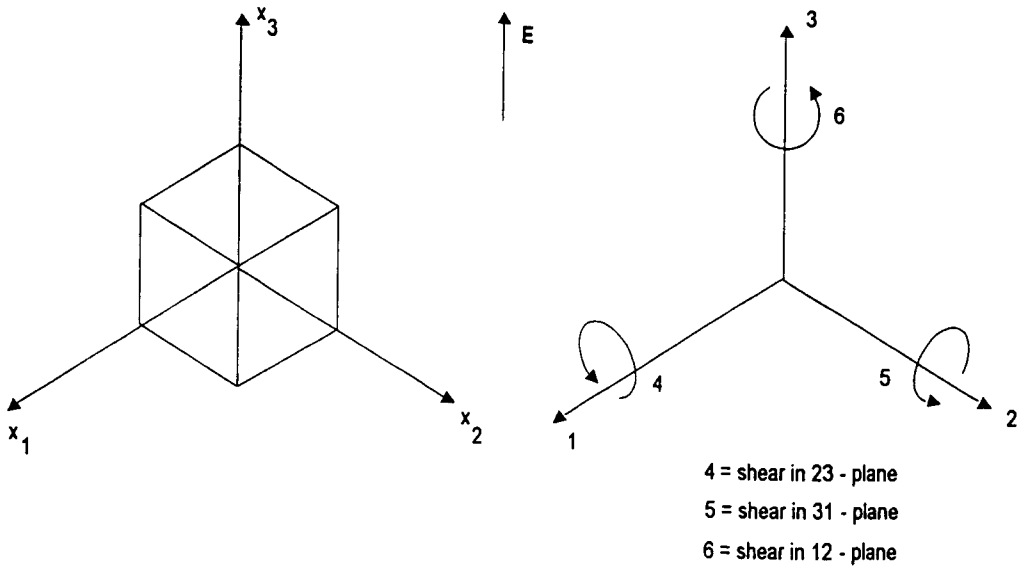

Fig.1.3 Illustration of the directions associated with the subscripts used in the matrix notation.

1.3 Piezoelectric Contribution to Semiconducting Properties

When thin films of III-V semiconductors are grown on substrates, there will, in general, be some lattice mismatch between the film itself and the substrate (Strite and Morkoç, 1992 ; Grey et al., 1995). This lattice mismatch will produce strain in the film. Since the semiconductor film is piezoelectric, these residual strains give rise to electric fields within the film. The electric field generated by the strain is capable of causing changes to the electronic band structure and optical characteristics of the semiconductors. These changes have been exploited in the design of devices based on single layers grown on substrates, or multi-layers using alternating materials. The work in this area has been recently reviewed (Rees, 1997).

The III-V compound semiconductors most commonly occur in either the wurtzite (6*mm*) or the zincblende ($\bar{4}3m$) crystal forms. The piezoelectric properties af these crystal classes are descibed more fully in chapters 3 and 4, however it is worth noting briefly that if the zincblende films are grown on

the [111] planes or if wurtzite films are grown on [0001] planes, then electric fields in the thickness direction (i.e. perpendicular to the plane of the film) can be induced by residual strains (Smith, 1997, and references therein).

The following examples illustrate some of the ways in which the piezoelectric effect has been exploited in semiconductor structures.

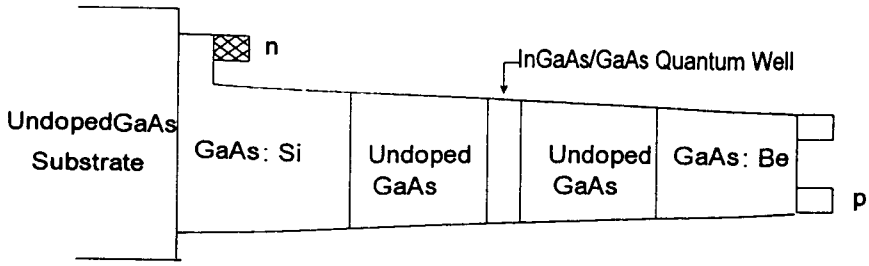

Fig.1.4 InGaAs/GaAs quantum well embedded into the intrinsic region of a *pin* diode grown on (111)B GaAs substrate (after Caridi, et al., 1990).

Fig.1.4 illustrates the influence of the piezoelectric effect in a device based on a zincblende semiconductor grown in the [111] orientation. This device makes use of an InGaAs/GaAs quantum well. The layers of different materials in the wells introduces strain into the structure. The strains in turn induce polarizations and associated electric fields. The electric fields cause a blue shift in the absorption band of the structure under zero bias. The measured blue shift indicates an electric field strength of order 10^7 Vm^{-1}. Piezoelectric fields can thus act as the internal bias of the *pin* diode structure and offer possibilities for devices requiring blue shifted absorption features such as self-electro-optic effect device (SEED) (Caridi, et al., 1990).

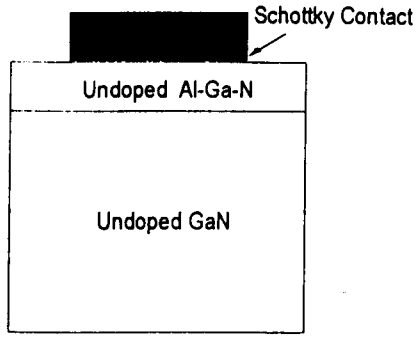

Fig.1.5 Diagram of a nominally undoped AlGaN/GaN heterostructure (after Yu et al., 1997).

Fig.1.5 illustrates a heterostructure made from wurtzite semiconductor grown in the [0001] orientation. A high sheet carrier concentration was found at the GaN/AlGaN interface, despite the absence of intentional doping in the structure. This is a consequence of piezoelectrically induced charges at the interface, which are caused by the lattice mismatch between the AlGaN barrier layer and the underlying GaN epilayer. An increase in the gate voltage swing along with improvements in speed and other advantages can be achieved from heterostructure field-effect transistors (HFET) fabricated from this GaN/AlGaN structure (Yu et al., 1997). Theoretical studies of the effects of the piezoelectric field in GaN/AlGaN structures on defect formation, charge transfer and electron transport have been reported recently (Hsu and Walukiewicz, 1998).

From the above examples it is apparent that the piezoelectric effect can produce a significant influence on semiconductor properties and the effect must be properly accounted for in the design of strained heterostructure devices. This in turn leads to a need for a set of reliable values of the various piezoelectric coefficients for the semiconducting

materials used. Some reports, involving a theoretical reassessment of the values of piezoelectric coefficients have appeared in recent times (Fisher et al., 1994 ; Chin, 1994). However experimental measurements of the piezoelectric coefficients appear to be lacking and should have significant value.

1.4 Piezoelectric Coefficient Measurements:Conventional Methods

1.4.1 Static and quasi-static methods

The earliest piezoelectric measurements, and probably the easiest to perform, use static methods. For example, measuring the piezoelectric coefficient using the inverse piezoelectric effect, would involve measuring the mechanical extension in a crystal for a given applied DC voltage, under conditions of zero stress within the crystal. The strain generated is then given by equation (1.4). Measurements of the amount of extension, which is usually small, require special means such as using strain gauges (Pointon, 1982), or interferometric techniques (Bottom, 1970).

Static measurements of the piezoelectric coefficient using the direct piezoelectric effect can be achieved by placing a weight on the crystal and observing the charges generated.

A problem with static methods is that the generated charge is small and may leak away before the test is complete. In addition any associated electronics must be DC coupled and hence is subject to slow drifts. Static measurements are, however useful for identification of the positive sense of the orthogonal x_1, x_2, x_3 axes in order to determine the sign of the piezoelectric coefficient (IEEE Standard on Piezoelectricity, 1988, p23).

If the coefficients are to be measured directly it is more usual to use low frequency AC measurements. Fig.1.6 shows the well-known Berlincourt

meter used for measuring d_{33}. In this meter a sinusoidal force is applied to a piezoelectric sample by an electromagnetic driver in the force head. The probes which make contact with the sample surface are specially shaped, in order to apply the stress in an appropriate way. The generated charge is measured. and the d_{33} calculated from the ratio of the charge to the force. Usually the instrument is calibrated to give a direct readout of d_{33}. Such instruments are normally suitable only for piezoelectric materials with reasonably large (i.e. >10 pCN^{-1}) coefficients (from the Berlincourt Piezo d_{33} meter manual, 1974)

Instruments such as the Berlincourt meter operate in a quasi-static mode. The measurements are performed at frequencies which are far below the mechanical resonance of the sample. Hence inertial forces are negligible and the strains are uniform throughout the material (Mason, 1950).

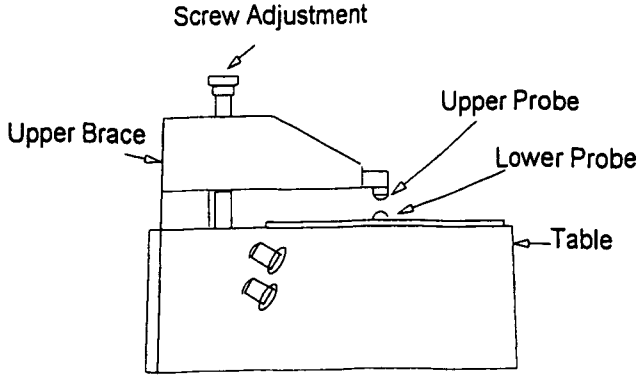

Fig.1.6 Berlincourt meter for measuring d_{33}. The force head uses an electromagnetic driver to apply force to a piezoelectric sample (from the Berlincourt Piezo d_{33} meter manual, 1974).

1.4.2 Resonance methods

Piezoelectric coefficients can also be measured by resonance methods (IEEE Standard on Piezoelectricity, 1988). These make use of the variation in electrical impedance in the frequency range close to a mechanical resonance. The impedance properties of the piezoelectric resonator can be represented by a simple equivalent electrical circuit as shown in Fig.1.7. For a more complex equivalent circuit, parasitic components due to the mounting of piezoelectric resonator are taken into account (Hafner, 1969).

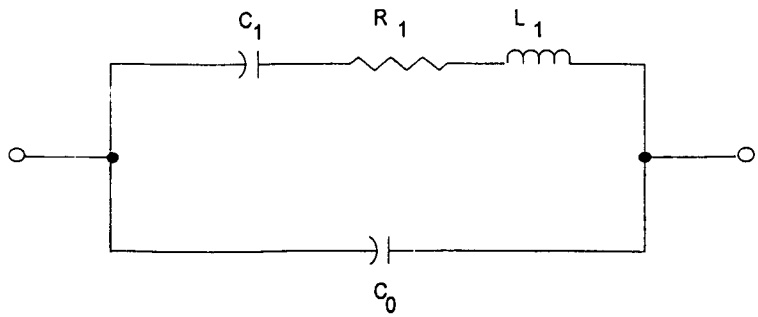

Fig.1.7 Equivalent circuit of a piezoelectric resonator (after IEEE Standard on Piezoelectricity, 1988).

Suitably shaped and oriented crystals, together with the application of an electric field in a particular direction can excite the vibrational mode desired such as length extensional, thickness shear, and thickness excitation modes (Kobiakov, 1980 ; Okamura and Minowa, 1989 ; Royer and Kmetik, 1992). The resonance method requires the ability to make accurate measurements of impedance near the appropriate mechanical resonance. For thickness coefficients, these resonances usually occur at quite high frequencies. The technique is capable of accurate results, however the measurements require more attention to detail than is the case for the direct methods described in the previous section.

1.5 Piezoelectric Coefficient Measurement in Thin Films

Measurements of the piezoelectric coefficients of thin (<1 μm) films present additional challenges. The d_{33} coefficient of thin plates of crystals with $3m$ symmetry such as $LiNbO_3$, $LiTaO_3$ have been determined using an optical heterodyne interferometer to measure the strains (Royer and Kmetik, 1992). In thin films of ferroelectric ceramics, such as lead-zirconate titanate (PZT), the d_{33} coefficient has been determined by using a normal load method to apply a stress and measuring the induced charges (Lefki and Dormans, 1994). In both cases the films were mounted on thick substrates. Therefore, the measured coefficient did not represent the true value of the coefficient for the bulk material, but rather an apparent value. The difference between the two is due to the clamping of the sample by the non-piezoelectric substrate. The situation is illustrated in Fig.1.8.

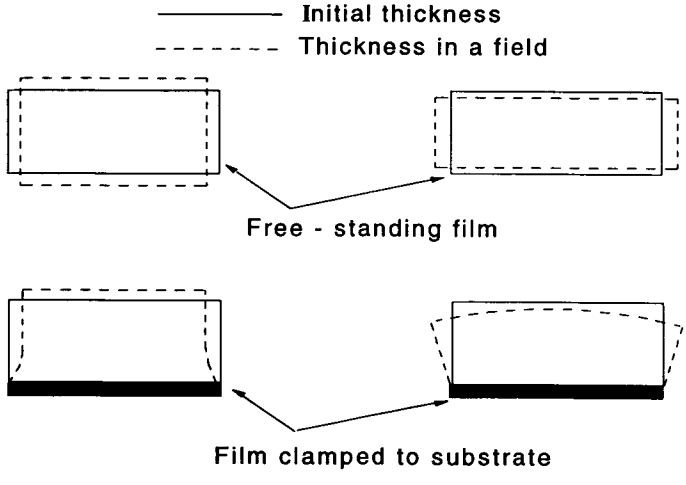

Fig.1.8 A diagram showing (not to scale) how a film clamped to a substrate is not free to expand or contract in the film plane.

It is possible to correct for this clamping (Royer and Kmetik, 1992; Lefki and Dormans, 1994). The following discussion assumes that the d_{33}

coefficient is to be measured using the inverse effect. The d_{33} coefficient is defined by:

$$d_{33} = \left(\frac{\partial S_3}{\partial E_3}\right)_T \tag{1.9}$$

where the 3 direction is the direction of the applied electric field, and is normal to the plane of the film.

The appropriate constitutive equation, written using the matrix notation is: (see table 1.1)

$$S_j = s^E_{jk} T_k + d_{ij} E_i \qquad j,k = 1,2,...,6;\ i = 1,2,3 \tag{1.10}$$

The expanded forms of this equation, written out only for the cases where E_3 is involved are :

$$S_1 = s^E_{11} T_1 + s^E_{12} T_2 + s^E_{13} T_3 + d_{31} E_3 \tag{1.11}$$

$$S_2 = s^E_{11} T_2 + s^E_{12} T_1 + s^E_{13} T_3 + d_{31} E_3 \tag{1.12}$$

$$S_3 = s^E_{13}(T_1 + T_2) + s^E_{33} T_3 + d_{33} E_3 \tag{1.13}$$

If the surface of the film is assumed to be free then T_3 = 0, and equation (1.13) becomes:

$$\left(\frac{S_3}{E_3}\right)_T = d_{33} + \frac{s^E_{33}(T_1 + T_2)}{E_3} \tag{1.14}$$

Since the film is clamped to a substrate, it is not free to expand or contract in the plane, hence:

$$S_1 = S_2 = 0 \tag{1.15}$$

From equations (1.11) and (1.12), with $T_1 = T_2$, it follows that

$$T_1 = T_2 = \frac{-d_{31}}{s^E_{11} + s^E_{12}} E_3 \tag{1.16}$$

Making use of equation (1.16) in (1.14), the expression becomes:

$$d_{33} = d'_{33} + 2\frac{d_{31}s_{13}^{E}}{s_{11}^{E} + s_{12}^{E}} \qquad (1.17)$$

In equation (1.17) d'_{33} is the clamped coefficient which would be measured. The second term represents a correction which should be added to the measured d'_{33} to obtain the true d_{33}.

1.6 Measuring the Piezoelectric Coefficients in Semiconductors

The piezoelectric semiconductors which were the focus of the present work were normally available only in thin film form. Hence the considerations outlined in the previous section were applicable. Two further factors were also of significance when determining the method to be used in measuring their piezoelectric coefficients. Firstly these materials have quite small piezoelectric coefficients (Bernardini et al., 1997), hence any measurement method must be quite sensitive. Secondly the materials have reasonably high conductivity and if the direct effect is used, the movement of free carriers within the sample can screen the piezoelectric field (Arlt, 1965 ; Arlt and Quadflieg, 1968 ; Wan et al., 1995). As a result, although conventional methods have been sometimes used, their application poses some problems.

As a result, it was decided for the present work to use the inverse piezoelectric effect to measure the coefficients, with the strain being measured by optical interferometry.

2

A Michelson Interferometer for Measurement of Piezoelectric Coefficients.

2.1 Introduction

As indicated in chapter 1, the piezoelectric *d* coefficient can be measured by either measuring the electric field generated in response to an applied mechanical strain, or by measuring the mechanical strain produced by an applied electric field. In the latter case, the mechanical movements which must be measured are very small. Optical interferometry provides a technique for doing this and the advent of cheap laser sources in recent years has made this technique increasingly attractive.

Several interferometer configurations have been used to measure field-induced piezoelectric strains (Okamura and Minowa, 1989 ; Royer and Kmetik, 1992 ; Tanaka et al., 1995 ; Wiederick et al., 1995). In the present work, the experimental setup was based on that developed by the group at PennState University (Zhang et al, 1988). The arrangement is essentially a Michelson interferometer, in which one surface of the specimen is used to reflect light,

while the opposite surface is clamped. This setup has been referred to as the *single-beam* interferometer, since light is reflected from only one surface of the specimen. This is in contrast to the dual beam arrangement where light is reflected from both sample surfaces. The dual beam arrangement becomes necessary in situations where the sample is likely to exhibit substantial bending mode vibrations (Pan and Cross, 1989). The single beam arrangement has been applied successfully to the determination of piezoelectric coefficients for Pb-based ferroelectric ceramics (Zhang et al., 1988; Li et al., 1994; Li et al., 1995 ; Kholkin et al., 1996).

The present work makes use of the single-beam Michelson interferometer for the determination of the piezoelectric coefficients of the compound semiconductors GaAs, GaN and AlN. The interferometric technique has a particular advantage for these materials since their piezoelectric activity is relatively small. The interferometer resolution is sufficient to measure piezoelectric coefficients which are less than 10 pmV^{-1} with good accuracy.

The following sections outline the principle of the Michelson interferometer, the setting up of the optical system and associated electronics, the method of measuring the field-induced displacement and the calibration procedure. The effects of spurious mechanical vibrations, noise limitations and the resolution of the interferometer are also discussed. Finally, a method for determining the sign of the piezoelectric coefficient from the interferometer measurements is outlined.

2.2 Principle of the Michelson Interferometer

The Michelson interferometer is probably the best-known of all interferometer arrangements, because of its use in the classic Michelson-Morley experiment. The interferometer consists basically of a beam splitter and

two mirrors. The beam splitter divides the incoming light into two beams which are then reflected from the two mirrors and re-combined at the beam splitter.

The Michelson interferometer produces an interference pattern whose intensity is dependent on the optical path difference between the two beams reflected from the two mirrors. If the path difference for the two beams is Δd, then the intensity I at the centre of the interference pattern, for monochromatic light of wavelength λ, can be written as (Hariharan, 1992):

$$I_1 + I_2 + 2\sqrt{I_1 I_2}\cos\left(\frac{4\pi\Delta d}{\lambda}\right) \qquad (2.1)$$

where the first two terms correspond to the intensity of the individual beams and the last term represents the interference nature of light. This intensity has the maximum and minimum values respectively as:

$$I_{\max} = I_1 + I_2 + 2\sqrt{I_1 I_2} \qquad \text{when } \cos(4\pi\Delta d/\lambda) = 1 \qquad (2.1a)$$

$$I_{\min} = I_1 + I_2 - 2\sqrt{I_1 I_2} \qquad \text{when } \cos(4\pi\Delta d/\lambda) = -1 \qquad (2.1b)$$

Equation (2.1) can thus be rewritten as:

$$I = \frac{1}{2}(I_{\max} + I_{\min}) + \frac{1}{2}(I_{\max} - I_{\min})\cos\left(\frac{4\pi\Delta d}{\lambda}\right) \qquad (2.2)$$

Figure 2.1 gives a graphical representation of equations (2.1) and (2.2).

If one or both of the interferometer mirrors vibrates, then the path difference between the two arms changes. If the amplitude of the vibration is less than a wavelength then, for a given amplitude, the resulting change in intensity depends on the initial path difference. The maximum change in intensity occurs if the initial path difference corresponds to a point where the intensity is mid-way between a maximum and minimum. One such point is labelled X in Fig. 2.1. For such points $\cos(4\pi\Delta d/\lambda) = 0$, and the path diffence Δd can be written as:

$$\Delta d = (2n+1)\frac{\lambda}{8} \tag{2.4}$$

The situation described by equation (2.4) is often referred to as the λ/4 condition.

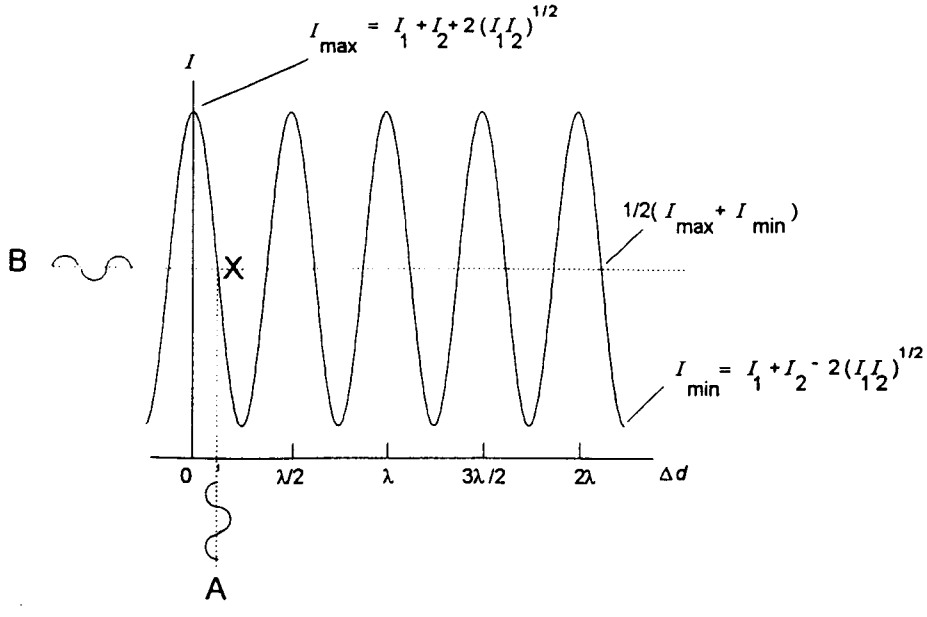

Fig.2.1 The intensity at the centre of the interference pattern of the Michelson interferometer, plotted against path difference. If the resting position correponds to the point X, then a sinusoidal variation in path difference A, produces a variation in intensity B.

2.3 Setting up the Interferometer

2.3.1 Experimental setup

The experimental arrangement of the interferometer used in the present work is shown schematically in Fig.2.2. A polarized He-Ne laser (Uniphase 1135p) is used as a light source. The laser beam is split into two beams; a probe and a reference beam. The probe beam is reflected from the sample, whose surface is made reflective by a metallized coating. The reference beam is reflected from a mirror which can be positioned by a piezoelectric transducer.

A condensing lens, placed before the beam splitter, focuses the beam on the sample surface and reference mirror. The probing and reference beams are recombined by the same beam splitter to form the interference pattern at the detector.

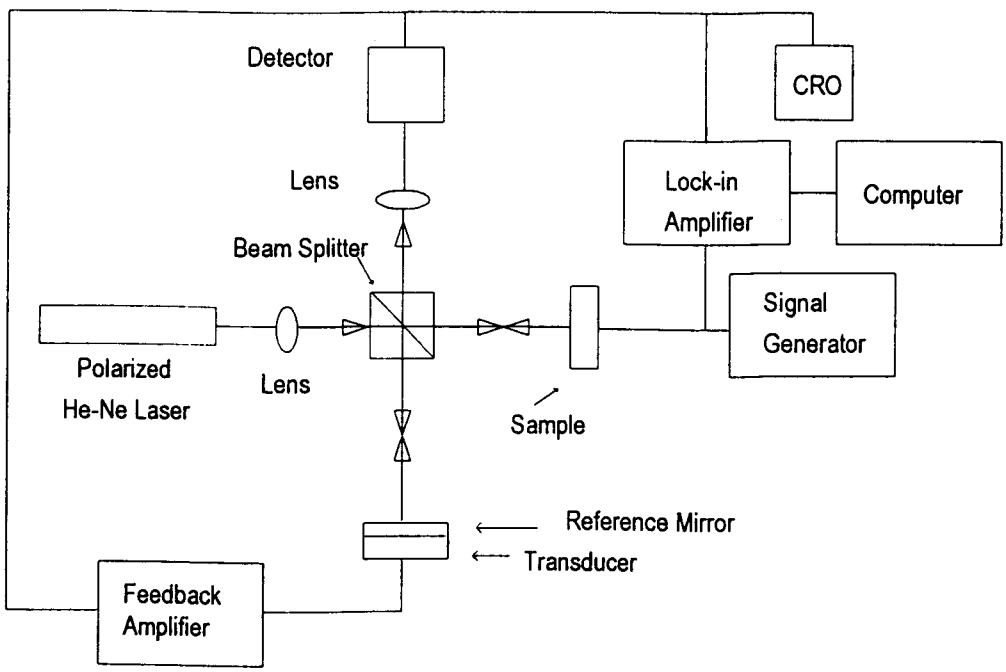

Fig.2.2 Schematic diagram of the Michelson He-Ne laser interferometer.

An AC voltage, of known amplitude and frequency, is applied to the sample using a signal generator (HP 8116A). The resulting piezoelectric strain in the sample produces a small (i.e. $<< \lambda$) displacement of the sample's reflecting surface, which in turn produces a small change in the intensity of the interference pattern. The centre of the interference pattern is adjusted to fall on the aperture of a *pin* photodiode detector (BPX 65). The detector converts the small changes of intensity into an electrical signal.

The output from the detector is measured using a lock-in amplifier (Stanford Research Systems 830). The reference input for the lock-in is driven directly from the signal generator. The lock-in amplifier is a two channel instrument and measures both the amplitude and phase of the detector output voltage. Knowing the output voltage and the driving voltage, the magnitude of the piezoelectric coefficient can be calculated, as described in section 2.4. The method for determining the sign of the measured piezoelectric coefficient is described in section 2.8.

2.3.2 Electronic stabilizer

The type of interferometer shown in Fig.2.2 has been investigated by Kwaaitaal et al (1980), who established theoretical and practical limitations for the setup. Their work indicated that Michelson interferometers can be used to measure vibrational amplitudes down to about 10^{-4} Å. However, in order to achieve this resolution, it is necessary to stabilize the interferometer against slow drifts and external vibrations. This can be done either by means of electronic control systems or by special optical arrangements.

The interferometer used in the present work is electronically stabilized. The reference mirror is mounted on a piezoelectric transducer which is driven by a feedback signal derived from the optical detector. The feedback amplifier also has a DC offset facility, which allows initial positioning of the reference mirror so that the interferometer can be placed in the position correponding to the point X in Fig. 2.1. After this initial positioning, feedback from the optical detector maintains the interferometer operating point at this fixed position in the interference pattern.

In order to measure the detector voltages which correspond to the maxima and minima of the interference pattern, the feedback is removed and

the reference mirror transducer is driven by a low frequency AC signal. As a result the reference mirror moves several wavelengths, resulting in an intensity change corresponding to several fringes. The large changes in intensity produced by this process can be observed on the oscilloscope and a typical oscilloscope trace is shown in Fig.2.3. The peak-to-peak volatge V_{pp} corresponds to the difference between the maximum and minimum intensity of the interference pattern. The cusps at the bottom of the trace in Fig. 2.3 correspond to a reversal in the direction of travel of the reference mirror. In Fig. 2.3 there is a movement of one wavelength of the reference mirror, giving a two fringe shift between reversals. The electronic stabilizer used in the interferometer is capable of moving the reference mirror by several wavelengths.

The mid-point between I_{max} and I_{min} (X in Fig.2.1) represents the desired operating point of the interferometer. To make a measurement, the DC offset in the feedback circuit is adjusted until the quiescent point is fixed at the mid-point of V_{pp}. The sample is then driven by an AC signal and the variation in intensity is measured by the lock-in amplifier.

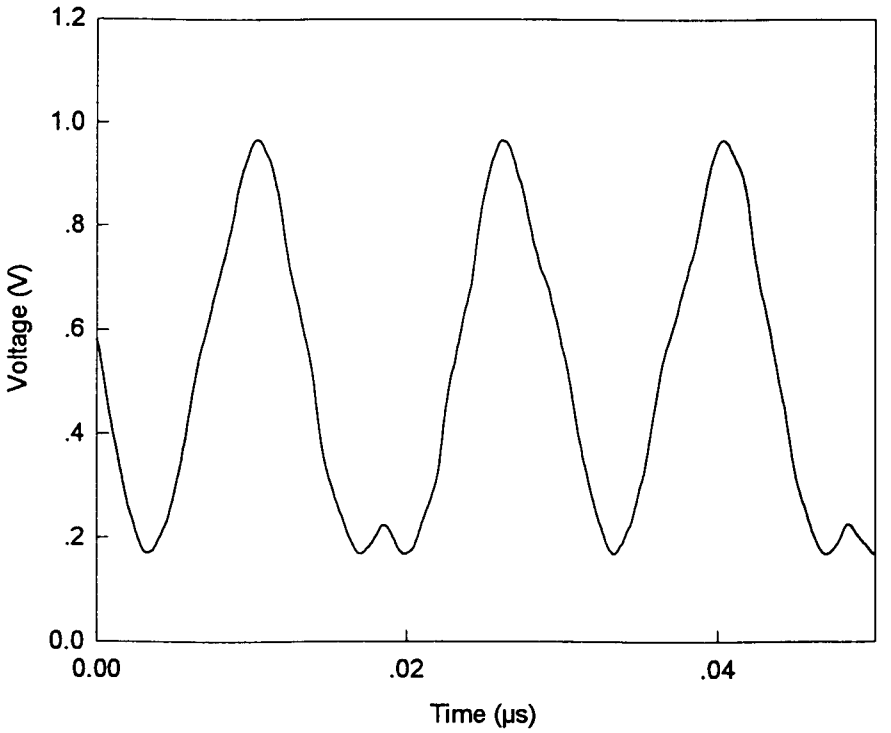

Fig.2.3 Variation of output voltage obtained when the reference mirror transducer is driven by a large AC signal. The peak-to-peak voltage corresponds to the peak-to-peak intensity. The distance of mirror travel in this case was one wavelength. The irregularities at the bottom of each second fringe correspond to the mirror reversing direction.

2.3.3 Drive voltage harmonic content

To ensure that the voltage used to drive the sample was really sinusoidal, the output of the signal generator was fed directly to the lock-in amplifier and the lock-in was set to measure the amplitude of the second harmonic. For all of the conditions used, the second harmonic content was negligible. The presence of second harmonic in the drive voltage is of significance for the electrostriction measurements described in chapter 6.

2.3.4 Detector response

The load resistance for the photodiode detector could be selected to be 10 kΩ, 3.3 kΩ, or 1 kΩ. The output response for each load resistance was measured using the circuit shown in Fig.2.4, with the light source being a red LED driven from the signal generator through a current limiting resistance. When using the 1 kΩ load resistance, a preamplifier (Stanford Research Systems 560) was inserted before the lock-in amplifier.

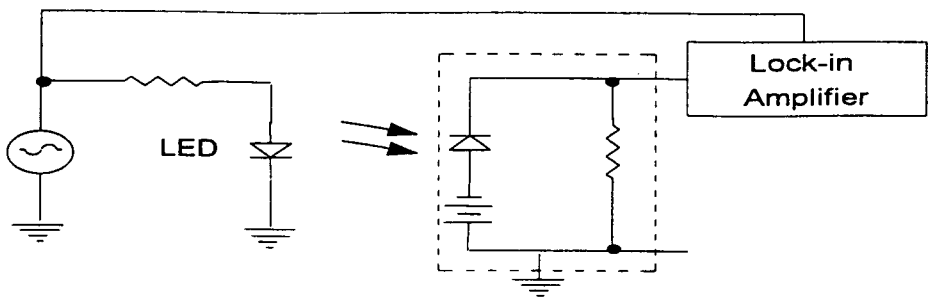

Fig.2.4 Circuit used for checking the frequency and phase responses of the detector. For the lowest load resistance, a preamplifier was inserted before the lock-in amplifier.

Fig.2.5 shows the magnitude and phase of the detector output voltage, as a function of frequency, for the different load resistances. The 10 kΩ resistance gives the highest output, but also has a frequency response which is restricted to 10 kHz. The 1 kΩ load gives the widest frequency response, but also has the lowest output. The phase response also varied with load resistance and frequency. At 1 kHz the load resistance has no observable effect on the phase response. However at higher frequencies the phase changes, with the largest change being associated with the highest load resistance.

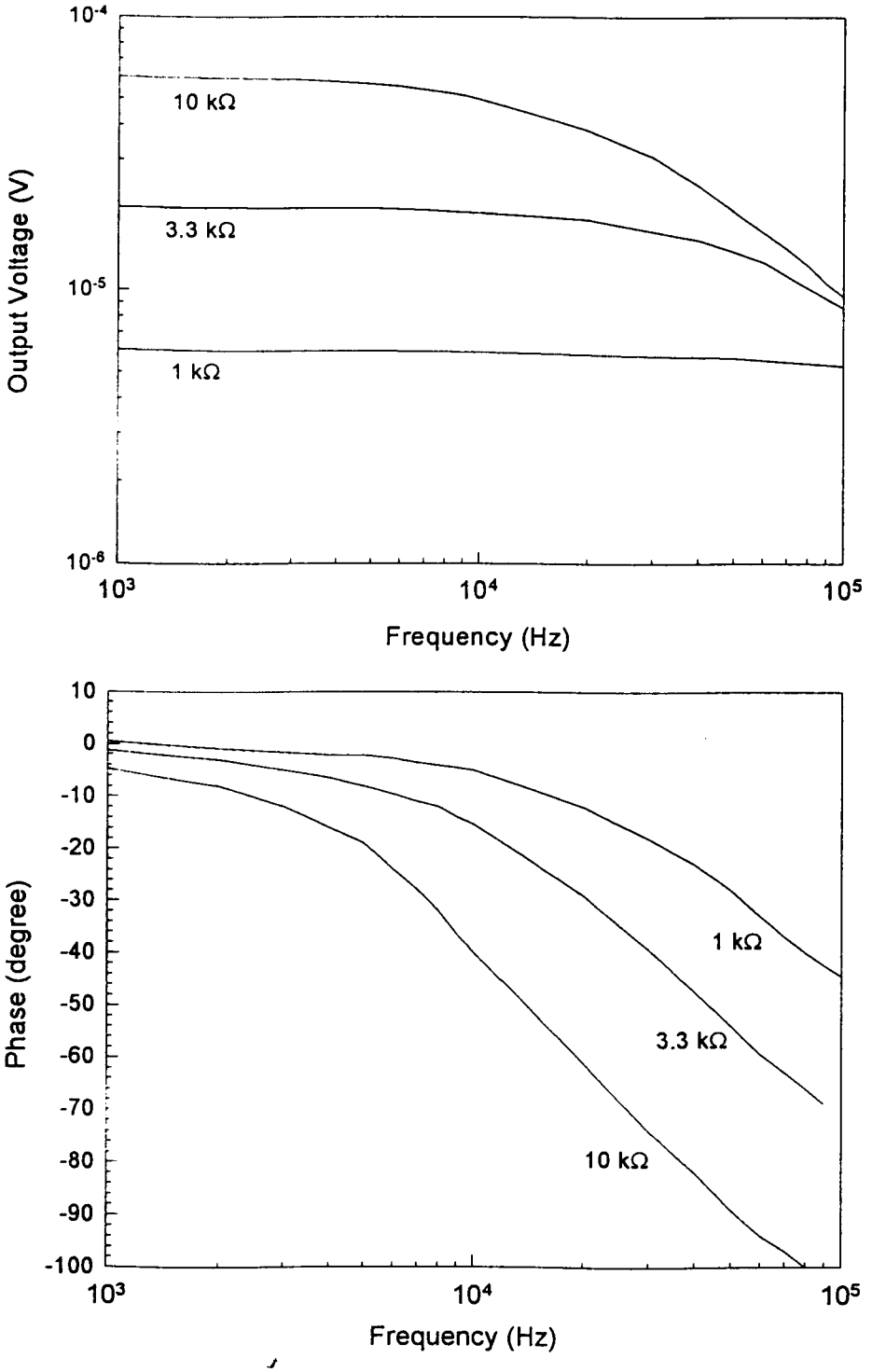

Fig.2.5 Detector output voltage (above) and relative phase (below) for different load resistances, measured using the setup shown in Fig. 2.4

2.4 Measurement of Electric Field Induced Strains

Fig.2.6 illustrates three different types of strain. These are a change in volume with no change in shape (bulk compressional strain), a change in length/thickness (tensile strain), and relative displacement of parallel layers (shear strains). Piezoelectrically induced tensile strains can be measured using the sample configuration illustrated schematically in Fig.2.7.

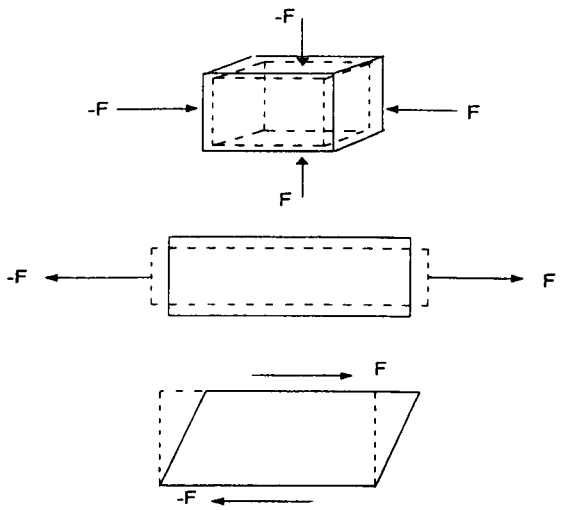

Fig.2.6 Illustration of (a) bulk (b) longitudinal and (c) shear strains.

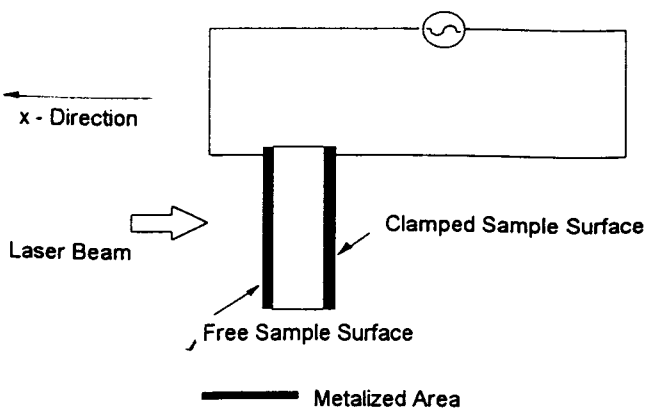

Fig.2.7 Configuration of the thickness excitation of a sample, giving rise to tensile strain.

Fig.2.7 illustrates the point that the free surface of the sample is used for two purposes : to act as an electrode and to reflect the laser beam. This can be done by either putting silver paint on the sample surface and polishing to a mirror surface or by depositing a metal such as aluminium onto the sample surface. The other surface of the sample must also be metalized, in order to act as the second electrode. When the sample is placed in the interferometer, the back surface of the sample is glued to a metal plate which is in turn fixed into a solid translation/rotation stage. The voltage applied between the two electrodes then produces an electric field having a component only in the thickness-direction (the x-direction in Fig.2.7).

If the sample has appropriate piezoelectric coefficients, the electric field in the thickness direction will produce a tensile stress parallel to the direction of the field. It may also generate tensile stresses in the directions perpendicular to the field. This will in turn produce strains in these lateral directions. The clamping of the sample in the lateral direction, by the optical mount, will limit the lateral strains and will also affect the tensile strain in the direction of the field.

For the arrangement shown in Fig.2.7, the measured tensile strain and the electric field have the same direction. Thus the piezoelectric coefficient measured is d_{ii}, where i can have the values 1, 2 or 3. The sample to be measured is usually in the form of a thin plate or film. The value of i corresponds with the particular crystal axis which is prependicular to the plane of the sample. For the quartz sample, discussed in section 2.5, this was the '1' axis, while for the semiconductor materials which are the subject of chapters 3 to 6, it was usually the '3' axis.

From equation (2.4), Δd can be written as : $\Delta d = d_{ac} + (2n+1)\lambda/8$, where d_{ac} is a small displacement of the sample surface, having the form $d_{ac} = d_0 \cos\omega t$. The interference signal at the detector is related to d_{ac} by

$$I = \frac{1}{2}(I_{\max} + I_{\min}) + \frac{1}{2}(I_{\max} - I_{\min})\sin\left(\frac{4\pi d_{ac}}{\lambda}\right) \qquad (2.5)$$

If the displacement is much smaller than the the distance required for a full fringe shift, then the sine function can be replaced by the sine argument, i.e., sin(x) = x. Equation (2.5) then reduces to

$$I = \frac{1}{2}(I_{\max} + I_{\min}) + \frac{1}{2}(I_{\max} - I_{\min})\left(\frac{4\pi d_{ac}}{\lambda}\right) \qquad (2.6)$$

Thus for small displacements, the intensity varies linearly with displacement. The voltage at the detector output, which is measured by the lock-in amplifier as V_{out} is given by

$$V_{out} = \left(\frac{2\pi}{\lambda}\right) V_{pp} d_{ac} \qquad (2.7)$$

where V_{pp} is the peak-to-peak voltage corresponding to the change in intensity caused by movements greater than one fringe shift. There will also be a DC voltage present at the detector output, associated with the first term in equation (2.6). However the lock-in amplifier responds only to AC voltage, so the DC level is not a part of V_{out}. The lockin reading is the rms value of V_{out}, which reflects the rms value of d_{ac}. The piezoelectric coefficient is the ratio of the strain to the field. For the simple geometry used here, this becomes:

$$d_{ii} = \frac{d_{ac}}{V} \qquad (2.8)$$

where V is the rms voltage driving the sample. Combining equations (2.7) and (2.8) gives:

$$d_{ii} = \frac{\lambda V_{out}}{2\pi V_{pp} V} \tag{2.9}$$

Thus the procedure for measuring the piezoelectric coefficient is firstly to apply a large voltage to the reference transducer and note the value of V_{pp}. Then the sample is driven by a known voltage V and the value of V_{out} is noted from the lock-in amplifier.

2.5 Initial System Calibration

The interferometer performance was checked from measurements performed on a sample whose piezoelectric coefficient is well-known. The material used for this purpose was a quartz crystal, since the values of the piezoelectric coefficients for quartz crystals are readily available in the literature. Quartz crystals are commonly available in thin plates with "x-cut" and "y-cut" orientations. The name reflects the crystal axis which is perpendicualr to the thinnest dimension of the crystal plate. The various forms of strain induced by an electric field in x-cut and y-cut quartz, are illustrated in Fig. 2.8.

Initial measurements were performed with an x-cut crystal, with dimensions 4.0x3.8x2.0 mm^3. This sample gave rise to some problems, however the results are reported here, since they illustrate some of the pitfalls to be avoided in the use of the interferometer. The thickness excitation configuration shown in Fig.2.7 was used. Since the field was applied normal to the plane of the x-cut sample, the relevant piezoelectric coefficient is d_{11} (Fig.2.8).

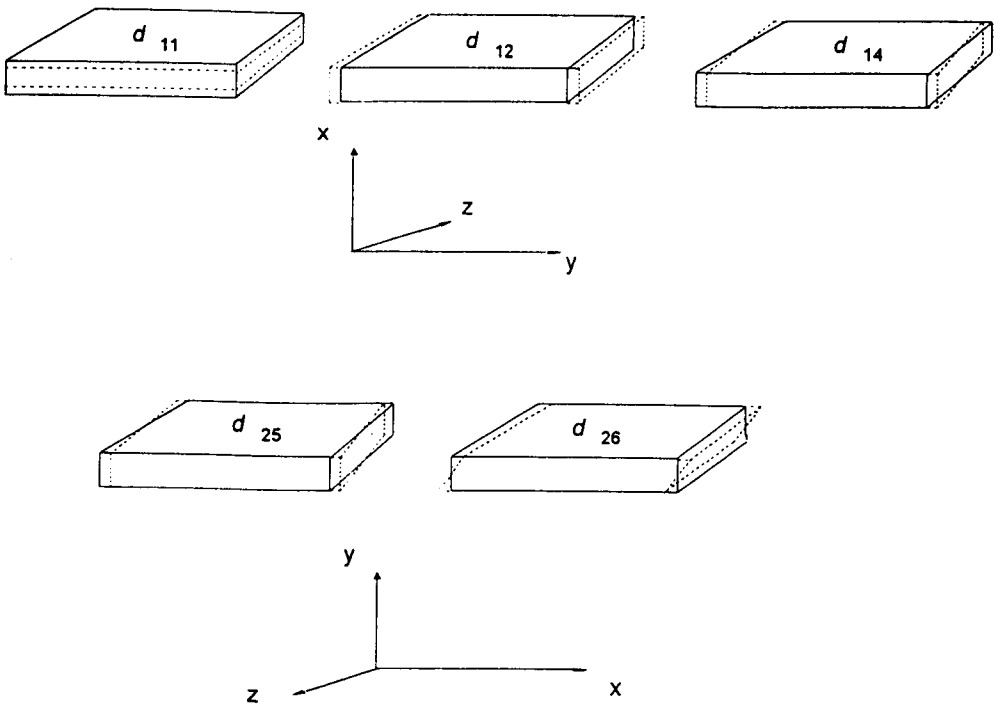

Fig.2.8 Piezoelectric strains in a quartz plate. The plate is assumed to be x-cut quartz in the upper three pictures and y-cut quartz in the lower two. The electric field is always perpendicular to the plane of the plate. In each case the particular piezoelectric coefficient involved is shown. (after Kuttruff, 1991). The d_{11} mode in x-cut quartz was used for calibration purposes.

The opposite surfaces of the sample were metallized by evaporating aluminium onto the sample using an Edwards Coating System E306A. The back surface of the sample was then bonded to an aluminium plate with conducting glue. The aluminium plate was used as one electrical contact to the sample. A 50 μm diameter gold wire, bonded with conducting glue to the top electrode, formed the other electrical contact. The use of a fine bonding wire helped to prevent the transfer of mechanical vibrations from the signal generator cable to the sample. The aluminium plate, with the sample, was attached to the optical mount in the interferometer.

The quartz sample was driven at a frequency 1 kHz, with a voltage whose amplitude was varied from 1 V to 16 V. Mechanical displacement in the sample was measured from the variation in intensity at the centre of the interference pattern. The displacement was found to vary linearly with driving voltage, as shown in Fig.2.9. The slope of the displacement versus voltage plot gave a value for the d_{11} coefficient of quartz of 2.34 pmV^{-1}. This value is within 2% of the literature value of 2.31 pmV^{-1} (Landolt-Börnstein, 1979). The variation of displacement with voltage for this sample was also measured at other frequencies. From 1 kHz to 4 kHz the mechanical displacement varied linearly with driving voltage. At frequencies above 4 kHz the readings became very unstable and it was not possible to obtain reliable measurements of displacement.

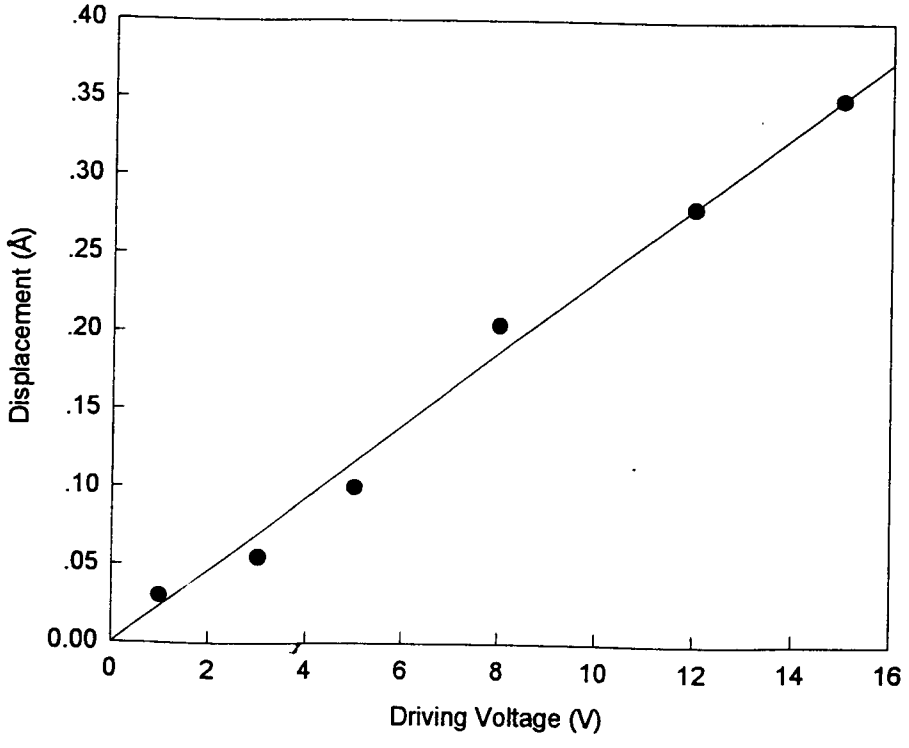

Fig.2.9 Variation in displacement with driving voltage, measured at 2 kHz, for a 4.0x3.8x2.0 mm^3 x-cut quartz plate.

The origins of the unreliability of the interferometer system, uncovered in the initial calibration runs, arose largely from mechanical resonances in the system. The way in which these effects were overcome is described in section 2.6.

2.6 Effects of Resonance

Low frequency resonances in the interferometer system were not unique to this project, similar effects were observed by Zhang et al (1988). The main origins of resonances observed in the present work were found to arise from mechanically induced vibrations of many of the optical components in the interferometer. It was found possible to greatly reduce resonance effects by careful attention to the design of the optical components. In particular, components were mounted on short, thick posts and the length of the optical paths were made as short as possible. Brass has a higher stiffness and density than aluminium, so a 5 mm thick brass plate was used to replace the original aluminium sample mounting plate. Care was taken to make the translation stage, on which the sample was mounted, as rigid as possible.

While these procedures were succesful in greatly reducing resonance effects, some resonances were found to originate from the form of the sample. Li et al. (1995) found that clamping and warping effects arising from the sample could be reduced by cutting samples which were nearly cubic in shape. Thus a second quartz sample, with dimensions 2.2x2.4x2.0 mm^3 was prepared and used to check the calibration. The electrodes and electrical contacts were as described in section 2.5. The results obtained from this sample, at a frequency of 1kHz, are shown in Fig.2.10a. Linearity of the piezoelectric response was observed for driving fields from 0.1 kVm^{-1} to 8.0 kVm^{-1}. Measurements at other frequencies were made, in order to check for the presence of resonance

effects. The measured d_{11}, plotted as a function of frequency from 1kHz to 100 kHz, was as shown in Fig.2.10b.

The resonances at low frequency were no longer observed. The effects of resonance in the region above 50 kHz were still evident and these are almost certainly associated with the sample itself and its mounting method. The mean d_{11} value for the 1-100 kHz frequency range was found to be 2.28 pmV^{-1}. The measured d_{11} was scattered from the mean value by less than 10%. The d_{11} coefficient measured in the 1kHz to 10 kHz range was found to be (2.30 ± 0.04) pmV^{-1}. In this range, the value was never more than 3% from the accepted value of 2.31 pmV^{-1} (Landolt-Börnstein, 1979). This frequency range was therefore used for most of the measurements reported in other chapters in this work.

(a)

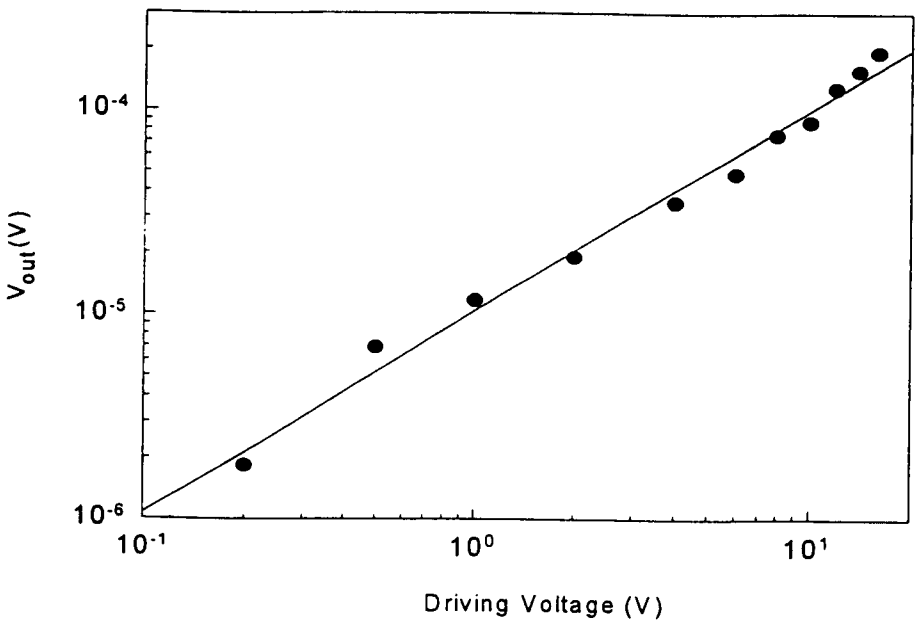

(b)

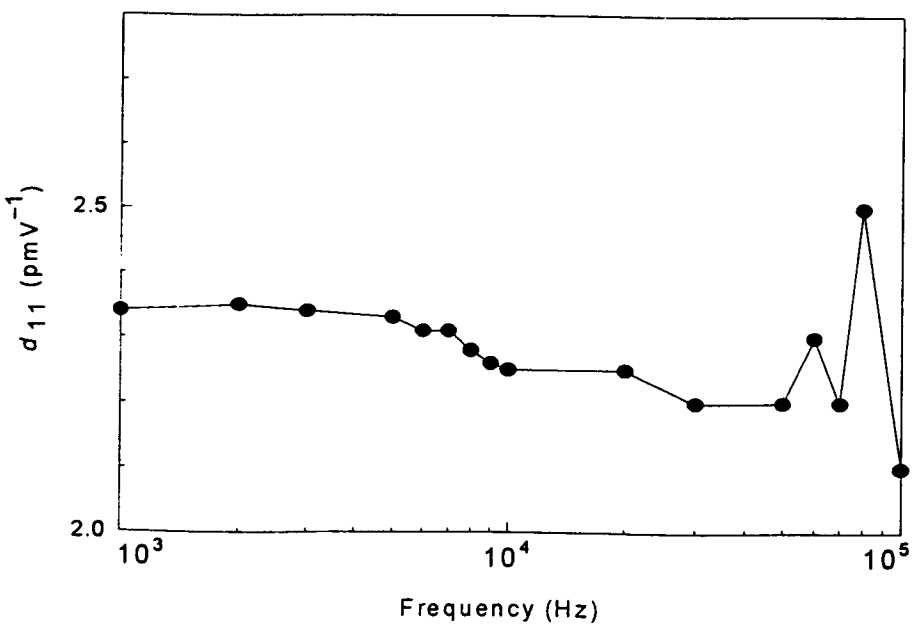

Fig.2.10 A plot of (a) detector voltage vs driving voltage at 1 kHz, and (b) the d_{11} value vs frequency for a quartz sample of dimensions 2.2x2.4x2.0 mm^3.

2.7 Noise Limitation and Interferometer Resolution

Kwaaitaal et al. (1980) have performed an extensive analysis of the noise limitations of both optically stablized and electronically stabilized Michelson interferometers. Their approach has been used as the basis of the noise analysis in the following sections.

Several noise sources contribute to the overall noise level in the interferometer. These include detector noise, electrical noise in the electronics, laser noise, mechanical noise and thermal effects. It is possible to predict noise figures for three noise sources :

(a) Detector noise: calculated mainly from shot noise and Johnson noise.

(b) Electrical noise: arising from the lock-in amplifier and the preamplifier, obtained from manufacturers' data.

(c) Laser noise: also obtained from data provided by the manufacturer.

Mechanical noise and thermal effects arise from the local environment and cannot be predicted. Since the final total noise figure can be measured, it is possible to deduce the relative importance of the various noise sources mentioned above.

2.7.1 Theoretical noise level

In the interference pattern the light incident at the detector causes an electrical current to flow in an external circuit. The photodiode current contains basically two components : the signal component which is coherent with the incident light variations, and the noise component which is not. The noise current in the detector was calculated based on the assumption that it consisted of shot noise and Johnson noise.

Shot noise is caused by the non-uniformity in the DC current flow in the photodiode. The shot noise current i_n , is given by

$$i_n = (2qI\Delta f)^{1/2} \tag{2.10}$$

where q is the electron charge (1.6×10^{-19} C), I the DC current and Δf the bandwidth of the measuring system. The DC current can be deduced from the measured DC voltage drop across the load resistance. The measurement bandwidth is determined by the time constant and filter slope of the lock-in amplifier. For the settings normally used here, the bandwidth was 0.0125 Hz. This gives a shot noise figure of 1.6 nV for the 1 kΩ load resistance.

Johnson noise arises from thermal fluctuations in the electron density within a resistor and is given by

$$V_n = (4kTR\Delta f)^{1/2} \tag{2.11}$$

where k is Boltzmann constant (1.38×10^{-23} JK^{-1}), T the temperature (typically 300° K), and R the resistance in ohms. The Johnson noise voltage generated across the 1 kΩ detector load resistance was calculated to be about 0.4 nV.

Amplifier noise was calculated by including the input noise in the lock-in amplifier and the low-noise preamplifier. In the lockin detection input signals of frequency f_{sig} within the detection bandwidth appear at the output at the frequency $f = f_{sig} - f_{ref}$, where f_{ref} is the reference frequency. Input noise near the reference frequency will appear as noise at the output. The input noise in the SR830 lock-in amplifier has a typical value of 0.7 nV for 0.0125 Hz bandwidth. For the same bandwidth, the input noise in the SR560 preamplifier in the low-noise gain mode has a value of 0.5 nV.

The laser contribution to the total noise comes from instability in the output amplitude of the laser. Manufacturer's specifications for the single-mode Uniphase 1135p He-Ne laser, indicate a maximum of 1% amplitude fluctuations

for a bandwidth from 30 Hz to 10 MHz. Assuming that this noise is reasonably uniform across the bandwidth, the relative noise in the laser for the 0.0125 Hz bandwidth of the lockin amplifier would be 3.5×10^{-7}. This follows from the fact that the noise voltage varies as the square root of the bandwidth. Referring to Fig. 2.3, it can be seen that a typical value of the quiescent output voltage is 0.6 V. This voltage will have a fractional fluctuation equal to the fractional fluctuation in laser intensity. Thus the noise voltage at the interferometer detector, arising from the laser fluctuations, would be expected to have a value of about 0.2 μ V.

The total noise is the square root of the sum of the squares of the various noise sources. It can be seen that the laser noise will dominate all of the other predictable noise sources and thus the total noise from these sources will be around 0.2 μV for a bandwidth of 0.0125 Hz. This figure represents the minimum noise level achievable for the interferometer, given the components used in its assembly.

2.7.2 Signal-to-noise ratio and theoretical detection limit

The path difference Δd between the two arms of the interferometer can be considered to be a steady component X, which is determined by the initial setting of the interferometer, plus the piezoelectric displacement x. Equation (2.2) can thus be written as:

$$I = \frac{1}{2}(I_{\max} + I_{\min}) + \frac{1}{2}(I_{\max} - I_{\min})\cos\left(\frac{4\pi(X+x)}{\lambda}\right) \qquad (2.12)$$

and this can be rearranged to give:

$$I = I_{DC} + (I_{DC} - I_{\min})\left(\sin\frac{4\pi X}{\lambda}\cos\frac{4\pi x}{\lambda} + \cos\frac{4\pi X}{\lambda}\sin\frac{4\pi x}{\lambda}\right) \qquad (2.13)$$

where I_{DC} is the intensity midway between I_{max} and I_{min}. If x << λ then equation (2.13) can be further simplified to:

$$I = I_{DC} + (I_{DC} - I_{\min})\left(\sin\frac{4\pi X}{\lambda} + \frac{4\pi x}{\lambda}\cos\frac{4\pi X}{\lambda}\right) \tag{2.14}$$

Since the photodiode current is proportional to the intensity, equation (2.14) can be expressed in terms of the photodiode current:

$$i = P\left[I_{DC} + (I_{DC} - I_{\min})\left(\sin\frac{4\pi X}{\lambda} + \frac{4\pi x}{\lambda}\cos\frac{4\pi X}{\lambda}\right)\right] \tag{2.15}$$

where P is a constant of proportionality which depends on the photodiode characteristics. Since the quantity x in equation (2.15) represents the mechanical signal, the current can be separated into two components; a steady DC component:

$$i_{DC} = P\left[I_{DC} + (I_{DC} - I_{\min})\left(\sin\frac{4\pi X}{\lambda}\right)\right] \tag{2.16}$$

and a signal component

$$i_{sig} = P\left[(I_{DC} - I_{\min})\left(\frac{4\pi x}{\lambda}\right)\left(\cos\frac{4\pi X}{\lambda}\right)\right] \tag{2.17}$$

The steady state current given by equation (2.16) will be very much larger than the signal current, hence the noise in the output will be predominantly the noise in the steady state component. From the discussion in section 2.7.1, it is apparent that this noise will be mainly determined by laser noise and thus will be 3.5×10^{-7} of the current. The signal-to-noise ratio (SNR) for the interferometer will thus be given by:

$$SNR = \frac{P\left[(I_{DC} - I_{\min})\left(\frac{4\pi x}{\lambda}\right)\left(\cos\frac{4\pi X}{\lambda}\right)\right]}{3.5\times10^{-7}P\left[I_{DC} + (I_{DC} - I_{\min})\left(\sin\frac{4\pi X}{\lambda}\right)\right]} \tag{2.18}$$

Equation 2.18 is useful for seeing how the various factors interact to determine the signal-to-noise ratio. The usual operating point is when X is an odd-integral number of λ/8 and for such points, the SNR will be a maximum for a given fringe contrast. For these points, the SNR becomes simply:

$$SNR = \frac{(I_{DC} - I_{\min})\left(\frac{4\pi x}{\lambda}\right)}{3.5 \times 10^{-7} I_{DC}} \qquad (2.19)$$

Figure 2.3 indicates that the quantity $(I_{DC}-I_{min})/I_{DC}$ will have a typical value of 0.75. For a laser of wavelength 632.8 nm this gives the-signal-to-noise ratio of $4.25 \times 10^{13} x$. Hence the signal-to-noise ratio of 1 would be obtained if x was of the order of 10^{-14} m. This figure represents a measure of the ultimate resolution available for the interferometer used in this work. As indicated in section 2.7.1, this figure is mainly limited by the laser noise. In the work of Kwaaitaal et al. (1980), the signal-to-noise ratio was calculated, assuming that shot noise in the detector was the main noise source. The detection limit of the interferometer was deduced, based on this assumption. The calculations of section 2.7.1 indicate that amplitude fluctuation in the laser would be the major contributor to the calculable noise sources in the current interferometer, a similar resolution limit of 10^{-14} m was obtained.

2.7.3 Noise measurement

The calculations in sections 2.7.1 and 2.7.2 give a noise figure based on factors which are predictable. However the final noise level in the interferometer also depends on environmental factors such as building vibrations and thermal effects and these are not predictable.

In order to assess the total noise level in the interferometer, noise measurements were carried out using the lock-in amplifier. These

measurements were made at times when building noise was at a minimum (usually in the evenings). The Stanford SR850 lock-in amplifier has a useful feature which allows it to display the noise level present in the signals being fed into it. With a sample mounted in the interferometer, but with no drive voltage connected, the lock-in was set to display the noise signal. The resultant noise, plotted as a function of frequency, is shown in Fig.2.11. The minimum noise level of 0.2 μV, calculated in section 2.7.1, is also included in this figure.

The noise spectrum includes a variety of noise sources that can be of electrical, thermal, or mechanical origin. At frequencies below 1 kHz the noise rises rapidly as the frequency decreases. The noise in this frequency range is probably due to building noise and reaches fairly high levels despite the effects of the feed back arrangement. At frequencies above 10 kHz the level of external noise sources are reduced and the total noise level drops towards the limiting figure calculated in section 2.7.1.

Based on the noise behaviour shown in Fig. 2.11, it might be expected that frequencies above 10 kHz would give the best measurements of piezoelectric coefficients. Unfortunately in this region, the bending modes, mentioned in section 2.6, become a problem. The best compromise was to use frequencies from 1 kHz and 10 kHz. In this range the noise level, for the usual lockin configuration, was approximately 4 μV. For the signal-to-noise ratio of 1, this gives a resolution of 5×10^{-14} m. More realistically, if it was desired to measure displacements with a noise level of 10% or less, then displacements greater than 5×10^{-13} m would be required.

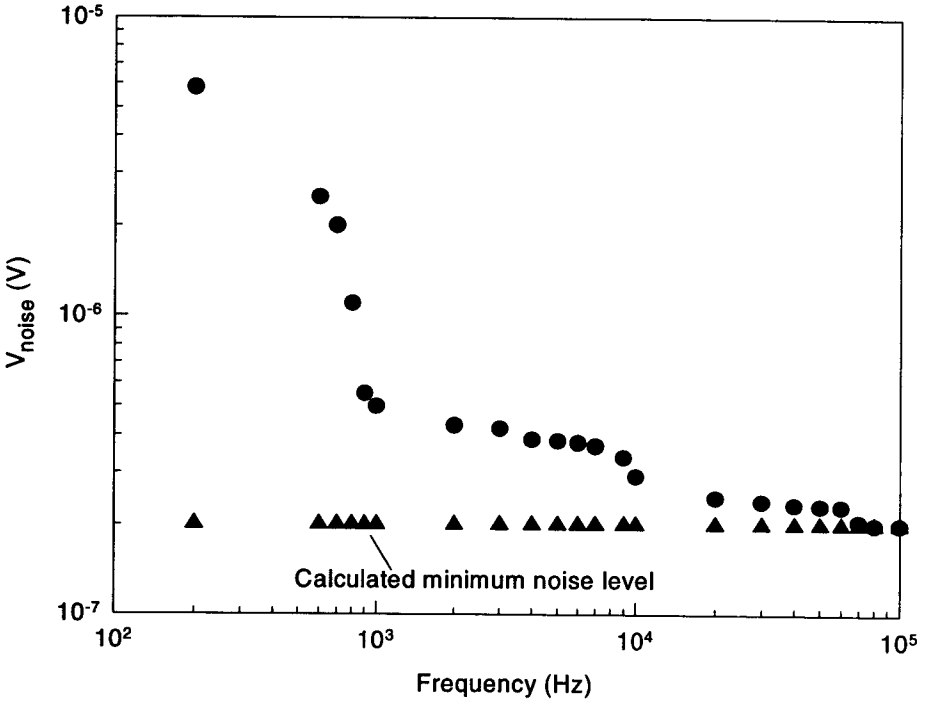

Fig.2.11 Measured noise spectrum and the calculated minimum noise level for the interferometer.

2.7.4 Interferometer resolution

The sensitivity of the interferometer was checked experimentally. Measurements on the 2.2x2.4x2.0 mm^3 quartz sample were made to deduce the interferometer resolution over the frequency range from 1 kHz to 100 kHz. Voltages of 0.1, 0.2 and 1.0 V were used to drive the sample. Fig.2.12 shows the output voltage obtained in each case.

The SNR was obtained directly from the ratio of the output voltage in Fig.2.12 to the noise voltage shown in Fig.2.11. At 1 kHz, if the output voltage from noise measurement, which is about 0.5 μV, is compared with the output voltage at the driving voltage of 0.1 V, 0.2 , and 1.0 V, the values of SNR ≈ 3, SNR ≈ 7 and SNR ≈ 20 were obtained respectively.

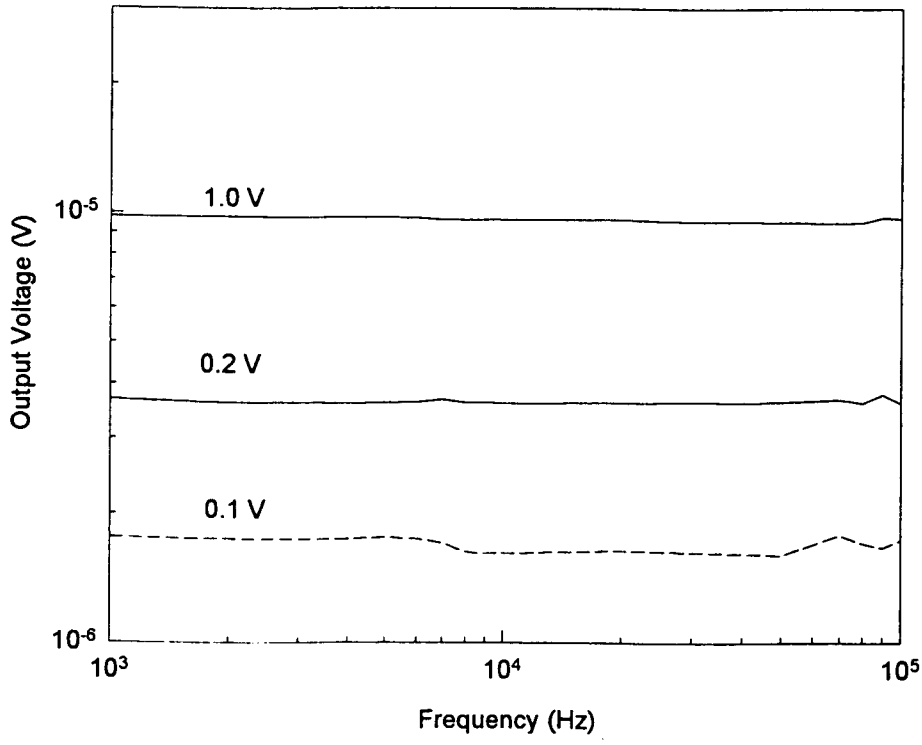

Fig.2.12 Frequency dependence of the output voltage in the quartz sample measured at the driving voltages of 0.1, 0.2 and 1.0 V.

2.8 Determination of the Piezoelectric Coefficient Sign

The convention for assigning a sign to the piezoelectric coefficient is specified in the IEEE Standard on piezoelectricity (1988, p23). Firstly it is necessary to define the positive direction of the crystal axes. A piezoelectric coefficient is taken to be positive when a positive charge is induced in the positive direction of the axis under a positive (extensional) stress. For the inverse piezoelectric effect, which is what is measured in this work, the coefficient is positive when an applied electric field pointing along the positive direction of the crystal axis, produces a positive strain (i.e. an increase in dimension along the axis).

The present work has developed a means for determining the sign of the measured piezoelectric coefficients from the interferometer output. The technique relies on the fact that when feedback is used in the interferometer, then not all interferometer conditions are stable. Referring to Fig. 2.1, it may be thought that the point X could be arranged to fall at the mid-point of either the positive or negative slope of the fringes. However when the feedback is connected, as shown in Fig. 2.2, one of these points becomes unstable. Which of the two slopes is unstable is determined by the phase of the feedback and the stable point can be moved from the positive slope to the negative slope, or vice versa, simply by reversing the leads to the feedback amplifier. Once the connections have been made, then an increase in path length in the sample arm will always produce an intensity change of the same polarity - either an increase or a decrease. This in turn means that, provided the feedback leads are not changed, it is possible to tell from the phase of the detector output voltage, the direction of travel of the sample surface.

In practice, it is only necessary to place in the interferometer a sample for which the sign of the piezoelectric coefficient and the direction of the crystal axes are known. The phase of the output produced by this sample is noted. All subsequent samples will produce output with either the same phase, or a phase shifted by 180°. Provided that the direction of the crystal axis in the sample is known, the sign of the coefficeint can be deduced. Alternatively, if the sign of the coefficient is known the phase can be used to determine the direction of the crystal axes in the sample.

The material used for the reference sample was the ferroelectric polymer, poly(vinylidene fluoride) (PVDF). The sign of the piezoelectric coefficient d_{33} for PVDF is known to be negative (Nalwa, 1995, p210). The

reason for using PVDF was that the direction of the '3' axis is determined by poling the sample and is thus known unambiguously.

The technique was confirmed by checking the known sign of the quartz calibration sample.

2.9 Conclusions

The interferometric technique is a useful technique for measuring piezoelectric coefficients, especially in materials where the coefficients are less than 10 pmV^{-1}. Both the magnitude and sign of the coefficient can be determined. Measurements of mechanical displacements with a resolution of around 10^{-3} Å are readily achieved without recourse to highly sophisticated vibration isolation systems. A calibration check using quartz indicated that the interferometer could easily achieve a basic accuracy of better than ±3% for a *d* coefficient of the order of 10^{-12} mV^{-1}. Limitations in the measurement arise mainly from external mechanical vibrations, although the effects of these can be minimised by careful design of the mounting of the optical components and the sample.

3

The Piezoelectric Coefficient of Gallium Arsenide

3.1 Introduction

Gallium arsenide (GaAs) is an important III-V semiconductor for which a number of material parameters have been measured. Reviews by Blakemore (1982) and Adachi (1985) provide a summary of these measurements, although only in Adachi's review have the piezoelectric properties been mentioned, with citations dating back to the 1960's.

As indicated in chapter 1, piezoelectric effects can exert a significant influence on zincblende semiconductor properties. Interest in the application of the piezoelectric properties of GaAs was stimulated by the theoretical work of Smith (1986, 1988). This work predicted that large strain-induced electric fields could be generated in strained layers grown on the (111) plane. The significance of this particular crystal direction is discussed in section 3.4. These strain-induced electric fields are capable of causing changes in the electronic band structure and hence in the optical properties of the

structures. As a consequence, a number of researchers have investigated the effects of the strain-induced field in strained-layer heterostructures grown on polar substrates of GaAs, such as [111] A, [111] B and [111] B-misoriented substrates (Grey et al., 1995 ; David, et al., 1994 ; Caridi et al., 1990 ; Sánchez-Rojas et al., 1994 ; Harken et al., 1995).

The piezoelectric fields in zincblende semiconductors grown in the [111] direction have been used to modify the operating characteristics of devices fabricated from these materials. For example a bistable switching, in the absence of external bias, of a self-electrooptic device composed of InGaAs/GaAs systems grown on [111]B GaAs (Pabla et al., 1994), a voltage threshold shift in a field-effect transistor containing nominally undoped GaAs grown on a [111] GaAs substrate (Kuech et al., 1990). Details of the work on strained layer piezoelectric devices and their performance improvement have recently been reviewed (Smith, 1997 ; Rees, 1997).

3.2 Review of Previous Work

There appear to be very few reports of measurements of the piezoelectric coefficients of GaAs in the literature, and those that do exist date back mainly to the 1960's. This fact formed an additional impetus for the measurements reported here.

Results from previous determinations of the values of the piezoelectric coefficient of GaAs are summarized in table 3.1. Values of the piezoelectric coefficients *d*, *e*, and *g* have been reported. The definitions of these coefficients are given in chapter 1. Only the *d* coefficient was measured in the present work.

GaAs belongs to the cubic point group $\bar{4}3m$. The piezoelectric tensor for this point group, written in the reduced Voigt notation, has the form:

$$\begin{pmatrix} 0 & 0 & 0 & d_{14} & 0 & 0 \\ 0 & 0 & 0 & 0 & d_{14} & 0 \\ 0 & 0 & 0 & 0 & 0 & d_{14} \end{pmatrix}$$

For the $\bar{4}3m$ group, d_{14} is readily obtained from e_{14} or g_{14} using the simple relations $d_{14} = s_{44}^{E} e_{14}$ or $d_{14} = \varepsilon_{11}^{T} g_{44}$. In order to aid comparisons, values of e_{14} and g_{14} have been converted to an equivalent d_{14} in table 3.1. This has been done using figures of 1.68×10^{-11} m^2N^{-1} for s_{44}^{E} and 13.18 for the relative permittivity.

The earliest reported measurement of the piezoelectric coefficients of GaAs were carried out by Hutson and White (1962), the values were obtained from measurements of wave velocities. Zerbst and Boroffka (1963) and Charlson and Mott (1963) measured the piezoelectric coefficients using the resonance method. One of the problems which arises with GaAs is its relatively high electrical conductivity. This creates a difficulty when attempting to measure the piezoelectric coefficient directly, since stress-induced fields are cancelled by charge migration within the material. Hambleton (1965), avoided this difficulty by measuring the charge generated by a static load at 77 K. The low temperature increased the dielectric time constant to a point where measurements could be made.

Table 3.1 gives the values of the piezoelectric coefficients of GaAs as reported in the literature. An interesting point emerges from these early reports. The first three references in table 3.1 give the coefficient as being positive. In fact the methods used (wave velocities and resonance) would not give the sign of the coefficient; presumably this was simply assumed to be positive. In the static measurement of Hambleton, the sign of the coefficient affects the polarity of the measured charge. Hambleton appears to have assumed that the coefficient was positive and was thus lead to postulate that

the Ga atoms must have negative charge while the arsenic atoms were positive. This observation is in contrast to the x-ray intensity measurement on GaAs (Kröger, 1965). From this measurement, the difference in electro-negativity of Ga and As has been deduced to result in ionic bonding with positive Ga atoms and negative As atoms. Subsequent work has shown that almost certainly the gallium atoms are positive and that the piezoelectric coefficient is negative.

Table 3.1 Values of the piezoelectric coefficient of GaAs as reported in the literature. For cases where the *g* or *e* value has been reported, the values have been converted to *d* for comparison. The *d* values are shown in brackets, in units of pmV^{-1}.

Reference	Value	Method/Theory
Experimental Determinations		
Hutson and White (1962)	$e_{14} = 0.12\ Cm^{-2}$ (2.02)	Plane-Wave Velocities
Zerbst and Boroffka (1963)	$g_{14} = 1.37 \times 10^{-2}\ m^2C^{-1}$ (1.60)	Resonance Method
Charlson and Mott (1963)	$d_{14} = 2.60 \times 10^{-12}\ CN^{-1}$	Resonance Method
Hambleton (1965)	$d_{14} = 2.63 \times 10^{-12}\ CN^{-1}$	Static Compression Method
Arlt and Quadflieg (1968)	$e_{14} = -0.16\ Cm^{-2}$ (2.69)	Piezoelectric Hall Effect
Theoretical Predictions		
McKitterick (1983)	$e_{14} = -0.14\ Cm^{-2}$ (2.35)	Density-functional Theory
Gironcoli et al.(1989)	$e_{14} = -0.10\ Cm^{-2}$ (1.68)	Linear-Response Theory

Arlt and Quadflieg (1968) used an ingenious method to overcome the problems of high conductivity. They vibrated a sample in a magnetic field. Piezoelectric fields were generated by the stresses caused by the vibrations. These fields gave rise to compensating currents, which were measured by the Hall effect. Thus the piezoelectric coefficient was deduced, not from the field itself, but by the charge compensation currents which resulted. In addition they were able to deduce the sign of the coefficient from the phase of the currents, and give it correctly as being negative.

Theoretical calculations of piezoelectric coefficients from crystal structure are difficult. There have been two attempts to calculate the value of the piezoelectric coefficient of GaAs. McKitterick (1983) has predicted the e_{14} value of GaAs from first-principles using a density-functional calculation. In this work, the e_{14} value was calculated from the charge density induced by the displacement of individual atoms. The calculations of the total induced charge density was made at several finite wave vectors of the phonon, and then extrapolated to the limit of zero wave vector. From the extrapolation, the e_{14} value obtained is in good agreement both in magnitude and sign with the work of Arlt and Quadflieg (1968).

By contrast, Gironcoli et al. (1989) have calculated the piezoelectric coefficients of several III-V semiconductors by calculating the stress induced by an electric field at zero strain (i.e. assuming no atomic displacement). The stress was assumed to vary linearly with the field. From this approach a negative e_{14}, with smaller magnitude than that of McKitterick (1983) was reported.

It is also interesting to note that experiments with GaAs performed previously have mostly made use of the direct piezoelectric effect, which can be unreliable, especially in materials of relatively high conductivity (Mason

and Jaffe, 1954). In these materials the piezoelectric polarization is effectively screened off by free carriers (Arlt, 1965 ; Arlt and Quadflieg, 1968).

Overall, it seems fairly certain that the piezoelectric coefficient of GaAs is negative. The present work, using the interferometric technique, actually measures the inverse piezoelectric effect. Thus the results obtained for GaAs have several points of interest. Firstly as a check of the magnitude and sign of the coefficient itself and secondly to see if the direct and inverse effects do have the same coefficient. Although thermodynamics predicts that the direct and inverse coefficients should be equal, it is possible that the measured values may differ in materials where the electrode area does not remain constant during the measurement (Anderson and Kepler, 1981).

3.3 Crystal Structure and [111] Plane

GaAs has the cubic zincblende (ZB) lattice with a symmetry $\bar{4}3m$. This group is probably the simplest structure which shows piezoelectricity. Fig.3.1a shows the conventional unit cell containing four GaAs molecules. The four nearest neighbours of each atom in the lattice are of the opposite type (Ga has four As neighbours and As has four Ga neighbours). The nearest neighbours form a tetrahedron, with tetrahedral directions [111], $[1\bar{1}\bar{1}]$, $[\bar{1}\bar{1}1]$, and $[\bar{1}1\bar{1}]$.

In general, the induced electric field will have both longitudinal and transverse components. However for material grown with the [111] growth axis, the strain-induced electric fields are in the [111] direction, while for material with the [110] growth axis the strain-induced electric field is transverse (Smith, 1988; Caridi et al., 1990). This means that the piezoelectric coefficient, referred to the conventional cubic crystal axes in

GaAs, can be obtained from either a shear strain exited by a field in a [110] direction or a thickness expansion excited by a field in the [111] direction (Mason, 1964, p174).

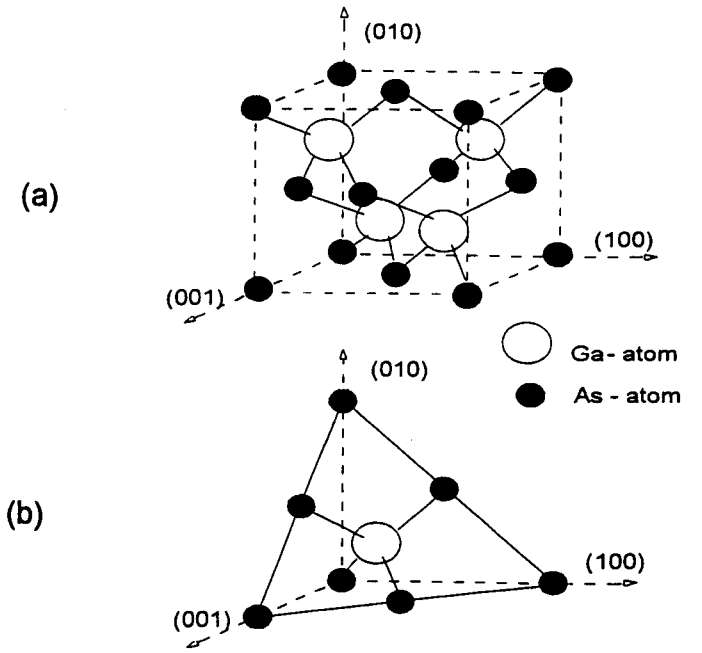

Fig.3.1 (a) Conventional unit cell for GaAs. (b) Truncation of the GaAs unit cell by the [111] plane. (After Blakemore, 1982).

Fig.3.1b shows the GaAs structure truncated on a (111) plane. It can be seen that the surface of a crystal, grown in the [111] direction, will have surfaces containing all Ga atoms or all As atoms. The convention is to label the (111) surfaces of GaAs crystals as either A (Ga atoms) or B (As atoms). The identification of the A and B surfaces of a (111) crystal is important if the sign of the piezoelectric coefficient is to be ascertained. Commercial GaAs wafers are described as [111]A or [111]B depending on which surface has been prepared for subsequent processing. In the work of Arlt and Quadflieg

(1968), both the magnitude and sign of the e_{14} coefficient were determined by piezoelectric Hall effect measurement made on the [111]A GaAs. The sign of the piezoelectric polarization charges on the A-face were found to be negative when the crystal expanded in [111] direction. It was this observation which lead Arlt and Quadflieg to the conclusion that e_{14} was negative.

3.4 Crystal Symmetry and the Piezoelectric Tensor

Since the length, width, and thickness of a [111] B GaAs sample do not coincide with the conventional crystallographic axes, it is worth considering the symmetry elements of the GaAs crystal structure and the way in which physical properties, such as the piezoelectric coefficients, transform under a rotation of axes. The general transformation of the piezoelectric tensor is described in chapter 1. Further details for the specific case of GaAs are outlined in the following sections.

3.4.1 Effect of crystal symmetry on the piezoelectric tensor

GaAs belongs to the highly symmetric cubic class $\bar{4}3m$, which has only one independent piezoelectric coefficient. The $\bar{4}3m$ notation implies that the symmetry elements are a 4-fold inversion ($\bar{4}$) axis parallel to the x_3 axis, a 3-fold (3) or triad axis parallel to the x_1 axis, and a mirror plane (m) along a plane bisecting the external angle between the $+x_1$ and x_2 axes (see chapter 1, Fig.1.3).

Nye (1985, p118) describes a method of determining the effect of crystal symmetry on physical properties by direct inspection. This method can be used to show how crystal symmetry determines the form of the piezoelectric tensor. The method is based on the fact that certain symmetry operations must leave the piezoelectric tensor component unchanged. An

apparent change of sign in the tensor component is used to identify those components which must be zero.

All the symmetry information of class $\bar{4}3m$ can be obtained from a single diagram, referred to as a stereogram, as shown in Fig.3.2. The symmetry elements are the $\bar{4}$ axis including a 2-fold (2) or diad axis parallel to x_3, and the $\bar{4}$ and the diad axes parallel to x_1.

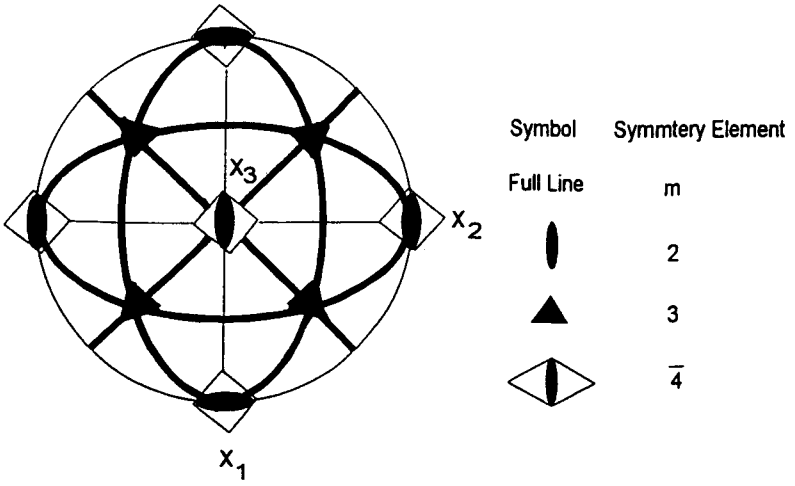

Fig.3.2 A stereogram showing the symmetry elements of class $\bar{4}3m$. The x_1 and, x_2 axes lie in the plane of the page while the x_3 axis is perpendicular to this plane (Nye, 1985, p288).

For convenience, the three cartesian reference axes x_1, x_2, and x_3 are referred to as 1-, 2-, and 3-axes, respectively. A systematic consideration according to the symmetries existing in the $\bar{4}3m$ crystal class is :

(i) The operation of the diad axis parallel to the 3-axis : The axes are transformed by the operation of the diad axis as follows : 1 transforms to –1, 2 to –2, and 3 to 3. Then the moduli are transformed according to the transformed axes, for example, d_{111} transforms into $-d_{111}$, and becomes

zero because the sign is changed, but d_{113} transforms into itself, and therefore is not zero. The nonzero moduli after the operation are :

$$d_{113}, d_{123}, d_{213}, d_{223}, d_{311}, d_{312}, d_{322}, d_{333}$$

(ii) The operation of the $\bar{4}$ axis parallel to the 3-axis : 1 transforms to -2, 2 to 1, and 3 to -3. Due to the $\bar{4}$-axis is an operation of 90° rotation followed by inversion, the modulus must transforms into itself. Then the nonzero moduli after the operation are :

$d_{113} = -d_{223}$, $d_{213} = d_{123}$, $d_{311} = -d_{322}$, $d_{312} = d_{321}$,

$d_{123} = d_{213}$, $d_{223} = -d_{113}$, $d_{322} = -d_{311}$,

$d_{333} = -d_{333}$.

(iii) The operation of the diad axis parallel to the 1-axis : 1 transforms to 1, 2 to –2, and 3 to –3. Some of the nonzero moduli listed in (ii) become zero and the remainder is

$$d_{123} = d_{213}, \quad \text{and} \quad d_{312} = d_{321}$$

(iv) The operation of the $\bar{4}$ axis parallel to the 1-axis : 1 transforms to –1, 2 to –3, and 3 to 2. After the operation there is only a single piezoelectric coefficient $d_{123} = d_{213} = d_{312}$.

3.4.2 Transformed piezoelectric coefficient

For a [111] GaAs sample it is necessary to transform the piezoelectric coefficients from the conventional crystal axes to a set where one axis is perpendicular to the (111) plane. The transformed piezoelectric coefficients can be obtained by rotating from the original coordinate system to the new one as follows.

The transformation law for a third-rank piezoelectric tensor is given by equation (1.7):

$$d_{ijk}' = a_{il} a_{jm} a_{kn} d_{lmn} \tag{3.1}$$

where d_{ijk}' are the piezoelectric moduli in the new coordinate system, d_{lmn} are the coefficients in the old system and the a_{ij} are the direction cosines of the new axes relative to the old. That is, a_{ij} is the cosine of the angle between the new i axis and the old j axis. In the interferometer arrangement, the field is applied in the 3 direction and, in the usual arrangement, only those displacements in the 3 direction are measured. Thus the coefficient of interest in the transformed coordinate system is d_{333}'. The nonzero piezoelectric components in the usual crystal coordinate system are $d_{123} = d_{213} = d_{312}$. The transformation between these particular components is:

$$d_{333}' = a_{31}a_{32}a_{33}d_{123} + a_{31}a_{33}a_{32}d_{132} + a_{32}a_{31}a_{33}d_{213} + a_{32}a_{33}a_{31}d_{231}a_{33}a_{31}a_{32}d_{312} + a_{33}a_{32}a_{31}d_{321} \tag{3.2}$$

where a_{31}, a_{32}, a_{33} are the cosines of the angle between the new 3 axis, which is in the [111] direction, and the original crystal axes which have the directions [001], [010] and [100] (Fig. 3.1). Thus $a_{31} = a_{32} = a_{33} = 1/\sqrt{3}$.

Each term in equation (3.2) can be written in the matrix notation as described in chapter 1, resulting in $d_{14} = 2d_{123} = 2d_{213} = 2d_{312}$ and $d_{33}' = d_{333}'$. Putting all this into equation (3.2) finally yields :

$$d_{33}' = \frac{d_{14}}{\sqrt{3}} \tag{3.3}$$

where d_{14} is the piezoelectric coefficient for GaAs referred to the normal crystal axes and d_{33}' is the piezoelectric coefficient referred to a set of axes in which the '3' axis is perpendicular to the <111> plane. It should be noted that d_{33}' and d_{14} have the same sign.

3.5 Measurement of The d_{14} Coefficient

3.5.1 Sample preparation

The GaAs samples used in the present work were prepared from commercial [111]B wafers, having a 2° orientation of the 3 axis towards the $[2\bar{1}\bar{1}]$ direction. The wafers were n^+, polished on both sides and with a thickness of 0.4 mm. The wafers were kindly supplied by Dr. J. P. David, Department of Electronic and Electrical Engineering, University of Sheffield, England. Samples measured approximately 5 mm by 5 mm.

3.5.2 Electrode material

Problems can arise when attempting to make ohmic contacts to GaAs. As a check on the influence of the electrode material on the measured piezoelectric response of GaAs, three different metals, namely aluminium, gold and indium were tried. In the case of aluminium and gold, the metals were simply evaporated onto the GaAs surfaces. In the case of indium (Sze, 1969), the indium was first evaporated onto both surfaces of the sample, followed by the evaporation of a thin layer of gold. The evaporated alloy was then diffused into the sample under a nitrogen atmosphere in a furnace (Lenton Thermal Designs 1200) annealed at 300 °C for 3 minutes.

Initial experiments used a circular electrode of 2.0 mm diameter. The electrode on the free surface of the sample acted as one of the mirrors in the interferometer. The other surface of the sample, with the electrode, was

glued, with conducting epoxy, to a brass plate. The arrangement of the sample and electrical contacts were as for the quartz sample described in chapter 2. The electrode/n^+-GaAs/electrode thus formed a metal-semiconductor-metal (MSM) structure. Charlson and Mott (1963) point out that the type of contact at the metal-semiconductor interface may have an effect on the uniformity of the piezoelectric excitation in GaAs. Charlson and Mott used the resonance method (chapter 1, section 1.4.2), in which the impedance properties of GaAs are probably affected by the high conductivity of the sample. The measurements performed to check the influence of the electrode material can then be used as a check on the effect of the metal-semiconductor contacts to the piezoelectric response.

For each electrode material, the thickness excitation measurement was made at a constant driving frequency but with varying voltages. Fig.3.3 shows the plots of displacement vs driving voltage for the different electrode materials. It can be seen that the results for aluminium and gold are distinctly non-linear. However the annealed indium/gold contact gives a quite linear relationship. It is assumed that this linear response results from the better ohmic contact between the metal electrode and the semiconductor sample.

For the indium electrodes, measurements of displacement versus driving voltage were made over the full range of frequencies from 1 kHz to 100 kHz. The slope of these plots was measured to obtain d_{33}', then equation (3.3) was used to obtain the value of d_{14}. The value of d_{14} was found to be 2.7 pmV^{-1} at 1 kHz. However a problem emerged when using the small circular electrodes. It was found that as the frequency of measurement increased towards 10 kHz, the observed value of d_{14} showed a marked decrease. This problem was overcome by varying the electrode arrangement as described in section 3.5.3.

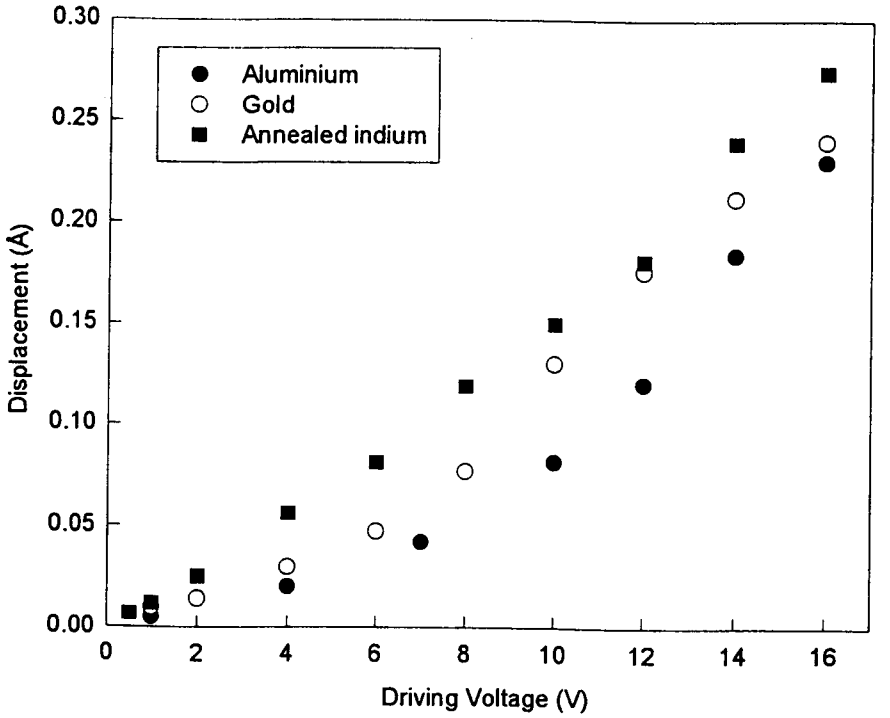

Fig.3.3 Variation of mechanical displacement with driving voltage for n^+-(111)B GaAs with aluminium, gold, and annealed indium (with a thin layer of gold on the top of indium) electrodes measured at 1 kHz.

3.5.3 Effect of electrode dimensions

As a general rule, when piezoelectric measurements are made, the recommendation is that as much as possible of the surface be electroded (Cady, 1964, p237).

To check the effect of electrode area, samples were prepared with as much as possible of the surface covered by indium electrodes. Measurements of the piezoelectric coefficients were carried out over the range from 1 kHz to 100 kHz. A plot of the frequency dependence of the d_{14} coefficient, measured on samples with full area electrodes, is shown in

Fig.3.4. A significant feature of this plot is that the large decrease in measured d_{14} around 10 kHz, which was observed in the samples with 2 mm electrodes, is much less significant. The value of d_{14} at frequencies below 8 kHz was independent of electrode area and this was taken as an indication that the value measured in this range of frequencies was the correct value.

Large variations in the response were observed at frequencies above 30 kHz. These are due to resonances. The d_{14} value was reasonably constant within the frequency range of 1-10 kHz. The magnitude of the d_{14} coefficient in this frequency range was found to be (2.7 ± 0.1) pmV^{-1}.

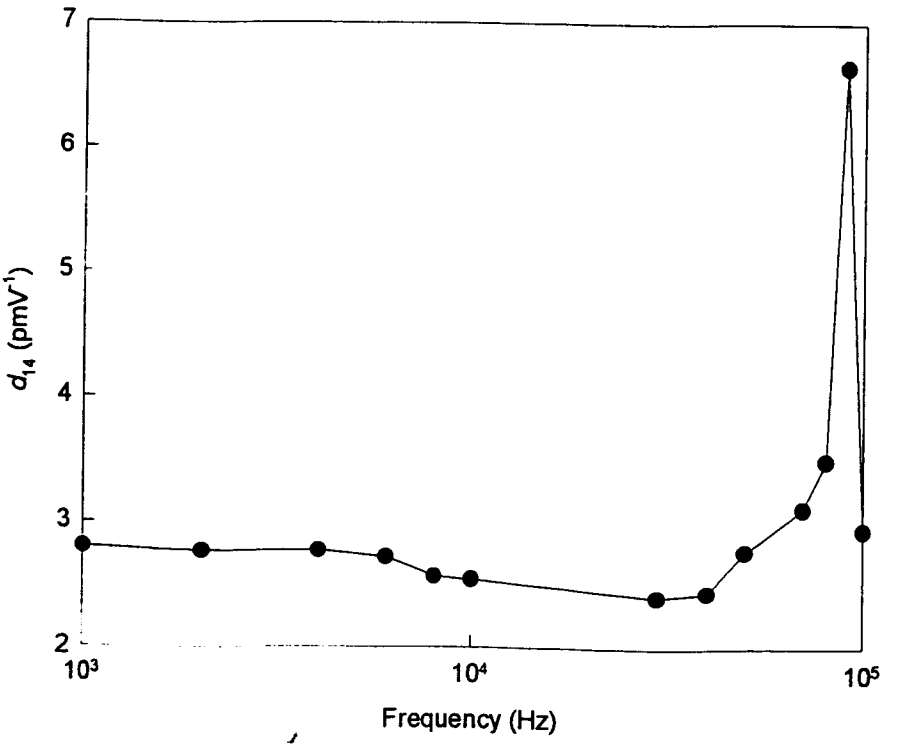

Fig.3.4 Plot of the frequency dependence of the measured d_{14} for (111)B GaAs. The annealed electrode covered the full sample surface.

3.5.4 The sign of the d_{14} coefficient

The sign of the d_{14} coefficient was determined as described in chapter 2. First the driving voltage was connected to a PVDF sample for which the free surface had been connected to the positive terminal of the poling supply. The GaAs samples was then driven by the same source, with the B crystal face acting as the free surface. For this configuration the output phase of the signal obtained with the GaAs sample differed by 180° from that measured with the PVDF sample.

For the PVDF sample the positive direction of the 3 axis was towards the free surface. For the GaAs sample the positive direction was away from the free surface. The fact that the samples give responses which are 180° out of phase when their 3 axes point in opposite directions indicates that the sign of their d_{33} coefficients are the same. Since d_{33} for PVDF is known to be negative, the coefficient for GaAs is thus confirmed to be negative.

As a double check, the GaAs sample was prepared with the [111]A surface as the free surface. This sample produced an output of the same phase as the PVDF reference sample.

3.6 Conclusions

This is the first time that the interferometric technique has been used to determine the magnitude and sign of the d_{14} coefficient for GaAs. The electrode material and dimensions play a role in the observed piezoelectric response. An electrode consisting of annealed indium, with a thin layer of gold on the top is the most suitable electrode for GaAs. For samples prepared from a commercial [111] oriented wafer, it was found essential to ensure that a large area of the surface was electroded. Such samples gave reliable measurements of the d_{14} coefficient in the frequency range from

1 kHz to 10 kHz. The measured d_{14} coefficient of GaAs determined in this frequency range was found to be (-2.7 ± 0.1) pmV^{-1}. This value is consistent with most previous determinations, in particular the Hall measurements of Arlt and Quadflieg (1968).

Given that GaAs has a reasonably high electrical conductivity, it might be expected that methods based on the direct piezoelectric effect would give values lower than the true value, due to significant levels of charge movement in the sample. The interferometric method measures the inverse effect and avoids the conductivity problem, since the sample is driven by a low impedance voltage generator. The results confirm the equality of the measured coefficients for the direct and inverse piezoelectric effect.

4

Extensional Piezoelectric Coefficients of Gallium Nitride and Aluminium Nitride

4.1 Introduction

In recent years, interest in the piezoelectric properties of materials in thin layer form has increased because of the range of applications of devices such as microactuators, microsensors, ultrasonic motors, etc., which are based on piezoelectric thin films (Kim and Muller, 1987 ; Wenzel and White, 1988 ; Moroney et al., 1989). A number of piezoelectric multilayer structures for piezoelectric applications have been fabricated from III-V nitride semiconductors including gallium nitride (GaN) and aluminium nitride (AlN). Experimental values of the measured physical properties of GaN and AlN films have been reviewed by Strite and Morkoç (1992). However, to date, there are no experimental values available for the piezoelectric coefficients of GaN and very few reports have appeared on the piezoelectric coefficients for AlN. Obtaining such experimental data for the piezoelectric coefficients is therefore of considerable value and interest.

4.1.1 Review of previous work

A summary of the *d* coefficients as reported in the literature for AlN is given in table 4.1. Theoretical values of the *e* coefficients for GaN and AlN are also included in this table.

Table 4.1 Values of the *d*-coefficients (in units of pmV^{-1}) for AlN and the *e*-coefficients (in units of Cm^{-2}) for AlN and GaN as reported in the literature.

Reference	d_{15}	d_{31}	d_{33}	Method/Theory
Hutson (1963)	4	−2	5	Method unknown, data quoted by Tsubouchi et al. (1981)
Tsubouchi et al.(1981)	−4.08	−2.65	5.53	SAW Velocity Measurement
Kamiya (1996)		−2.71	6.72	Hartree-Fock Periodic Approach
		e_{31}	e_{33}	
Bernardini et al.(1997)	(AlN)	−0.60	1.46	Berry-Phase Approach
	(GaN)	−0.49	0.73	Berry-Phase Approach

The earliest reported values were those of Hutson (1963). Hutson's work and that of Tsubouchi et al. (1981), which were derived from surface acoustic wave (SAW) phase velocities measured on single-crystal AlN films, show good agreement for the d_{15} coefficient and the largest discrepancy for the d_{33} coefficient. There is a contradiction in the sign of d_{15} in these two reports. Kamiya (1996), calculated the *d* coefficients of wurtzite AlN, using a Hartree-Fock periodic calculation. In the calculation, it was assumed that an external electric field induced ionic displacement, which in turn caused ionic polarization. The ionic polarization obtained from the theoretical effective charges was then used to calculate the d_{33} and d_{31} coefficients. Kamiya,

however, reported a slightly larger value of the *d* coefficients in his work which was found to follow from an overestimated value of the effective charge.

Theoretical work by Bernardini et al. (1997) provided the *e* coefficients for both wurtzite-type GaN and AlN using the Berry-phase approach. This approach was applied to the piezoelectric polarization which was related linearly to the strain. This group reported that the calculated *e* values of AlN were up to ten times larger than in some other III-V semiconductors, such as GaAs, GaSb, and II-VI compounds such as ZnS. This work represents the first reported attempt to calculate the *e* coefficients of GaN.

4.1.2 Applications of piezoelectric effect of GaN and AlN

In addition to the semiconductors having zincblende structure, such as GaAs, piezoelectric effects can also influence the properties of wurtzite semiconductors such as GaN and AlN. In fact for all nitride films grown on non-lattice matched substrates, the residual strains generate electric fields within the structure. These fields can modify the electronic structure and optical properties of the film. GaN-based sensors, consisting of a strained layer of GaN, have been produced. These sensors exhibit a large change in resistance for small changes in strain. This type of sensor has high sensitivity and can be used for the measurement of vibration, force and pressure, over a wide range of frequencies (Bykhovski et al., 1996).

In the case of AlN, high-frequency and low-dispersion surface acoustic waves have long been used successfully in surface acoustic wave devices (O'Clock and Duffy, 1973 ; Gualtieri and Kosinski, 1994 ; Liaw and Hickernell, 1995). The SAW efficiency of the devices can be determined by the values of the elastic, piezoelectric, and dielectric constants and temperature coefficients. A high sensitivity piezoelectric pressure sensor

fabricated from AlN film has been recently reported, and the characteristics of the sensor are found to be very attractive for integration into field effect transistor structures (Matthes et al., 1992).

As indicated in chapter 1, multilayers of semiconductors can be grown intentionally strained in order to produce electric fields within the structure. A theoretical study of strained multilayers of GaN and/or AlN, grown with a [0001] orientation, indicates that the generated electric field can modify the performance of devices made from these materials (Bykhovski et al., 1993). The same group (Bykhovski et al., 1995) have studied the strain induced electric fields in a GaN-AlN-GaN structure. The structure was as shown in Fig.4.1.

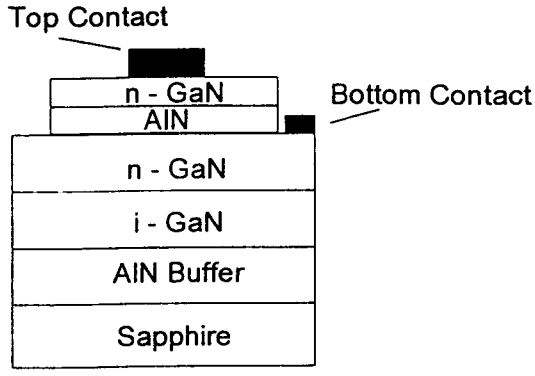

Fig.4.1 GaN-AlN-GaN structure (after Bykhovski et al., 1995).

With a sufficiently thin AlN layer in the structure, the strain induced electric fields can shift the flatband voltage and produce an accumulation region on one side and a depletion region on the other side of the AlN layer. The accumulated piezoelectric charges were found to affect carrier distribution near the interfaces in the structure. This finding suggests the possibility of fabricating GaN- and AlN-based optoelectronic devices with

lower threshold current density. A knowledge of the strain induced polarization and the corresponding voltage shifts is essential for designing such devices.

4.2 Crystal Structure and the Piezoelectric Coefficients

The crystal structure of nitride films is strongly influenced by the substrate material and orientation. GaN, and possibly AlN, may form in the zincblende structure when grown on cubic substrates (Paisley et al., 1989 ; Mizuta et al., 1986). However, the equilibrium form of epitaxial and polycrystalline films of GaN and AlN grown on substrates such as sapphire, silicon, and silicon carbide is usually found to be wurtzite (Strite and Morkoç, 1992).

The wurtzite crystal structure has hexagonal 6*mm* symmetry, with four atoms per primitive cell. The piezoelectric tensor of wurtzite crystals has three nonzero components : d_{33} , $d_{31}(= d_{32})$, and d_{15} $(= d_{24})$ (Nye, 1985, p 124). The first two of these involve extensional strains and the determination of these coefficients is described in the remainder of this chapter. The third component involves shear strain and a method of determining this, using the interferometer, is described in chapter 5.

Fundamentally, the wurtzite structure is similar to the zincblende structure, which is fcc with two atoms per cell (Martin, 1972). The fundamental relation between the two structures is that there are two tetrahedra in the wurtzite lattice, each of which can be related to the tetrahedra in the zincblende lattice by a simple rotation. Therefore, a close correspondence of the tensor representations of physical properties can be established between the two structures. In particular, there exist relationships between the piezoelectric coefficients of each structure (Birman, 1958, Berlincourt et al., 1963):

$$d_{14} = \sqrt{3} d_{33}' \tag{4.1}$$

and

$$d_{14} = -2\sqrt{3} d_{31}' \tag{4.2}$$

The primed quantities in equations (4.1) and (4.2) relate to the wurtzite phase, while the unprimed quantities relate to the zincblende phase. From equations (4.1) and (4.2), the following relationship is obtained :

$$d_{31}' = -\frac{1}{2} d_{33}' \tag{4.3}$$

4.3 Experimental Techniques

4.3.1 Sample preparation

4.3.1.1 GaN films

GaN has long been grown in thin film form by various methods and many physical properties of GaN have been measured on films of widely varying quality. Very recently, GaN free standing platelets have been fabricated, thus enabling some measurement of single crystal properties for bulk GaN (Detchprohm et al., 1996; Melnik et al., 1997).

In the present work, a polycrystalline GaN film grown on doped silicon with [100] orientation and a commercial wafer of GaN, epitaxially grown on silicon carbide with [0001] orientation, were used.

The polycrystalline film was grown by B. Zhou in the Semiconductor Science and Technology Laboratories (SSTL) at Macquarie University, Australia. The film was grown by laser assisted chemical vapour deposition (LCVD). X-ray diffraction confirmed the wurtzite structure, with a [0002]

orientation. The film was found to be *n* type, a consequence of unintentional doping during the growth process. The thickness of the film was 1 μm. Further details of the film properties have been provided elsewhere (Zhou, 1996).

The commercial GaN wafer, was obtained from Technologies and Devices International, Inc., USA. The growth method of the film is hydride vapour phase epitaxy (HVPE). This film had a thickness of 2.5 μm, with [0001] orientation.

4.3.1.2 AlN films

AlN has been synthesized in a single-crystal form, having a wurtzite structure (Mroz,Jr., 1992). However the growth of high-purity crystals of AlN is difficult. On the other hand, AlN has been grown successfully in thin film form (Strite and Morkoç, 1992).

In the present work, two samples of polycrystalline AlN films grown on doped [100] silicon in the SSTL at Macquarie University were used. Both samples were films grown under low damage growth conditions at low temperature and were intended for use as insulating layers for metal-insulator-semiconductor applications.

The first sample was CVD grown by Li at a temperature of 200°C. This sample was 1 μm thick and had a thin oxide layer, of about 0.1 μm thickness, on the surface. Further details of the properties of this film have been reported elsewhere (Li, 1991).

The second sample was grown by Butcher using laser ablation, or pulsed laser deposition, which gives an alternate to CVD and permits growth at temperatures below 90° C. This film is referred to as laser ablated film. Details of this film's properties have been reported elsewhere (Butcher,

1997). X-ray diffraction spectrum of both films show a principal [100] AlN peak, hence confirming the wurtzite structure.

4.3.2 Measurement of the d_{33} and d_{31}.coefficients

The piezoelectric tensor component of initial interest was d_{33}. For the wurtzite structure, the '3' direction is usually associated with the direction of the crystallographic c-axis. In the 6*mm* crystal class the positive direction of the '3' axis is defined in such a way as to make d_{33} positive (IEEE Standard on Piezoelectricity, 1988). Fig.4.2 shows the wurtzite crystal structure. In a wurtzite-type film the c-axis is usually perpendicular to the plane of the film. If an electric field is applied parallel to the c-axis, the d_{33} coefficient can be obtained directly from the ratio of the resultant displacement normal to the film plane to the applied voltage.

The second tensor component of interest is d_{31}. In this case the coefficient relates the changes in lateral dimensions to the field in the 3-direction. Once d_{33} is known, d_{31} can be determined from equation (4.3). Since d_{33} is defined to be positive, d_{31} must be negative. The values measured for d_{31} and d_{33} are the clamped values (see chapter 1).

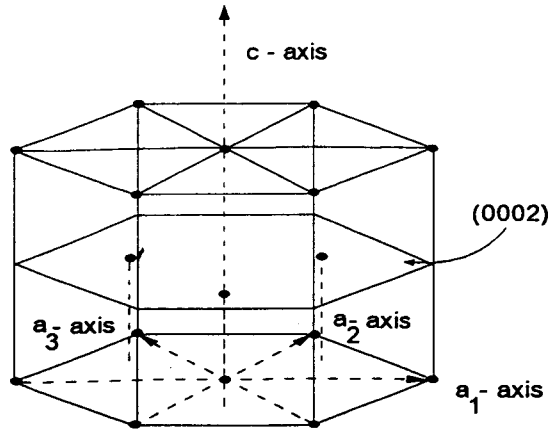

Fig.4.2 Illustration of the crystal axes for the wurtzite structure. In nitride films the c-axis is usually perpendicular to the film plane.

4.3.3 Resistivity measurement

A common feature of the samples described in this chapter, and one which distinguishes them from the GaAs material of chapter 3, is the fact that all of the GaN and AlN samples were in the form of thin films grown on a substrate. In the d_{33} measurement, the electric field is applied normal to the plane of the sample via an electrode on the film surface and another on the substrate. To measure the piezoelectric coefficient it is necessary to be sure that there is negligible voltage drop across the substrate. This will be the case if the resistance of a given area of the semiconductor film is much larger than an equivalent area of substrate. To check this, the film resistance was measured using the arrangement shown in Fig.4.3. The surface of the substrate was covered with an evaporated aluminium coating, while a circular aluminium electrode, of diameter 2 mm, was evaporated onto the film surface. The electrodes were connected to a voltage source and the current flow was measured using a Keithley 617 programmable electrometer. The internal supply of the electrometer was used as the voltage source.

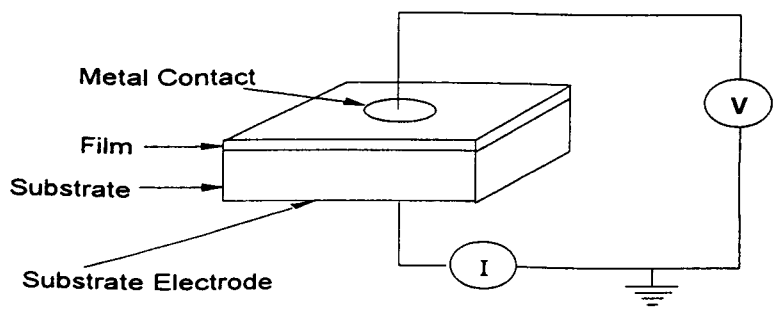

Fig.4.3 The arrangement used for measuring sample resistance.

This procedure measures the combined resistance of the film plus substrate in series. The samples grown in the SSTL, i.e. the polycrystalline

GaN and both AlN samples, were grown on substrates of known resistivity. For these films, the film and substrate resistances were deduced from the measured I-V plots and the known resistivity of the substrate. In the case of the commercial GaN wafer, the substrate resistivity was not known. For this sample, some of the GaN layer was etched away to expose the substrate and the I-V measurement repeated for the substrate alone.

4.4 Experimental Results

4.4.1 Film resistivity

The 1 μm polycrystalline GaN film was grown on an n^+-Si substrate. This substrate had resistivity of 0.01 Ωcm and was 0.3 mm thick. A typical I-V curve obtained from this film is shown in Fig.4.4.

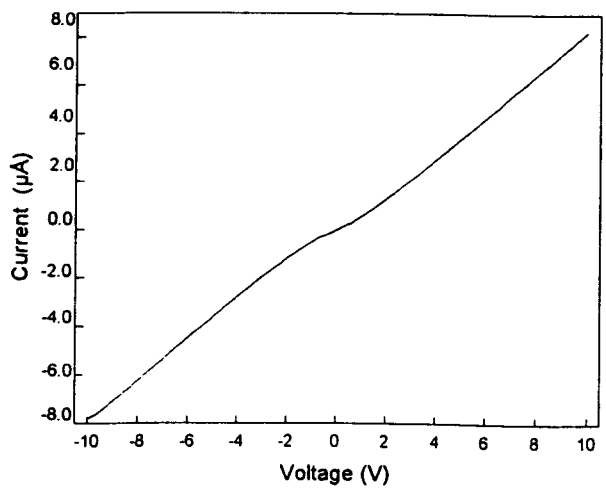

Fig.4.4 I-V curve of the polycrystalline GaN film.

The current varied linearly with the applied voltage, except in the region near the origin, where the voltage was small. The total resistance obtained from the slope of Fig. 4.4 is 1.25×10^6 Ω. The resistance of a circular area of substrate, corresponding to the area of the circular electrode is 0.1Ω.

In this case, even though the film is much thinner than the substrate, the resistance of a given area of the GaN film is about 6 orders of magnitude larger than the same area of substrate. It can thus be safely assumed that the voltage loss across the substrate is negligible.

Both AlN films were grown on the same Si substrate as the polycrystalline GaN. The total measured resistance of these films together with their substrates was found to be 3.0×10^8 Ω and 1.2×10^6 Ω. As for the GaN on silicon, the film resistance is much larger than that of the substrate.

For the commercial GaN wafer, the total resistance was found to be 1.0×10^6 Ω. The resistance of the substrate, measured after etching away a small area of GaN, was 5.0×10^3 Ω. In this case the resistances are closer than for the polycrystalline samples. Nevertheless the difference was still over 2 orders of magnitude, and voltage drops across the substrate have thus been neglected.

An additional effect, which could introduce error is the Maxwell-Wagner effect, in which sample and substrate capacitance combine to alter the field distribution. This effect would be significant if the capacitive reactance of the film being measured was not much greater than the imedance of the substrate. Because of the small area of the samples, the capacitance of both the substrate and the sample is much less than 1 pF. As a result the capacitive reactance, at 1.0 kHz is in excess of 10^8 Ω.

The net result of all of this is that the field across the sample can be simply calculate as described. However it is worth noting that a move to higher frequencies may well involve the need to re-consider this point.

4.4.2 Bending Effects

The polycrystalline GaN sample was the first sample measured during the course of the investigation described in this thesis. In order to ensure that a thickness coefficient (d_{11} or d_{22} or d_{33}) is measured correctly, it is important to ensure that the interferometer actually is measuring changes in sample thickness. This is particularly important for the single beam arrangement, where only the position of one surface of the sample is probed. In this arrangement, any bending in the sample would give rise to erroneous measurements. Considerable effort was expended in the initial stages of the measurements on the polycrystalline GaN sample to ensure that only thickness-mode vibrations were present. The method used to check for the presence of bending modes was to scan the probe beam across the sample surface, measuring the variation in amplitude of the field-induced vibrations. In the present arrangement it was possible to position the laser beam on the sample surface with a resolution of 100 μm.

The main factor which determined the presence of bending-mode vibrations was found to be the mounting of the sample. Fig.4.5a shows the variation in amplitude detected at various points across the film surface for a sample glued on edge to the brass plate and driven at a frequency of 1 kHz. The variation in vibration amplitude across the surface, in particular the larger amplitude towards the centre of the film, indicated bending-mode vibrations. If the sample was mounted by gluing flat to the brass plate, then the surface vibration was as shown in Fig.4.5b. The uniform vibration amplitude was taken as an indication that the predominant vibration is the thickness mode.

Driving voltages of different amplitude were applied to the sample glued to the brass plate. The variation of vibration amplitude at each driving voltage was observed as a function of frequency, and the results were as

shown in Fig.4.6. For a constant driving voltage, the variation in amplitude varied by less than 4% within the frequency range from 1 kHz to 10 kHz.

(a)

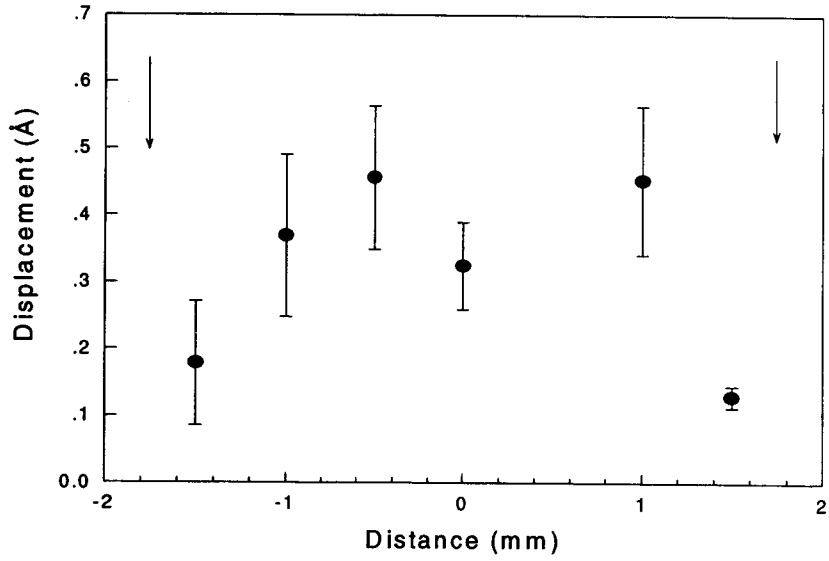

(b)

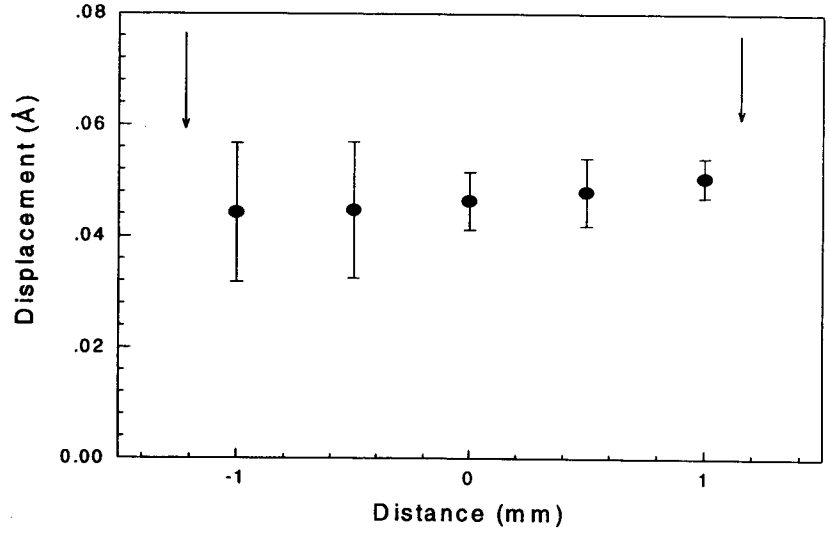

Fig.4.5 Variation in the amplitude of vibration across the sample surface, measured at 1 kHz. (a) edge mounted sample, and (b) the sample rigidly glued to the brass plate. The arrows mark the position of the electrode edges.

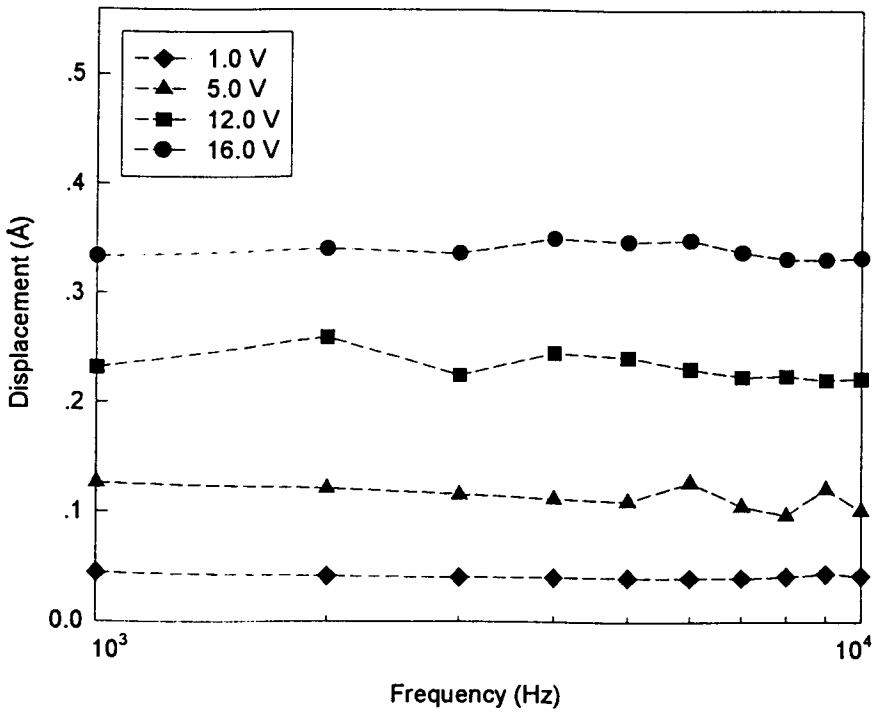

Fig.4.6 Frequency dependence of the amplitude of vibration in the GaN film driven by a range of driving voltage.

4.4.3 The d_{33} and d_{31} coefficients

Measurements of vibration amplitude were normally made at the centre of the film. The normal routine was to measure vibration amplitude for a range of voltages, plot the amplitude against the voltage and use the slope of the plot to calculate the piezoelectric coefficient. The procedure was repeated for a range of frequencies. The results for the four samples are shown in Fig.4.7 to Fig.4.9.

(a)

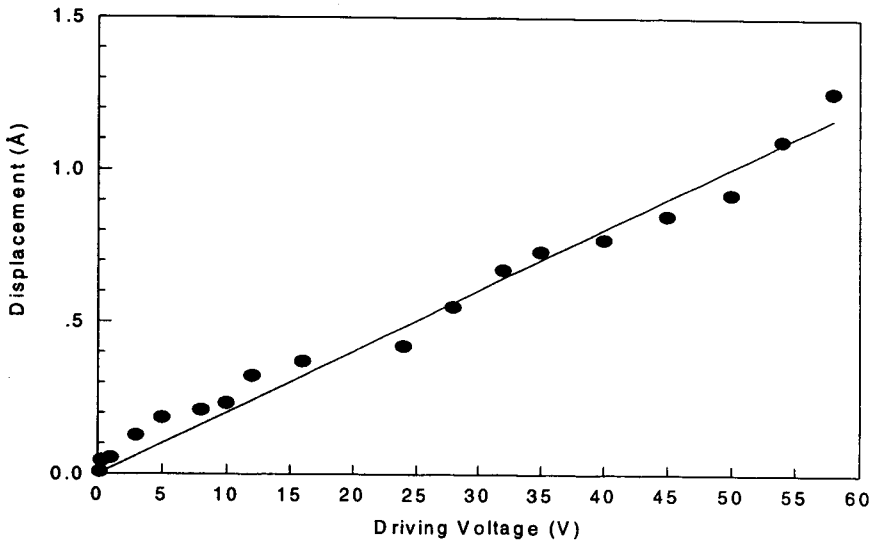

(b)

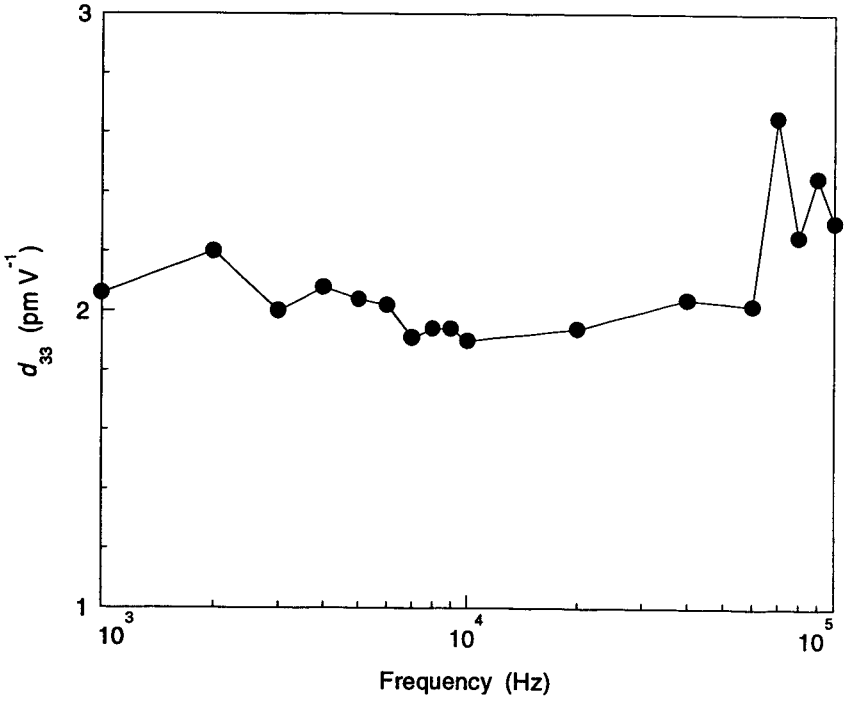

Fig.4.7 Electromechanical response for the polycrystalline GaN film. (a) Surface displacement versus driving voltage at 1 kHz, and (b) frequency dependence of the measured d_{33}.

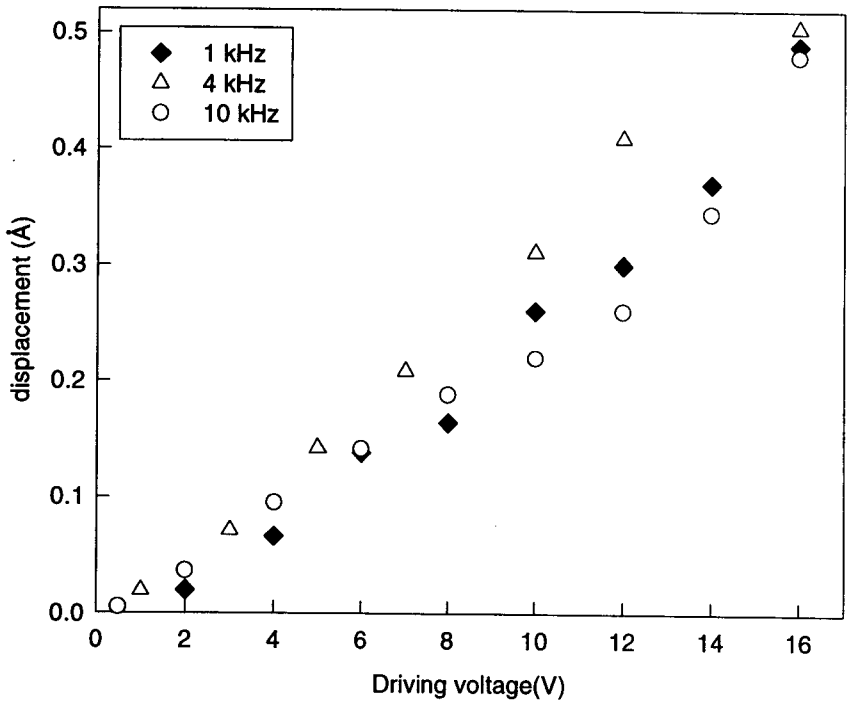

Fig.4.8 Electromechanical response obtained with the commercial GaN wafer. Variation of mechanical displacement with driving voltage measured for frequencies in the range from 1-10 kHz. In contrast to the plots of figure 4.7, in this case both the amplitude and frequency dependance are shown in the one plot.

(a)

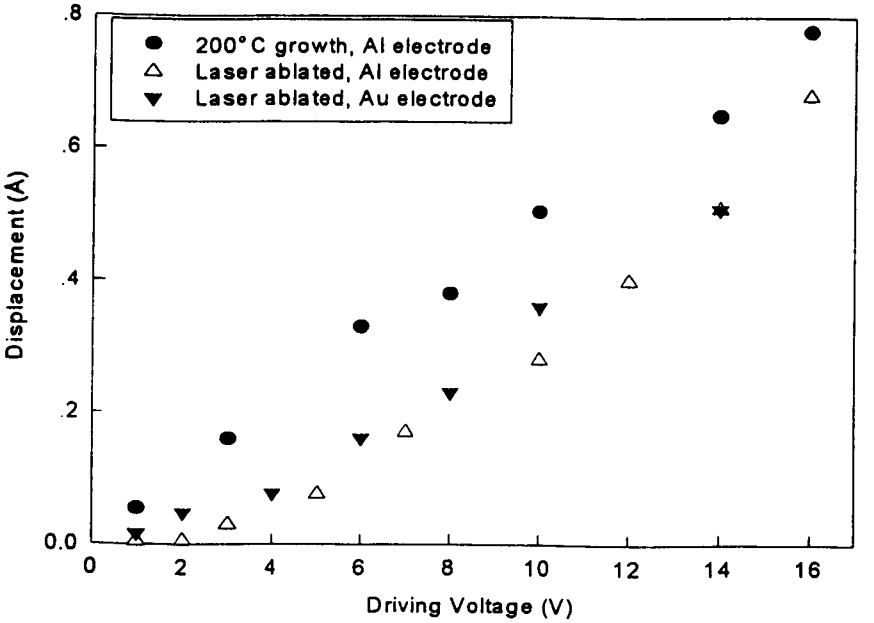

(b)

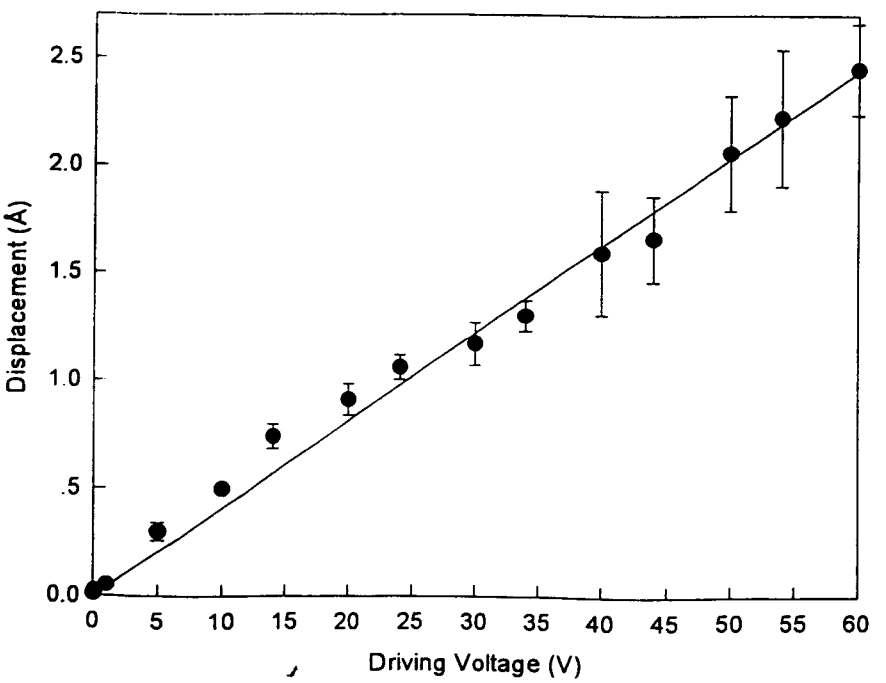

Fig.4.9 Variations of mechanical displacement with driving voltage measured (a) at 1 kHz for both AlN films, and (b) values averaged from data obtained in the range from 1 kHz to 10 kHz, for the 200° C grown AlN film.

Fig.4.7a shows the piezoelectric response in the polycrystalline GaN film for applied fields from 0.2 MVm^{-1} to 60 MVm^{-1}. The minimum field of 0.2 MVm^{-1} gave a displacement of 3×10^{-3} Å. This is not far above the resolution limit of the interferometer (chapter 2). The d_{33} of the film was obtained from the slope of this plot. The plots for other frequencies are not shown, however the values of d_{33} for the full range of frequencies from 1 kHz to 100 kHz are shown in Fig.4.7b. It is evident that bending mode vibrations were not totally suppressed at frequencies above 50 kHz.

The value of d_{33} for this film, obtained by averaging over the frequency range 1 kHz to 10 kHz, was (2.0 ± 0.1) pmV^{-1}. The corresponding value of d_{31}, obtained using equation (4.3) was (-1.0 ± 0.1) pmV^{-1}.

Fig.4.8 shows the response obtained with the commercial GaN wafer in the frequency range from 1 kHz to 10 kHz. The d_{33} value, averaged over the range, was found to be (2.8 ± 0.1) pmV^{-1}. Using equation (4.3), a d_{31} value was found to be (-1.4 ± 0.1) pmV^{-1}.

As might be expected, the piezoelectric coefficients of the polycrystalline GaN film are lower than those of the single-crystal GaN wafer. In the polycrystalline film, factors such as interfacial stress, defects and variation in c-axis alignment act to reduce the observed piezoelectric response. Thus the value obtained for the wafer is probably a more reliable indicator of the piezoelectric coefficient for bulk GaN. Nevertheless the value for the film is of interest, since this is the value which would be pertinent for devices based on such thin films. The difference between the two d_{33} values is about 30% and this gives an indication of the size of the effects arising from the phenomena mentioned above.

Fig.4.9a shows the piezoelectric response of both AlN films. For the laser ablated film, the piezoelectric response at low electric field did not follow the field linearly. At first it was felt that this non-linearity may be due to effects

at the electrode-semiconductor interface. However the effect was observed for both gold and aluminium electrodes. It is known that the film grown by laser ablation is much more porous than that grown by CVD. The crystallite size in the laser ablation film was also larger, about 200 nm, compared with 50 nm to 100 nm for the CVD film. It is possible that the non-linearity arises from these factors. An effort was made to deduce the d_{33} and d_{31} coefficients from a linear portion of the responses observed at 1 kHz for both gold and aluminium electrodes. The average values of d_{33} and d_{31} for this film were found respectively to be (3.2 ± 0.3) pmV^{-1}, and (−1.6 ± 0.1) pmV^{-1}.

Fig.4.9b shows the piezoelectric response of the AlN film grown at 200°C. The observed response was linear for fields from 0.1 MVm^{-1} to 60 MVm^{-1}. The value of d_{33}, measured across the range from 1 kHz to 10 kHz was found to be (4.0 ± 0.1) pmV^{-1}. Using equation (4.3) gives a value of (−2.0 ± 0.1) pmV^{-1} for d_{31}. The lower porosity of the CVD grown film suggests that the piezoelectric coefficients measured on it are a better indication of the true value of the piezoelectric coefficient of AlN.

4.4.4 Substrate clamping

All of the nitride films used in the present work were deposited on substrates. As indicated in chapter 1, the presence of the substrate restricts the strain in the plane of the films and this in turn reduces the thickness strain. The result is that the measured value of d_{33} is less than the true value of unconstrained material. If it is assumed that the substrate clamps the film such that the lateral strain is zero, then equation (1.17) can be used:

$$d_{33} = d'_{33} + 2\frac{d_{31}s_{13}^{E}}{s_{11}^{E} + s_{12}^{E}} \qquad (4.4)$$

where the coefficients on the right of equation (4.4) are the measured values, while the coefficient on the left is the corrected one.

In order to be able to use equation (4.4), a reliable set of values for the elastic compliances is required. The nonzero compliances for wurtzite crystals are s_{11} (= s_{22}), s_{33}, s_{12}, s_{13} (= s_{23}), s_{44} (= s_{55}), and $s_{66} = 2(s_{11}-s_{12})$ (Nye, 1985, p141). Several sets of data for GaN and AlN, both theoretical and experimental, are available in the literature.

The corrected d_{33} for GaN and AlN were calculated from equation (4.4) and then a corrected d_{31} was calculated using equation (4.3) The values obtained are shown in tables 4.2 and 4.3, respectively. In the calculations, the measured values from the commercial GaN wafer and from the 200° C grown AlN were used. These were felt to be the more reliable values for reasons already outlined. However it should be noted that the AlN film is polycrystalline and the values obtained from it are probably smaller than the true single crystal values.

Table 4.2 contains values of d_{33} and d_{31}, which have been corrected for substrate clamping, of GaN. The calculations based on the compliances of Takagi et al.(1996) and Wright (1997), which are the most recent values, gives the two similar d_{33} values. Thus these d_{33} values are more reliable, and then lead to the average values of the d_{33} and d_{31} coefficients of (3.4 ± 0.1) pmV^{-1}, and (−1.7 ± 0.1) pmV^{-1} respectively for bulk GaN.

Table 4.3 contains the d_{33} and d_{31} values, which have been corrected for substrate clamping, of AlN. The values were calculated, based on several different reported sets of elastic coefficients. The interesting point is that all sets give quite similar values for the corrected piezoelectric coefficients. The final, corrected values of the d_{33} and d_{31} coefficients are therefore found to be (5.1 ± 0.2) pmV^{-1}, and (−2.6 ± 0.1) pmV^{-1} respectively for bulk AlN.

Table 4.2 Values of the d_{33} and d_{31} coefficients, which have been corrected for substrate clamping, for GaN film. The compliance values (in units of 10^{-12} m^2N^{-1}) as reported in the literature used in the calculations are included.

Reference	s_{11}^E	s_{12}^E	s_{13}^E	d_{33} (pmV^{-1})	d_{31} (pmV^{-1})
Sheleg and Savastenko(1979)*	5.1	−0.9	−2.5	4.5 ± 0.1	−2.25 ± 0.10
Polian et al.(1996)**	2.6	−1.0	−0.6	3.9 ± 0.1	−1.95 ± 0.10
Takagi et al.(1996)**	3.5	−0.9	−0.5	3.3 ± 0.1	−1.65 ± 0.10
Wright (1997)***	3.3	−1.0	−0.6	3.5 ± 0.1	−1.75 ± 0.10

* Measured values from x-ray diffraction spectra.

** Measured values from Brillouin scattering.

*** Calculated values using the plane-wave pseudopotential method.

Table 4.3 Values of the d_{33} and d_{31} coefficients, which have been corrected for substrate clamping, for AlN film. The compliance values (in units of 10^{-12} m^2N^{-1}) as reported in the literature used in the calculations are included.

Reference	s_{11}^E	s_{12}^E	s_{13}^E	d_{33}	d_{31}
Tsubouchi et al.(1981)*	3.5	−1.0	−0.8	5.3 ± 0.1	−2.65 ± 0.10
McNeil et al.(1993)**	2.9	−0.9	−0.5	5.0 ± 0.1	−2.5 ± 0.10
Ruiz et al.(1994)***	2.5	−0.7	−0.5	5.1 ± 0.1	−2.55 ± 0.10
Wright (1997)****	3.0	−0.9	−0.6	5.1 ± 0.1	−2.55 ± 0.10

* Measured values from SAW phase velocity.

** Measured values from Brillouin scattering.

*** Calculated values using Hartree-Fock theory

**** Calculated values using the plane-wave pseudopotential method.

4.4.5 Piezoelectric coefficients of zincblende GaN and AlN

GaN and AlN can exist in either the wurtzite or the zincblende structure. The form which is present in thin film samples is largely determined by the growth conditions. As indicated in section 4.2, the zincblende and wurtzite structures are identical through the second nearest neighbour and the piezoelectric coefficients of the two structures are related by equations (4.1) and (4.2)

As for GaAs (chapter 3), e_{14} can be obtained from d_{14} using the relation $e_{14} = d_{14}c_{44}$. A c_{44} value of 101×10^9 Nm^{-2} (Takagi et al., 1996) was used in the calculation for GaN. A c_{44} value of 128×10^9 Nm^{-2} (Ruiz et al., 1994) was used for AlN.

The calculated zincblende coefficients are shown in table 4.4.

Table 4.4 Calculated piezoelectric coefficients for zincblende GaN and AlN.

Film	d_{33}' (pmV^{-1})	d_{14} (pmV^{-1})	e_{14} (Cm^{-2})
GaN	3.4	5.9	0.60
AlN	5.1	8.8	1.13

4.4.6 Direction of the 3 axis

As indicated in section 4, the IEEE standard defines the positive direction of the 3 axis in the 6mm crystal class in such a way as to make d_{33} positive. In this case then, the phase of the output voltage, when compared with the PVDF reference sample, gives the positive directin of the 3 axis, rather than the sign of the coefficient. It was found for all samples that the positive direction of the 3 axis pointed away from the substrate. This is a new

finding for these samples. Conventional X-ray diffraction patterns show that the 3 axis is perpendicular to the plane of the films, but cannot determine the positive direction of the axes. When the nitrides are grown on substrates, it is more common for the nitrogen atoms to grow on the surface rather than the aluminium or gallium atoms (Tansley, 1998). This in turn leads to the conclusion that in AlN and GaN the 3 axis points in a direction from the nitrogen atoms to the aluminium or gallium atoms.

4.5 Conclusions

The data reported in this chapter represent the first time that the piezoelectric coefficients for AlN and GaN have been measured by interferometry. For GaN this work represents the first reported measurements of piezoelectric coefficients by any method, apart from a publication by the author (Muensit and Guy, 1998).

The film resistivity is found to be several orders of magnitude higher than that of the substrate. The effects of bending become evident at low frequencies, if the sample is not mounted properly. If the sample is rigidly glued to the holder, the bending effects can be removed from the low frequency measurements. However, some resonance effects are still evident at frequencies above 50 kHz.

The values of the d_{33} and d_{31} coefficients for GaN are found to be (3.4 ± 0.1) pmV^{-1} and (-1.7 ± 0.1) pmV^{-1} respectively. Since these values were measured on a single crystal wafer and have been corrected for substrate clamping, the values should be a good measure of the true piezoelectric coefficients.

For AlN, the values of the d_{33} and d_{31} coefficients are found to be (5.1 ± 0.2) pmV^{-1}, and (-2.6 ± 0.1) pmV^{-1} respectively. Since these figures are measured on a polycrystalline sample it is quite probable that the true

values for bulk AlN would be somewhat higher. If the experience with GaN is taken as a guide, the single crystal values could be up to 30% higher than the values given here.

The piezoelectric measurements indicate that the positive c axis in the films points away from the substrate. The piezoelectric measurements thus provide a simple means for identifying the positive c axis direction.

These values are much smaller than those exhibited by materials normally used in actuator and sensor applications (Pointon, 1982). However, the fact that these two nitrides have increasing potential in semiconductor applications makes the values of considerable interest.

5

Shear Piezoelectric Coefficients of Gallium Nitride and Aluminium Nitride

5.1 Introduction

The piezoelectric coefficients discussed in chapters 3 and 4 required the measurement of longitudinal strain. Piezoelectricity can also generate shear strains and this chapter describes a method by which the shear coefficients can be measured.

The general piezoelectric tensor, written in abbreviated notation, is d_{ij}. The subscript i gives the component of the electric field and can have values ranging from i to 3. j gives the component of strain and can have values ranging from 1 to 6, with the values from 4 to 6 representing shear strains.

Chapter 3 describes the measurement of the coefficient d_{14} for GaAs. This tensor component involves a shear strain, however for GaAs the measurement was done by transforming to a new set of axes, for which d_{14} becomes d_{33}. The method relies on the availability of a sample having (111) crystal orientation. However not all shear coefficients can be measured by

transforming axes. Thus the present work sought to develop a technique for measuring shear strains, and hence the shear piezoelectric coefficients, using the same interferometer which was used for measuring longitudinal strain.

This chapter describes the measurement of the d_{15} coefficient for wurtzite GaN and AlN. The method of measuring the shear strain was developed during the course of this project and is believed to be unique. At this point in time not all problems have been solved, and these are discussed in the present chapter. However the method has given encouraging results. The value of d_{15} for AlN has been measured and shows good agreement with values quoted in the literature. The value of d_{15} for GaN has also been measured. The latter parameter appears never to have been measured prior to the present work..

Table 5.1 repeats some of the data from table 4.1. There appear to have been only two published reports of measurements of the d_{15} coefficient of AlN and none for GaN.

Table 5.1 Reported values of the d_{15} coefficient (in units of pmV^{-1}) for AlN.

Reference	d_{15}	d_{31}	d_{33}	Method
Hutson (1963)	4	–2	5	Method unknown, data quoted by Tsubouchi et al. (1981)
Tsubouchi et al.(1981)	–4.08	–2.65	5.53	SAW Velocity Measurement

5.2 A Method for Measuring Shear Coefficients

5.2.1 Measurement of shear strain

Shearing strains can be produced piezoelectrically by application of an electric field parallel to either an axis of shear or a plane of shear (Cady, 1964, p109). Fig.5.1 illustrates the case of simple shear strain in a rectangular shape ABCD. The axis of this shear is perpendicular to the plane of the diagram.

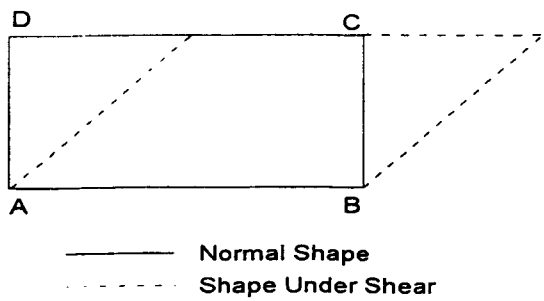

Fig.5.1 Deformation of a rectangular shape ABCD by a shear strain about an axis perpendicular to the plane of the page.

In the present work, the shear deformation of the films is produced piezoelectrically by a field parallel to the plane of shear. Since the film is rigidly attached to a substrate, then the surface AB in Fig.5.1 is fixed, while the surface DC moves.

Fig. 5.2 illustrates a method of mounting a sample in the interferometer in such a way that movement of the sample surface, resulting from shear strain, could be measured.

In this method, the sample is orientated such that its surface is parallel to the laser beam in the probe arm of the interferometer. A mirror is mounted on the sample surface with its plane perpendicular to the plane of

the sample surface. For small deformations, the shear strain depicted in Fig.5.2 is defined as (Weidner and Sells, 1965, p415) :

$$\tan\beta = \frac{d'}{t} \tag{5.1}$$

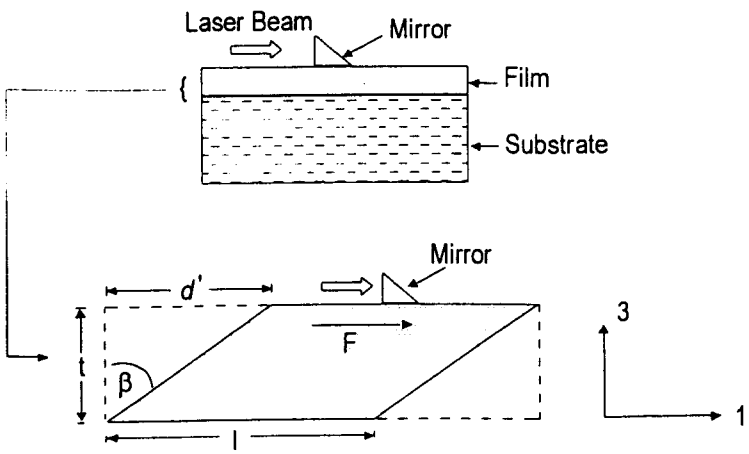

Fig.5.2 Side view (not to scale) of a method of sample mounting to permit the measurement of shear strains.

For a film of known thickness *t*, the strain can be obtained by measuring *d'*, the piezoelectrically induced movement of the surface.

It should be noted that some approximations are assumed here. Firstly it is assumed that the thickness of the film (the distance *t* in Fig.5.2) does not change as a result of the shear. Secondly, the sample is assumed to adhere to the ideal strained shape shown in Figs.5.1 and 5.2. This may not be valid in a dynamic situation, when inertial forces may cause the shape to deviate from the ideal. Both assumptions are reasonable if the strains are not large.

Given the direction of the axes shown in Fig.5.2, the component of strain measured would be S_5. The d_{15} coefficient relates this component of strain to the 1 component of the electric field:

$$S_5 = d_{15}E_1 \tag{5.2}$$

Thus d_{15} can be measured using the configuration of Fig. 5.2, by applying a known field in the 1 direction and using the interferometer to measure the motion of the sample surface.

5.2.2 Application of the field

In order to measure d_{15} correctly, a field, which would ideally be uniform, must be applied in the 1 direction of Fig.5.2. The simplest way of doing this would be to apply electrodes at the ends of the film, as shown in Fig. 5.3a. This diagram represents the film and electrodes in cross section.

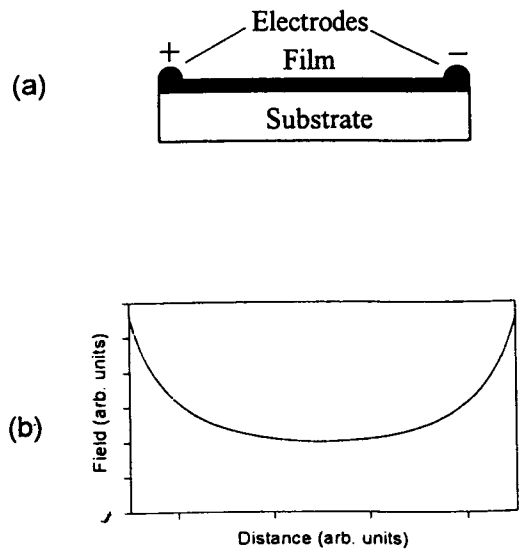

Fig.5.3 (a) Electrode arrangement for applying a field in the film plane. (b) Field distribution along a line between the electrodes, assuming that the electrodes behave as line charges.

If the film is very thin, then symmetry requires that the direction of the field in the film will be parallel to the plane of the film and the field should be reasonably uniform through the thickness of the film. The main problem is that the field will not be uniform along the length between the electrodes. If the electrodes are approximated as long, conducting cylinders, perpendicular to the plane of the diagram in Fig.5.3a, then the field due to each electrode will drop off inversely with distance from the electrode. The total field will thus vary as $(a^{-1}+b^{-1})$, where a and b represent the distances from the two electrodes. This variation is shown in Fig.5.3b. The left and right ends of the plot of Fig.5.3b represent the surfaces of the electrodes. The size of the field at the electrode surface depends on the size of the electrodes, relative to the inter-electrode distance. Fig.5.3b has been plotted for electrodes whose diameters are one tenth of the inter-electrode distance.

While the field between the electrodes does vary, it is still the case that the voltage between the electrodes is equal to $\int E \cdot dl$ along a line joining the electrodes. Hence the average field will be given by:

$$E = \frac{V}{l} \tag{5.3}$$

where l is the distance between the electrodes.

If it is assumed that the strain in the film is determined by the average field, then the d_{15} coefficient can be obtained from the measured displacement and applied voltage. Combining equations (5.1), (5.2) and (5.3) gives:

$$d_{15} = \frac{d'l}{Vt} \tag{5.4}$$

In fact using the average field is not strictly correct and some errors in the measurements will arise from this.

5.3 Experimental Techniques

5.3.1 Sample preparation

The CVD grown AlN film and commercial GaN wafers on both SiC and sapphire substrates (Cree Research, Inc., USA) were used. Samples were prepared in the form shown in Fig. 5.4. Conducting epoxy was applied to the opposite edges, along the length of the film to act as electrodes. Two 50 μm diameter wires were connected from these electrodes to two insulated electrical contacts. A mirror was attached to the film surface using non-conducting epoxy. The mirror was made from a small (1.5 mm by 1.5mm) piece of silicon wafer, with an evaporated alumium layer to form a reflective surface. An additional piece of silicon was glued to the back (fig. 5.2), to increase rigidity. The mirror was weighed, prior to mounting on the sample.

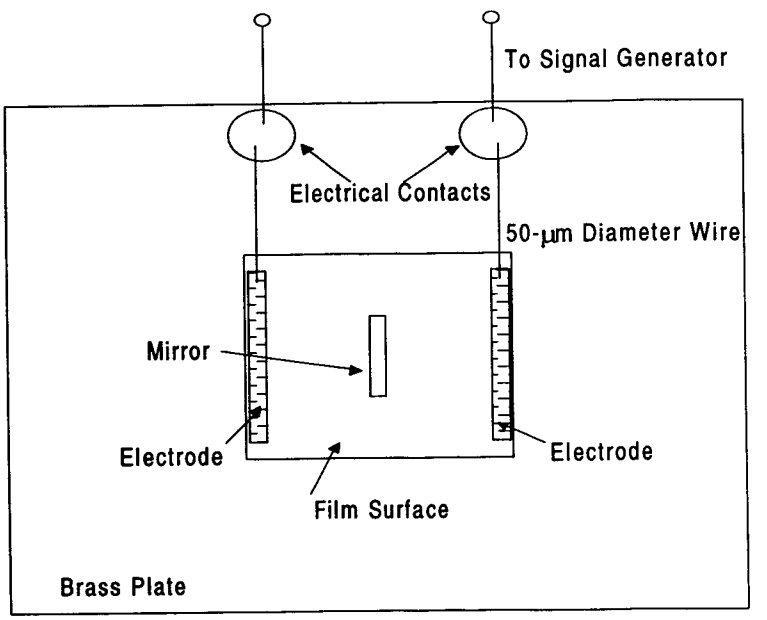

Fig.5.4 A diagram (not to scale) of the sample arrangement for measuring d_{15}. The film lies in the plane of the page, while the plane of the mirror is perpendicular to the plane of the page.

5.3.2 Determination of the d_{15} coefficient

The interferometer was used to measure the displacements caused by the shear deformation of the film. The measured displacement d' was evaluated using equation (2.7):

$$d' = d_o = \frac{\lambda}{2\pi}\frac{V_{out}}{V_{pp}} \tag{5.5}$$

From d', the known film thickness and length, and the applied driving voltage the d_{15} value was calculated using equation (5.4). The procedure was repeated for a range of driving voltages and frequencies.

5.4 Experimental Results

5.4.1 AlN

The initial attempts at these measurements used unbraced mirrors. The sample used was the CVD AlN film. Fig.5.5 shows the measured displacements as a function of frequency for two mirrors having slightly different masses. Two resonance peaks were observed, at frequencies of about 2 kHz and 6 kHz. These frequencies, being a fundamental and third harmonic, strongly suggest that the peaks are due to vibrations of the mirror, which is vibrating like a rod clamped at one end.

The mounting of the mirror was then made with more care, in particular a small bracing piece was placed at the back of the mirror to improve rigidity. The improved results are shown in Fig.5.6. The fundamental resonances were observed at frequencies of 1885 Hz and 1788 Hz

Measurements of displacement for various values of driving voltage were made on the film with the 3.6×10^{-5} kg mirror. The results were as shown in Fig.5.7. Relatively large displacements were observed at frequencies near resonance. The displacements were reasonably constant over the frequency

range from 3 kHz to 5 kHz, and these displacements were used to calculate the value of d_{15}.

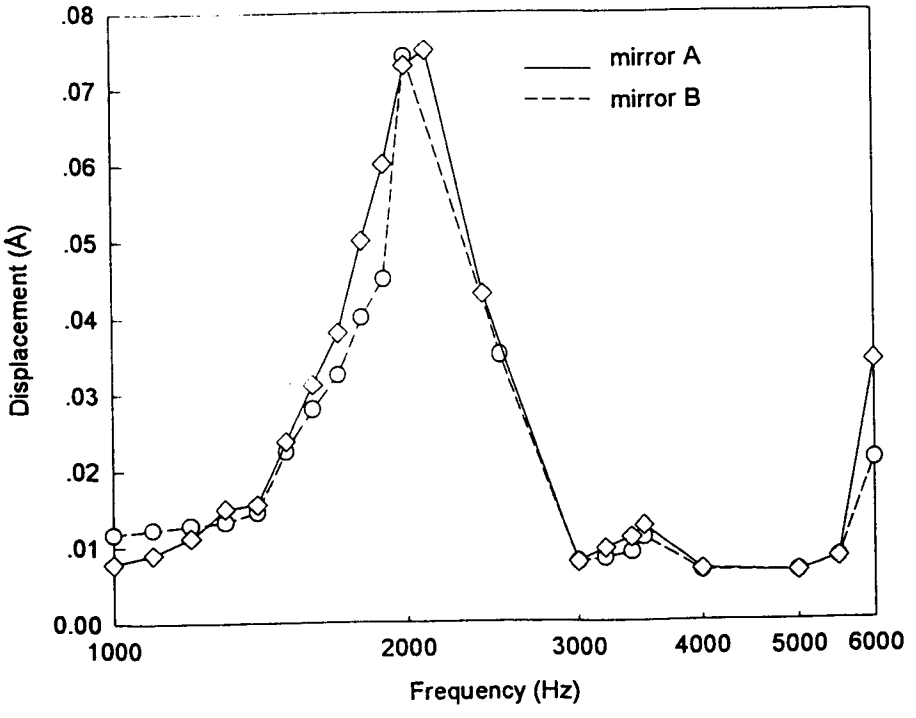

Fig.5.5 Frequency dependence of the measured displacement in AlN film under shearing stress measured at a driving voltage of 20.0 V.

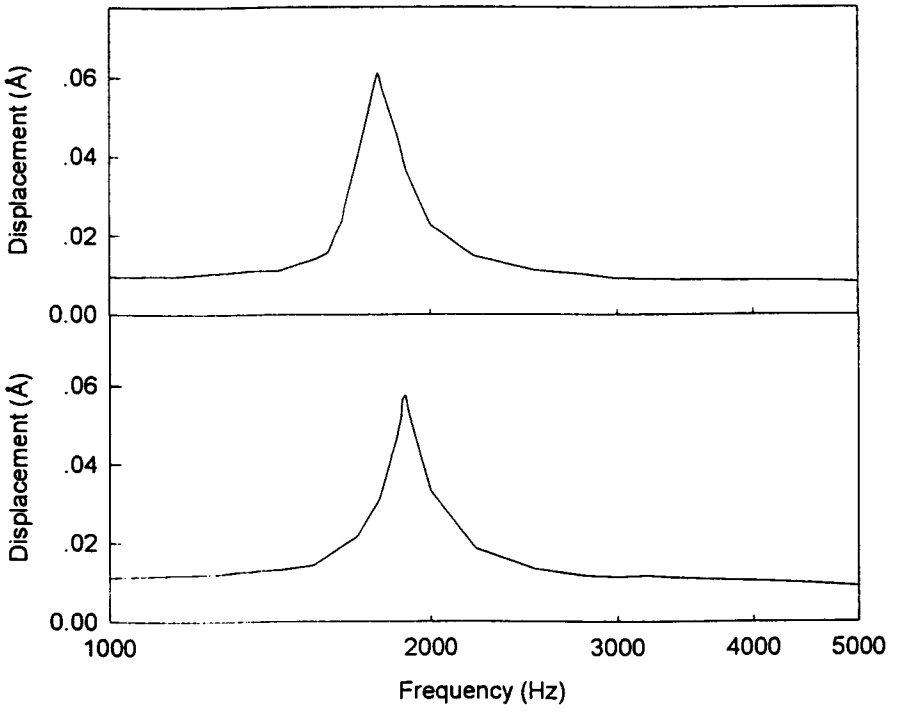

Fig.5.6 Shear displacement in an AlN film as a function of frequency. The driving voltage was 20.0 V. The mirror mass was 3.6×10^{-5} kg for the upper plot and 3.2×10^{-5} kg for the lower.

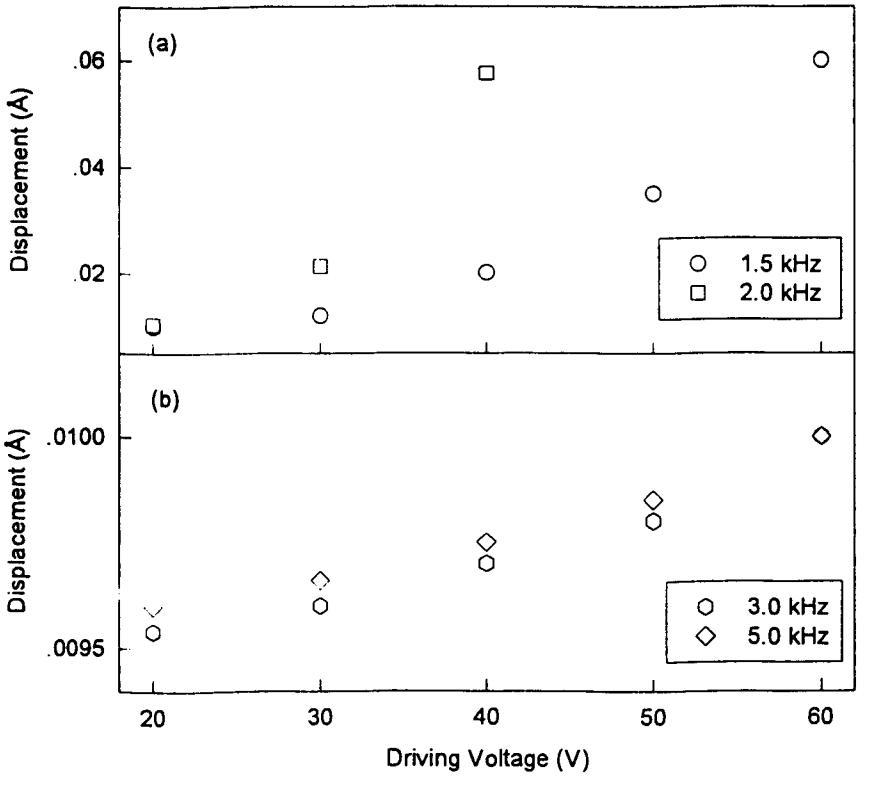

Fig.5.7 Shear displacement as a function of driving voltage for CVD grown AlN, (a) for frequency near resonance, and (b) in the range 3-5 kHz.

5.4.2 GaN

5.4.2.1 GaN with SiC substrate

Measurements were also made for the commercial 2.5 μm GaN wafer on SiC. A mirror of mass 4.2×10^{-5} kg was glued onto the film. The frequency dependence of the measured displacement, and variations of displacement with driving voltage were as shown in Fig.5.8. The minimum field required in order to produce an observable output was 24 MVm^{-1}. The first and the second resonances were observed at 1750 Hz and 6 kHz, respectively. The measured displacements between the two resonances were substantially constant. At 3 kHz the displacement was observed to be linear with driving voltage.

5.4.2.2 GaN with sapphire substrate

Measurements were also made on a commercial, 1.3-μm thick GaN on sapphire wafer. A mirror of mass 4.3×10^{-5} kg was glued to the film. The results are shown in Fig.5.9. The fundamental resonance in this case was at 1920 Hz. As before, the response in the region between the resonance peaks was quite uniform.

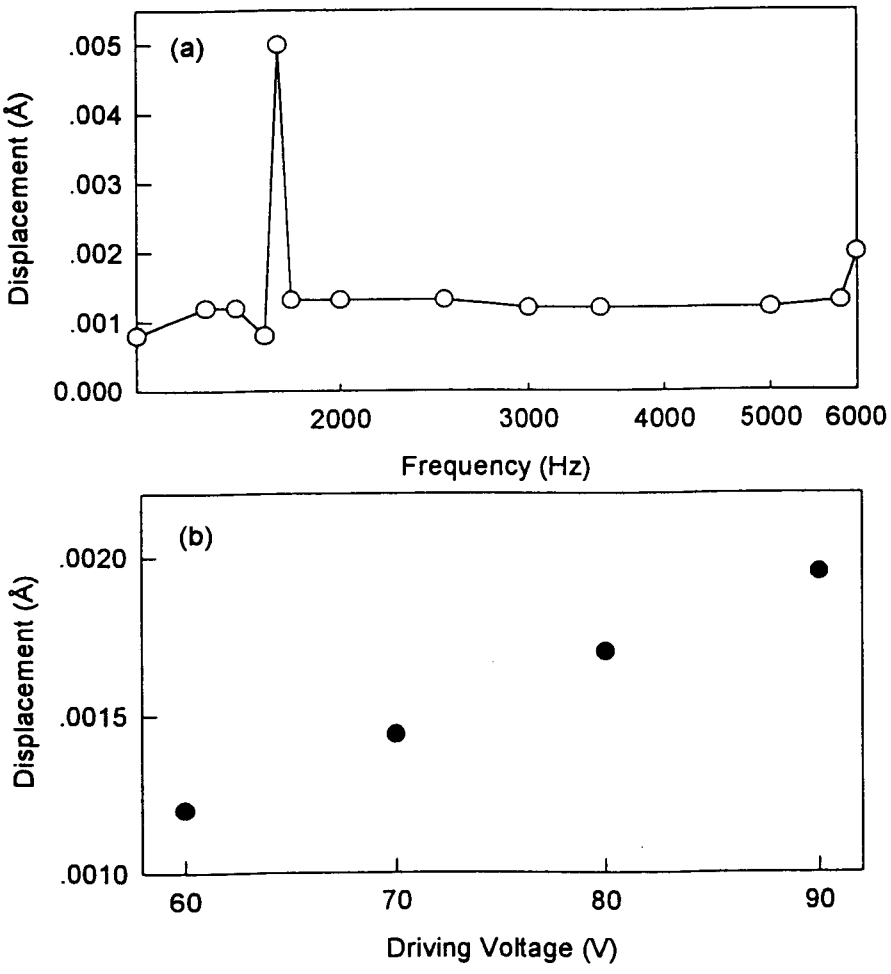

Fig.5.8 (a) Variation of displacement with frequency measured at a driving voltage of 60.0 V, and (b) variation of displacement with driving voltage measured at 3 kHz for the commercial GaN on SiC wafer.

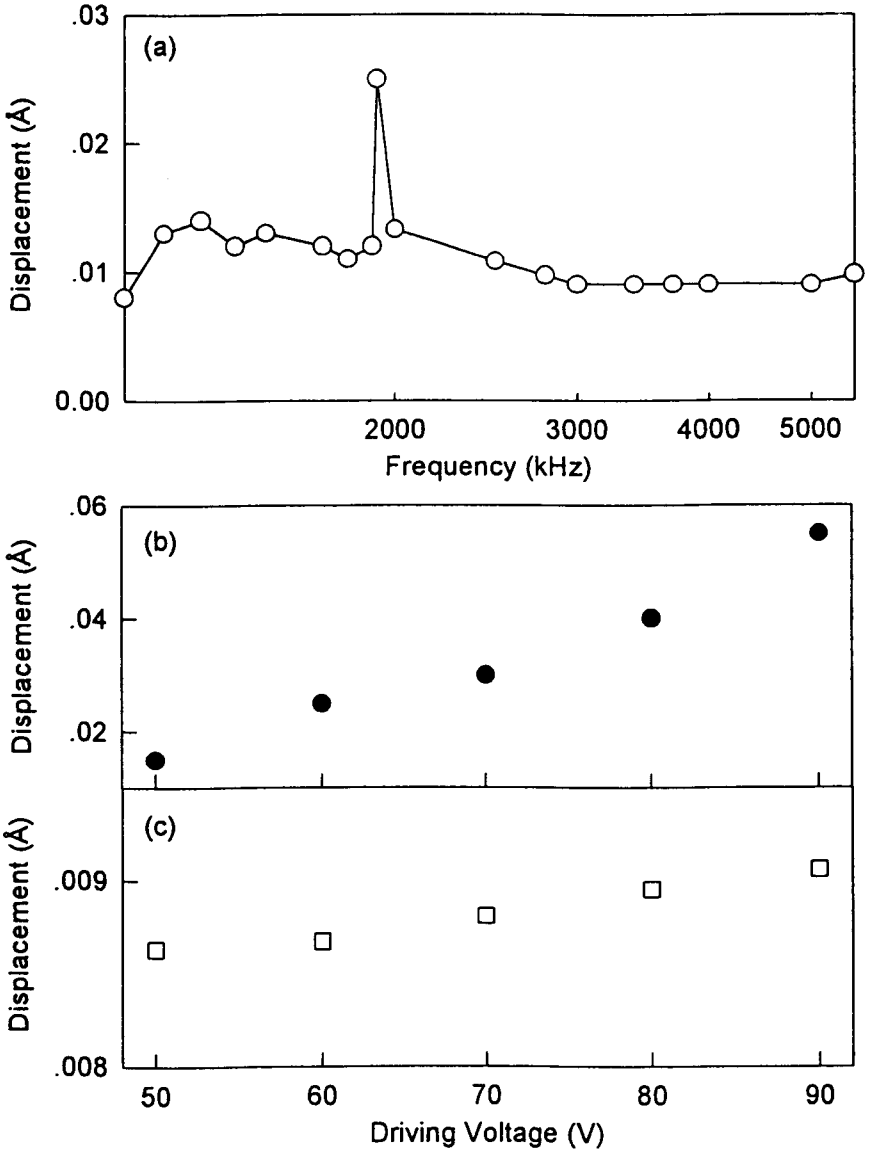

Fig.5.9 (a) Variation of displacement with frequency measured at a driving voltage of 30.0 V, (b) variation of displacement with driving voltage at 1.5 kHz, and (c) 3 kHz for the commercial GaN on sapphire wafer.

5.5 Discussion

In the d_{33} measurement (chapter 4), lateral clamping of the film by the substrate reduces the measured value of d_{33}. For the case of d_{15}, the application of the field in the 1-direction results in an angular movement of the film in the 31 plane, but no change in dimensions in the 21 plane. As a consequence, lateral clamping by the substrate was assumed to have negligible effect on the measured d_{15}.

The non-uniformity of the electric field distribution in the d_{15} measurement remains an issue which was not solved during the course of the present project. However it should be noted that the piezoelectric strain varies linearly with the field. This would normally mean that the strain would vary as the field variation shown in Fig.5.3b. However the film must remain intact, so in reality the strain would be reasonably constant across the sample surface and, as a result, internal stresses would be generated. The result of these stresses would be to reduce the strain near the electrodes and increase it away from the electrodes. Whether this would produce a uniform, average strain across the sample which would be related to the average field by d_{15} must remain a matter for conjecture at this stage. There are additional complexities in the polycrystalline samples, arising from interfacial effects.

The assumptions made in the present case seem to represent a reasonable approach, in order to take the first steps in measuring d_{15} by the interferometric technique.

An additional item of interest in the d_{15} measurement is the orientation of the '1' axis. In the measurements described, it may be noted that no attention was paid to aligning the electrodes in such a way as to generate a field along the '1' axis. Indeed even ascertaining the direction of the '1' axis in the samples was not carried out. For the polycrystalline samples there is no

evidence even to suggest that the '1' axes of all crystallites point in the same direction. However, in the 6*mm* class, the coefficients d_{15} and d_{24} are equal. This means that whether the field is applied in the '1' or '2' direction does not matter. Indeed, given the symmetry of the 6*mm* class, a field applied in any direction in the 1-2 plane, will generate a movement of the free sample surface parallel to the field and of a magnitude in accordance with d_{15}. For this reason the IEEE Standard on Piezoelectricity gives the direction of the +x axis for the 6*mm* class as arbitrary.

5.5.1 The d_{15} coefficient of AlN

The d_{15} coefficient of each of the films was calculated from the slope of the displacement vs driving voltage plots. The data used for these plots was that measured in the frequency range from 3 kHz to 5 kHz.

For AlN/Si (Fig.5.7b), the slope was $(1.0 \pm 0.1)\times10^{-15}$ mV^{-1}. This slope leads to a value of (-3.6 ± 0.1) pmV^{-1} for the d_{15} coefficient.

This value is about 12% lower than that reported by Tsubouchi et al. (1981). Given the difficulties noted above, i.e., non-uniform field and polycrystalline sample, the agreement is an encouraging indicator of the validity of the method. The samples used by Tsubouchi et al. (1981) were single crystal AlN film

5.5.2 The d_{15} coefficient of GaN

For GaN/SiC (Fig.5.8b), the slope of the displacement vs voltage plot was found to be $(2.0 \pm 0.1)\times10^{-15}$ mV^{-1}. This leads to a value for the d_{15} coefficient of GaN of (-3.0 ± 0.1) pmV^{-1}.

For GaN/sapphire (Fig.5.9c), the slope was 1.2×10^{-15} mV^{-1}, leading to a d_{15} value of (-3.2 ± 0.1) pmV^{-1}.

It may be thought that the low resistance SiC substrate would lead to errors by effectively short-circuiting the field in the high resistivity GaN. It should be emphasised again that the driving voltage was obtained from a low impedance generator and the voltage was monitored at the electrodes themselves. Thus it was always the case that the line integral of the field along the film between the electrodes was equal to the potential difference between the electrodes. The only question relates to the uniformity of this field. Indeed in this context it may be that the low resistance substrate is beneficial, in that it would constitute a distributed, low impedance voltage divider for the film.

Against this background, the value of d_{15} for GaN was taken as an average of the values from the two samples, with sufficient uncertainty to include both values. The value proposed is thus (-3.1 ± 0.1) pmV^{-1}. This value was obtained from samples prepared from commercial wafers having single crystal orientation. Thus the interfacial effects, present in polycrystalline samples, are not a factor.

5.6 Conclusions

The interferometric technique has been used to measure the shear piezoelectric coefficient d_{15} for AlN and GaN. This work represents the first application of this technique to measure this particular coefficient. Some difficulties still remain to be solved in the method. In particular the effects of mirror resonance need to be addressed and a more accurate determination of the field distribution in the film is required.

The measured d_{15} for AlN was found to be (-3.6 ± 0.1) pmV^{-1}. This compares with a value of -4.08 pmV^{-1}, measured from SAW wave velocities by Tsubouchi et al.(1981).

The measured d_{15} for GaN was found to be (-3.1 ± 0.1) pmV^{-1}. This represents the first reported measurement of this coefficient.

6

Electrostriction in Gallium Nitride, Aluminium Nitride and Gallium Arsenide

6.1 Introduction

Electrostriction is a quadratic coupling of strain and field, which is present in all materials, including gases and liquids. Interest in the phenomenon of electrostriction has been increased recently because of the development of new ceramic materials with very large electrostrictive coefficients. Many applications take advantage of these ceramics as sensors, actuators and tunable transducers (Sundar and Newnham, 1992).

It has been suggested that electrostriction is the origin of piezoelectricity in at least some ferroelectric materials, such as barium titanate ($BaTiO_3$) and the PVDF family of ferroelectric polymers (Zhenyi et al., 1994 ; Devonshire, 1954). In these materials, the spontaneous polarization has been thought to bias the inherent electrostrictive response, thus producing a piezoelectric effect. It seems that there has been no work done on the electrostrictive properties of the compound semiconductors. It was

thus of some interest to see if a significant part of the electromechanical effects in these materials was electrostrictive in nature. The investigation of electrostriction is of more than passing interest, given the potential for the application of these materials in semiconductor devices.

The present work aims to investigate for the first time electrostriction in the III-V compound semiconductors: GaN, AlN and GaAs.

Electrostriction can be measured either using the direct effect, in which the strain induced by an applied field is measured, or the inverse effect, in which the change of dielectric permittivity under mechanical stress is measured. As in the case of piezoelectricity, thermodynamics requires that the coefficients for the direct and the inverse effects are equal.

In the present work the direct effect was exploited, using the interferometer described in chapter 2 to measure the electrostrictive strain. This type of interferometer has previously been used successfully in measuring the electrostrictive coefficients of ferroelectric ceramics (Zhang et al., 1988).

6.2 Background.

6.2.1 Fundamental relations.

Constitutive equations describing direct and inverse electrostriction can be derived from the Gibbs free energy and the elastic Gibbs function (Meng and Cross, 1985; Sundar et al, 1995). For simplicity, it is assumed that factors such as applied stresses, temperature, magnetic field, etc. are constant and that the strain is due entirely to the electric field. Under these conditions, the strain can be expressed in terms of the field as (Nye, 1985, p257):

$$S_{ij} = d_{ijk}E_k + M_{ijkl}E_kE_l \tag{6.1}$$

The first term on the right of equation (6.1) represents the inverse piezoelectric effect, with d_{ijk} being the components of the third-rank piezoelectric tensor. The second term gives the quadratic dependence of strain on the field. It is this term which is referred to as *electrostriction*, and the M_{ijkl} are the electrostrictive strain coefficients. M is a fourth rank tensor, which is symmetric in i and k, and in j and l. Electrostriction is distinguished from piezoelectricity by its quadratic dependence on the field. This quadratic dependence means that a reversal of the field will not reverse the direction of strain. In piezoelectric materials it is often only the linear term which need be considered, since the quadratic terms are usually relatively small. However, the quadratic term becomes important for crystals having a centre of symmetry, since they cannot be piezoelectric.

As is the case for piezoelectricity, a number of electrostrictive coefficients can be defined. These depend on which of the electrical or mechanical variables are taken to be independent. If the electric field is taken as the independent variable, then the electrostrictive constitutive equations for non-piezoelectric materials, written in full tensor notation are (Sundar et al, 1995):

$$S_{ij} = s^E_{ijmn}T_{mn} + M_{ijkl}E_kE_l \tag{6.2}$$

$$T_{ij} = c^E_{ijmn}S_{mn} + m_{ijkl}E_kE_l \tag{6.3}$$

where s^E_{ijmn} and c^E_{ijmn} are the compliance and the stiffness tensors for constant electric field. M_{ijkl} and m_{ijkl} are the electrostriction coefficients.

If polarization is used as the independent electrical variable, the equations become (Sundar et al, 1995):

$$S_{ij} = s^{P}_{ijmn} T_{mn} + Q_{ijkl} P_k P_l \tag{6.4}$$

$$T_{ij} = c^{P}_{ijmn} S_{mn} + q_{ijkl} P_k P_l \tag{6.5}$$

The constitutive equations for the inverse effect have the form (Sundar and Newnham, 1992):

$$E_k = -2Q_{ijkl} T_{ij} P_l = -2q_{ijkl} S_{ij} P_l \tag{6.6}$$

$$P_k = 2M_{ijkl} T_{ij} E_l = 2m_{ijkl} S_{ij} E_l \tag{6.7}$$

Equations (6.6) and (6.7) are frequently written in a form which uses the permittivity or dielectric stiffness. Thus for example the first expression in equation (6.7) can be written as $\varepsilon_{kl} = 2M_{ijkl} T_{ij}$. From the constitutive equations listed above it is seen that there are four electrostrictive coefficients; *M, m, Q* and *q*. These coefficients are not all independent. For example, combining equations (6.2) and (6.3) gives $M = -sm$, or $m = -cM$. Similarly, from equations (6.4) and (6.5), $Q = -sq$, or $q = -cQ$. In the present work, only one of the four electrostrictive coefficients is of concern: the electrostrictive strain coefficient *M*.

While the electrostrictive coefficients are fourth rank tensors, their symmetry means that they can be described using the reduced matrix notation outlined in chapter 1. The first two and last two subscripts are combined into one, using the convention described in section 1.2.5. The matrix element M_{mn} is obtained from the tensor component M_{ijkl} by the rules (Nye, 1985, p248) :

$M_{mn} = M_{ijkl}$, when n = 1,2, or 3

$M_{mn} = 2M_{ijkl}$, when n = 4,5, or 6.

Table 6.1 Examples of electrostriction measurements reported in the literature.

Reference	Direct Effect
Misawa et al.(1976)	Electrically induced stress in SiO_2 film measured by using a laser interferometer; $M_{13} = 1.4 \times 10^{-22}$ m^2V^{-2}.
Zhang et al. (1988)	Electrically induced strains in PMN* measured by using a single-beam Michelson interferometer; the M_{11} value is 1.03×10^{-16} m^2V^{-2}.
Van Sterkenberg(1991)	Electrically induced strains in eight alkali halides measured by using a double-beam Michelson interferometer; M_{11} , M_{12} and M_{44} values are of the order of 10^{-21} m^2V^{-2}.
Zhenyi et al. (1994)	Electrically induced strains in PVDF measured by using the double-beam Michelson interferometer; the M value is 1.63×10^{-17} - 3.3×10^{-17} m^2V^{-2}.
Wang et al.(1995)	Electrically induced strains in polyurethane elastomers measured by using the laser interferometer; M_{33} values are of the order of 10^{-18} m^4V^{-2}.
	Inverse Effect
Meng and Cross (1985)	Changes of the dielectric constant of CaF_2 with the stress applied by a compressometer; M_{11} , M_{12} and M_{44} are of the order of 10^{-20} m^2V^{-2}.
Sundar et al.(1995)	Changes of the dielectric constant with the stress applied by the compressometer; Q_{33} values are of the order of 10^{-3} m^4C^{-2} for ferroics , and 10^{-2} m^4C^{-2} for glass ceramics.

* Lead magnesium niobate

6.2.2 Crystal symmetry and electrostrictive coefficients

For wurtzite GaN and AlN, with 6*mm* symmetry, the nonzero electrostrictive coefficients, written in matrix notation, are M_{11}, M_{12}, M_{13}, M_{31}, M_{33} and M_{44} (Nye, 1985, p251). The normal interferometer arrangement applies a field in the 3 direction and also measures the displacement in this direction. It is thus the M_{33} coefficient which is most readily measured, since $S_3 = M_{33}E_3^2$ (equation (6.2)).

For zincblende GaAs, with $\bar{4}3m$ crystal symmetry, the nonzero electrostrictive coefficients are M_{11}, M_{12} and M_{44} (Nye, 1985, p251). The subscripts here refer to the conventional crystal axes for GaAs. In order to provide a complete set of electrostrictive coefficients of GaAs, samples with [100] and [110] orientations are required. The coefficients M_{11} and M_{12} can be directly determined by measuring the longitudinal and transverse strain in a [100] sample. M_{44} can be obtained by measuring the longitudinal strain in the [110] direction for a field in the same direction (Meng and Cross, 1985 ; van Sterkenburg, 1991).

For [110] and [111] oriented crystals, new longitudinal coefficients can be defined. The longitudinal electrostrictive coefficient for a [110] sample is defined as:

$$M'_{110} = \frac{1}{2}M_{11} + \frac{1}{2}M_{12} + \frac{1}{4}M_{44} \qquad (6.8)$$

For a sample with [111] orientation, the longitudinal electrostrictive coefficient M'_{111} is defined as:

$$M'_{111} = \frac{1}{3}M_{11} + \frac{2}{3}M_{12} + \frac{1}{3}M_{44} \qquad (6.9)$$

The samples used in the present work had [111] orientation. The electrostrictive coefficient measured is thus that defined in equation (6.9).

6.3 Electrostriction Measurements

For crystals lacking a centre of symmetry, such as the materials studied in this work, the electrically induced strains will contain both piezoelectric and electrostrictive components. While there are also components of the strain which involve even higher orders of the field, these will be small and are neglected. The strain would thus be given by equation (6.1).

Since the field and displacement are always in the 3 direction, it is possible to dispense with the tensor notation in equation (6.1), and to write

$$S = dE + ME^2 \tag{6.10}$$

If a field consisting of a DC bias field E_b and an AC component E_{AC} is applied, then the strain will be

$$S = d(E_b + E_o \cos\omega t) + M(E_b + E_o \cos\omega t)^2 \tag{6.11}$$

where $E_{AC} = E_o \cos\omega t$.

This expression can be expanded to

$$S = E_b(d + M) + \frac{1}{2}ME_o^2 + (d + 2ME_b)E_o \cos\omega t + \frac{1}{2}ME_o^2 \cos 2\omega t \tag{6.12}$$

The first two terms on the right of equation (6.12) represent a steady strain. In the interferometer measuring system such steady strains are compensated by the feedback arrangement and so are not recorded at the output. Superimposed on this steady strain is a varying strain which has the same frequency as the driving voltage (the third term in equation (6.12)), together with a strain which has double the driving frequency (the fourth term). It is the third term in equation (6.12) which is of major interest here. This term indicates that both the piezoelectric and the electrostrictive coefficient could be obtained by measuring the strain component with

frequency ω, for a range of bias fields. The value of M could also be obtained by measuring the 2 ω component of strain.

The way in which a varying bias field affects the amplitude of the strain in an electrostrictive (i.e. quadratic) material, is illustrated in Fig.6.1.

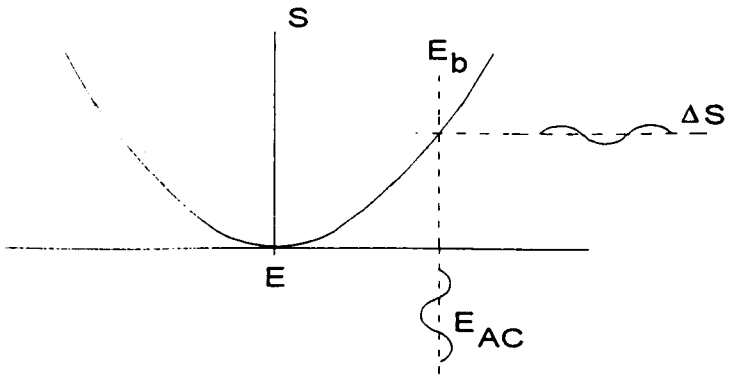

Fig.6.1 Illustration showing the way in which a DC bias can affect the strain in an electrostrictive material.

It is convenient to follow the procedure of Zhenyi et al. (1994), and define a thickness coefficient d_T, given by

$$d_T \equiv \frac{\partial S}{\partial E_{AC}} = d + 2ME_b \qquad (6.13)$$

The thickness coefficient can be obtained by measuring the variation in strain with applied field E_{AC}, for a fixed value of the bias field. The displacement for a constant driving field can be measured for a range of bias fields. Plotting d_T against E_b should give a straight line whose slope is $2M$ and whose intercept on the d_T axis is d.

6.4 Other Quadratic Effects

Other phenomena can give rise to quadratic electromechanical effects, and these need to be considered in the electrostriction measurements.

6.4.1 Maxwell stress

When an electric field is applied to a sample, then the electrostatic attraction between the electrodes generates a stress in the material. The strain which results from this stress varies quadratically with the field and also depends on the mechanical compliance of the material.

The strain S_3^M, resulting from the Maxwell stress, is given by equation (6.14) (Wang et al., 1995). If all fields and strains are in the same direction, it is possible to simplify the expression by omitting the tensor notation.

$$S^M = -\frac{1}{2}\varepsilon_o \varepsilon s E^2 \qquad (6.14)$$

where ε_0 is the permittivity of free space (8.854×10^{-12} $C^2N^{-1}m^{-2}$), ε is the dielectric constant, and s the compliance of the material.

6.4.2 Thermal expansion

When a voltage is applied to a material, current flows in the material and some heating results. The amount of heating varies quadratically with the applied voltage. This heating in turn leads to thermal expansion, which will also vary quadratically with the applied voltage. An exact calculation of the magnitude of the effect becomes difficult, because of the heat losses involved, however a rough estimate is readily made.

It is assumed that the heat dissipated in each half-cycle of the applied voltage goes entirely into heating the sample. This energy is:

$$\Delta Q = \frac{V_o^2}{2R}\frac{t}{2} = \frac{V_o^2}{4Rf} \tag{6.15}$$

where V_0 is the peak value of the applied voltage, R is the sample resistance, t is the period and f is the frequency.

The resulting change in temperature will be

$$\Delta T = \frac{\Delta Q}{mc} = \frac{V_o^2}{4Rfmc} \tag{6.16}$$

where c is the specific heat capacity and m is the mass of the sample.

If the thickness of the sample is t and the thermal expansion coefficient is α, then the expansion resulting from the heating will be

$$\Delta t = \frac{\alpha t V_o^2}{4Rfcm} \tag{6.17}$$

This calculation will over-estimate the expansion, since heat losses to the surroundings will reduce the amplitude of the temperature fluctuations.

6.5 Experimental Techniques

6.5.1 Sample preparation

Electrostriction measurements were carried out on the polycrystalline GaN, the CVD grown AlN and the commercial wafers of GaN on SiC. The electrodes used for all of these materials were evaporated aluminium. Samples were also prepared from the n^+-[111]B GaAs wafer. Aluminium, gold, and indium electrodes were used for the GaAs. The measurement of the piezoelectric coefficients of these materials is described in chapters 3, 4 and 5.

6.5.2 Interferometer setup

Samples were mounted in the interferometer in the same way as for the d_{33} measurements described in chapters 3 and 4. The signal generator was used as the source of the AC driving voltage, and the generator offset was used to supply the bias field. The strains at the driving frequency, were measured for a range of bias and driving voltages.

Strains at twice the driving frequency were also measured, to check that the value of M from the third and fourth terms in equation (6.12) were consistent. The 2ω term was measured by setting the lock-in amplifier to measure the second harmonic.

6.5.3 Dielectric measurement

A prediction of the likely size of the Maxwell stress effect requires a knowledge of dielectric constant of the film. For this reason, the dielectric constant for each film was measured.

The capacitance of the films were measured using an HP 4192A impedance Analyzer. The sample arrangement was as for the I-V measurements described in chapter 4. The dielectric constant was calculated, by assuming that the sample approximated to a simple parallel plate capacitor:

$$\varepsilon_r = \frac{Ct}{\varepsilon_o A} \tag{6.18}$$

where t is the thickness of the film, A the electrode area and C the measured capacitance.

6.6 Experimental Results

6.6.1 Dielectric constant

A typical dielectric plot for the single crystal GaN film is shown in Fig.6.2. The capacitance of this film over the frequency range from 1 kHz to 100 kHz was 0.1 nF and did not vary greatly with frequency. Given the 2.5 μm film thickness and 2 mm electrode diameter, this gives a dielectric constant of 9.0. Over the same frequency range, the dielectric constants for polycrystalline GaN and AlN films were 7.2 and 7.9 respectively.

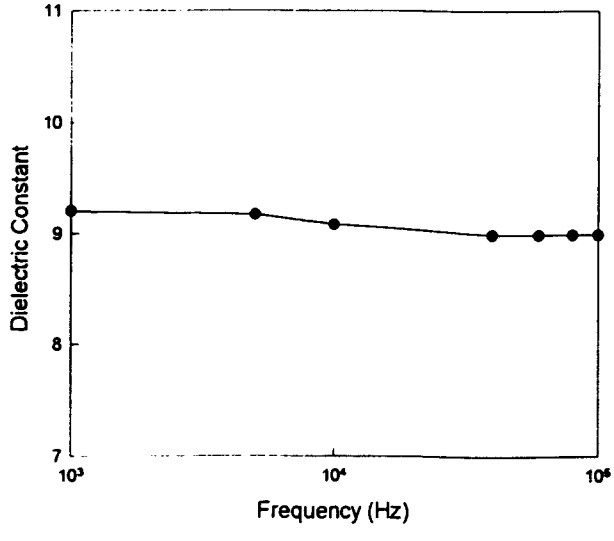

Fig.6.2 Plot of dielectric constant as a function of frequency for the commercial GaN wafer.

6.6.2 Results for GaN and AlN

Figs.6.3, 6.4 and 6.5 show the actual surface displacement and calculated thickness coefficient for the polycrystalline GaN, polycrystalline AlN, and the commercial GaN wafer. The operating frequency for all measurements was 2.0 kHz, and the driving voltages used were in a range of

2.0 V to 20.0 V. For each sample, the displacements at the driving frequency were measured. The thickness coefficient was calculated from the measured displacements using equation (6.13).

All samples show a minimum displacement at zero bias field. Symmetry in the detected displacement for positive and negative bias was observed in the polycrystalline GaN and AlN films (Figs.6.3 and 6.4). The plots of d_T vs bias field at each driving voltage for polycrystalline GaN and AlN are reasonably linear over the range of the applied field (Figs.6.3b and 6.4b).

For the commercial GaN wafer, it is apparent that the displacements are not symmetric, but tend to show a larger increase for negative bias than for positive (Fig.6.5a). The plot of d_T vs bias field (Fig.6.5b) was not linear. For a given bias, this film possessed the largest d_T, while it was smallest in AlN.

(a)

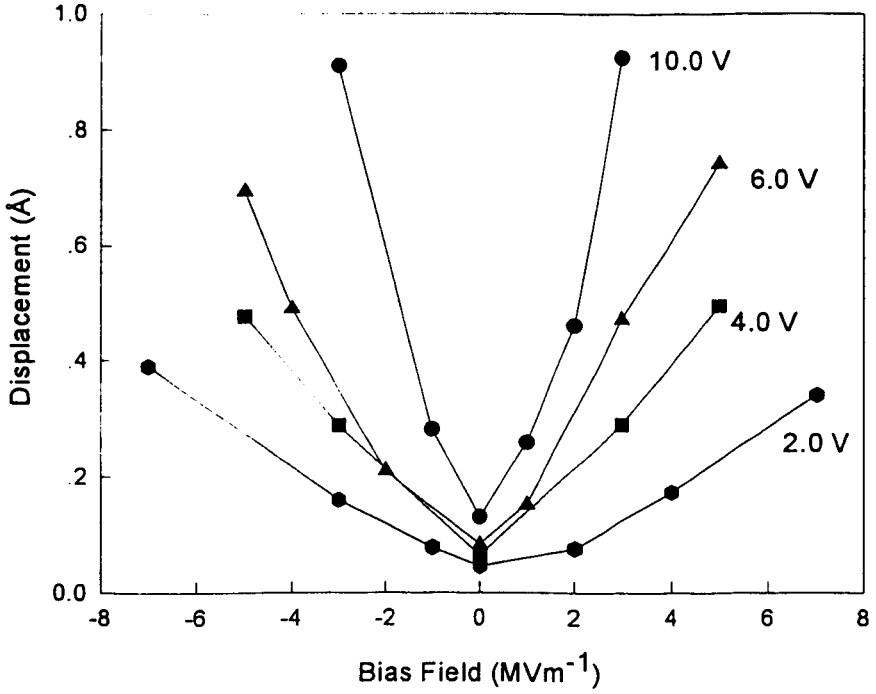

(b)

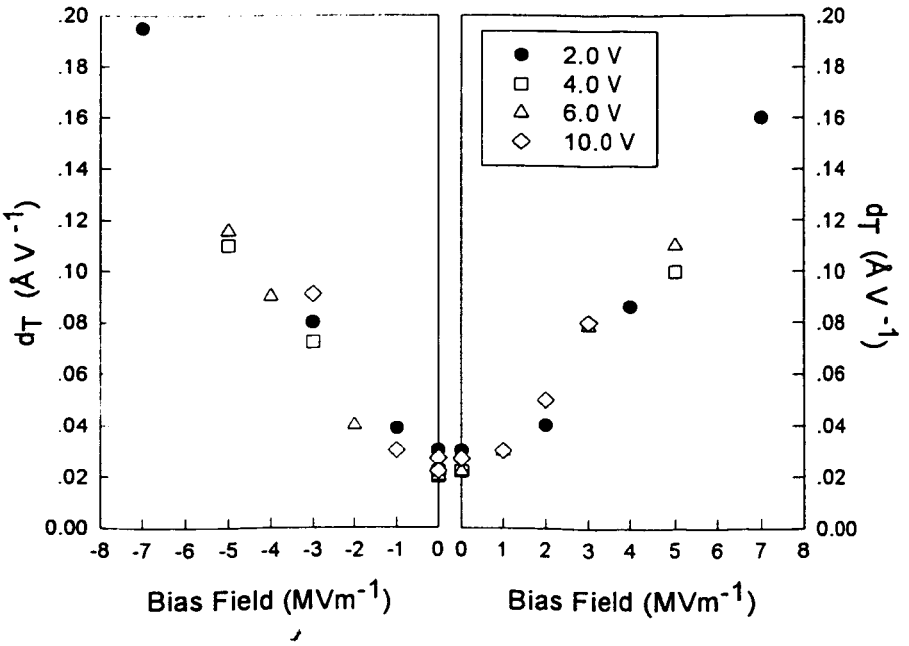

Fig.6.3 Results for the polycrystalline GaN film measured at 2 kHz.

(a) Variations of displacement with bias field for four different driving voltages. (b) Plots of the thickness coefficient for negative (left) and positive (right) bias field.

(a)

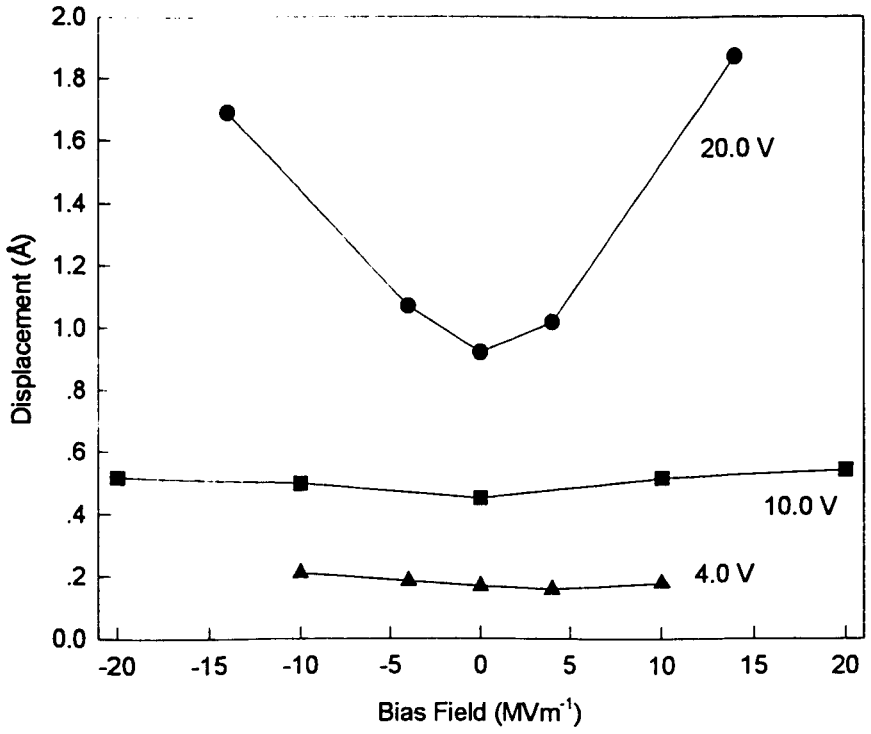

(b)

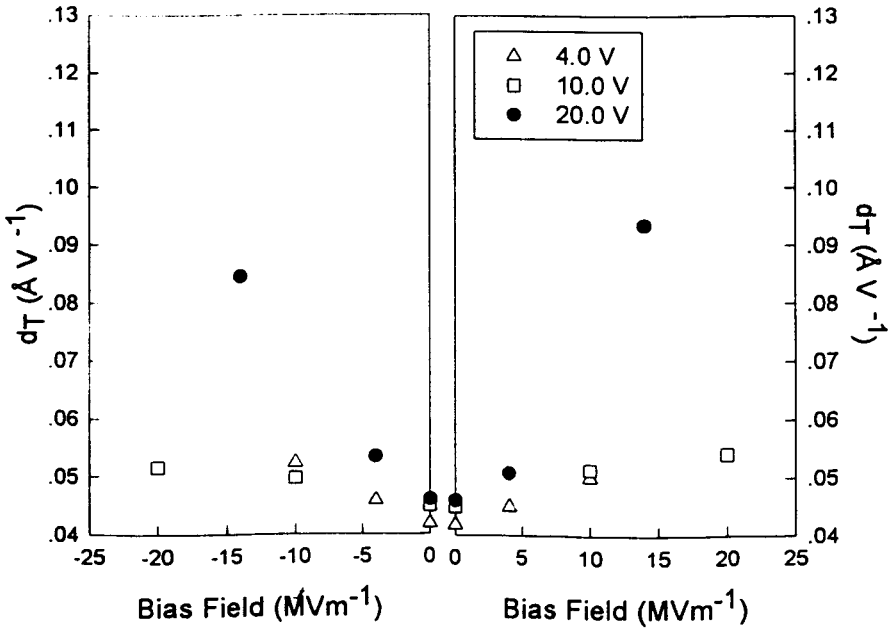

Fig.6.4 Results for the polycrystalline AlN film measured at 2 kHz.

(a) Variations of displacement with bias field for three different driving voltages. (b) Plots of the thickness coefficient for negative (left) and positive (right) bias field.

(a)

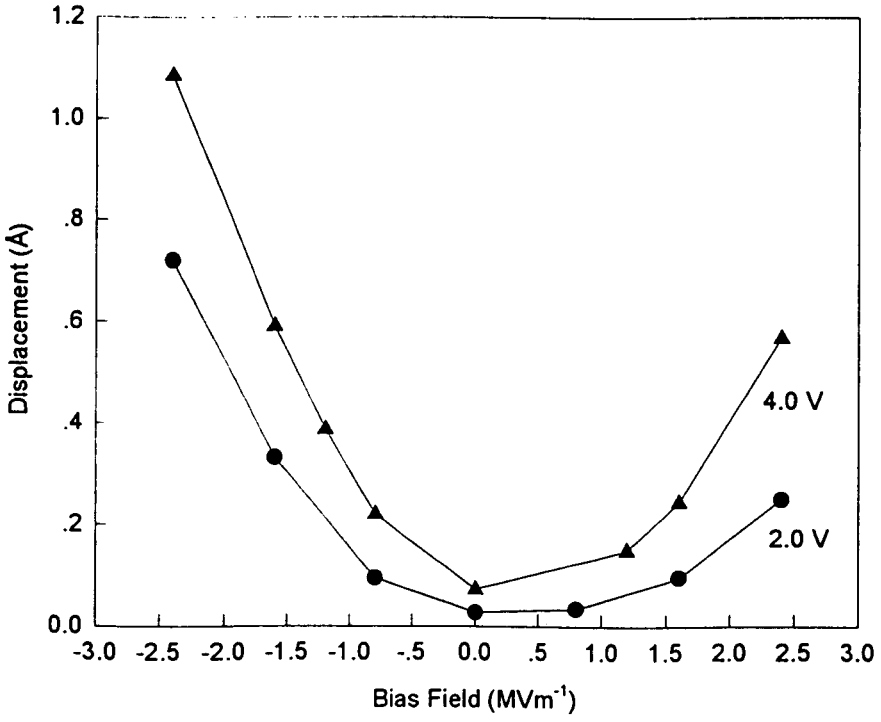

(b)

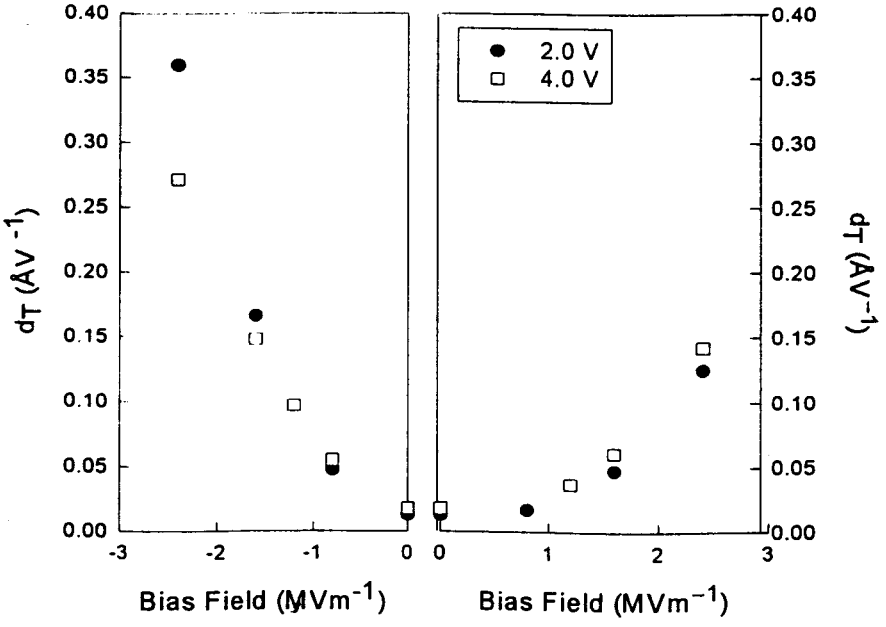

Fig.6.5 Results for the commercial GaN wafer measured at 2 kHz.

(a) Variations of displacement with bias field for two different driving voltages.

(b) Plots of the thickness coefficient for negative (left) and positive (right) bias field.

6.6.3 Results for GaAs

Similar measurements were made on [111]B GaAs samples, with Al, Au, and In electrodes. The results are shown in Figs.6.6 to 6.8. It is interesting to observe that the response varied significantly with the electrode material.

From Figs.6.6 and 6.7, where the electrodes were aluminium and gold, respectively, the measured displacements show a larger increase for negative bias than for positive. It is also evident that the minimum displacement did not occur when the bias field was zero. This offset is probably due to voltage barriers at the electrode-GaAs contacts which behaved differently under zero, positive, and negative bias. For the indium electrode (Fig.6.8), the minimum displacement did coincide with zero bias, although the response was still asymmetric.

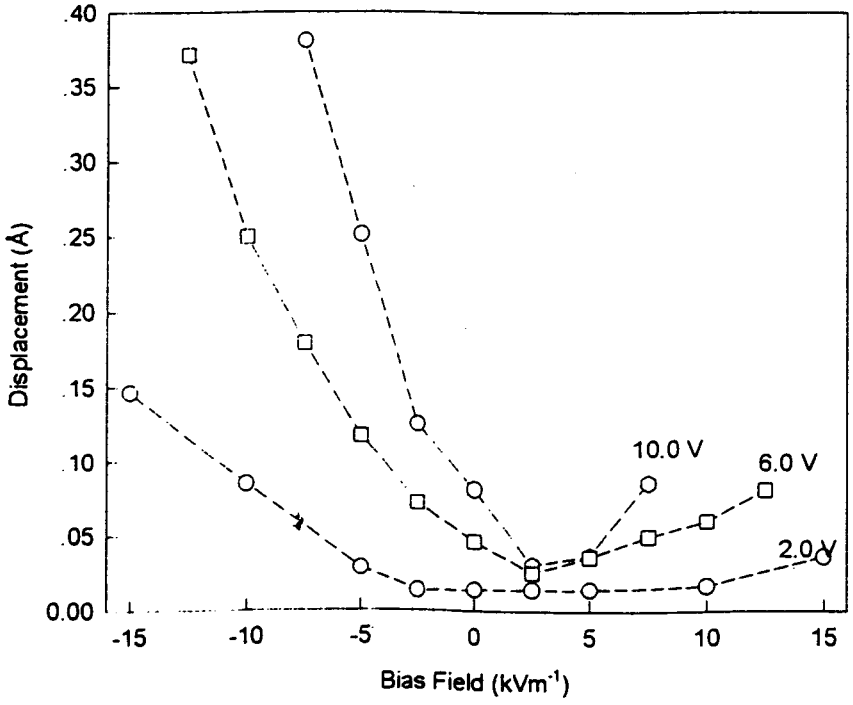

Fig.6.6 Variations of displacement with bias for [111]GaAs with Al electrode.

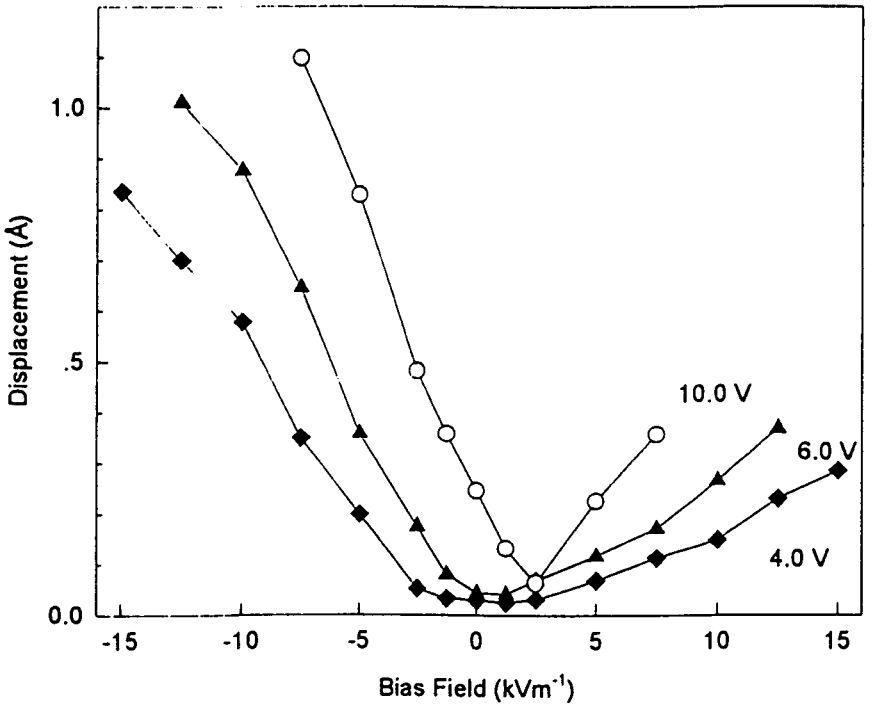

Fig.6.7 Variations of displacement with bias for [111]GaAs with Au electrode.

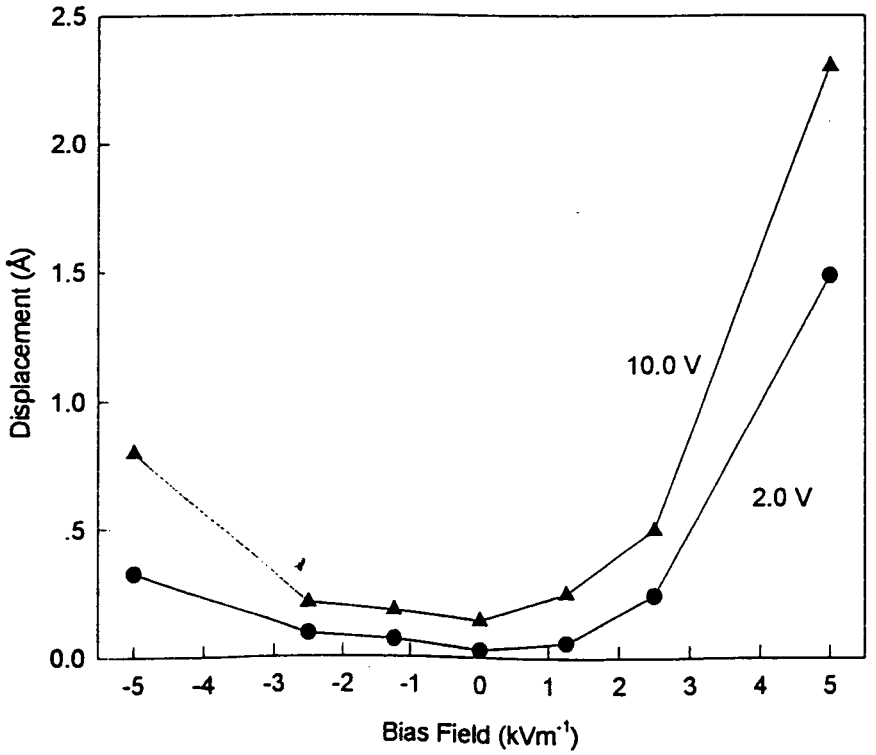

Fig.6.8 Variations of displacement with bias for [111]GaAs with In electrode.

6.7 Discussion

6.7.1 Maxwell stress effect contribution

In order to calculate the contribution due to Maxwell stress using equation (6.14), values of the compliance and dielectric constant are required. Values for compliances were obtained from the literature, while values for dielectric constants were those indicated in section 6.6.1. Table 6.2 gives the Maxwell stress contributions to M_{33} for each of the materials, calculated directly from equation (6.14).

Table 6.2 Estimation of Maxwell Stress contribution to the M_{33} coefficients.

Sample	$s^*(10^{-12}\ m^2N^{-1})$	ε_r	$-1/2\varepsilon_0\varepsilon_r s(10^{-23}\ m^2V^{-2})$
Polycrystalline GaN	2.8	7.2	-8.9
Polycrystalline AlN	2.6	7.9	-9.1
Single crystal GaN	2.8	9.0	-11.2

* Measured values for GaN taken from Polian et al. (1996), and for AlN from MacNeil et al. (1993).

In order to assess the contribution of Maxwell stress to the overall electromechanical response equation (6.13) should be recalled. This indicates that the values in table 6.2 should be compared with the slopes of Figs. 6.3b, 6.4b and 6.5b. The slopes in these figures have an order of magnitude of $10^{-17}\ m^2V^{-2}$. The Maxwell stress is thus several orders of magnitude smaller than the total observed response and may safely be neglected for the materials being studied here.

6.7.2 Thermal expansion contribution

Equation (6.17) was used to calculate the effect of thermal expansion in the polycrystalline GaN and AlN films. Table 6.3 summarises the required data for GaN and AlN. The thermal expansion coefficients are direction dependent and values are given for expansion along the a and c crystallographic axes. The room temperature specific heat of AlN has a value of 0.732 $Jg^{-1}K^{-1}$(Berger, 1997, p123). This value was also used for GaN.

Table 6.3 Material parameters of GaN and AlN for the thermal expansion calculation. α(a) is the thermal expansion coefficient in the direction of the a crystal axis, while α(c) applies to the c axis.

Sample	ρ^{*}(Ωcm)	$\rho_m{}^{**}$(gcm^{-3})	$\alpha(10^{-6}K^{-1})$
Polycrystalline GaN	$4.0x10^8$	6.1	5.6 (a), 3.2(c)***
Polycrystalline AlN	$9.4x10^{10}$	3.255	4.2 (a), 5.3 (c)****

*Chapter 4

**Berger (1997)

***Sheleg and Savastenko (1976)

****Yim and Paff (1974).

Using equation (6.17) and the relationships : $\rho = RA/t$ and $\rho_m = m/tA$, where A is the electrode area and t the thickness of the film, the thermal expansion contribution for the GaN and AlN films were calculated. The results of this calculation are shown in Fig.6.9. These results were calculated for an operating frequency of 2 kHz and a driving voltage in the range from 2.0 to 20.0 V. Since the resistivity of the film was much higher than that of the substrate (see chapter 4), it was assumed that there was negligible voltage

drop across the substrate. The contribution of thermal expansion of the substrate was thus neglected.

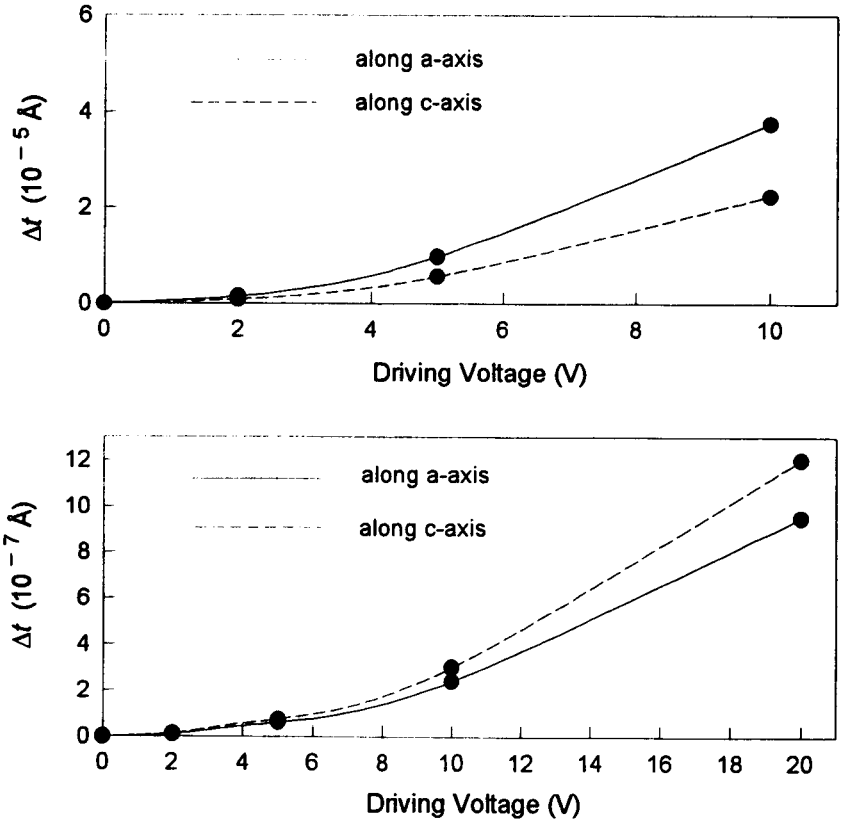

Fig.6.9 Lattice expansion as a function of driving voltage calculated at 2 kHz for the GaN (above), and AlN (below) films.

From Fig.6.9, it can be seen that the thermal expansion in GaN is much higher than in AlN. This is mainly due to the lower resistivity of the GaN films. Since the films have the c axis perpendicular to the plane of the film, it is the c axis expansion which is of most interest.

The calculated thermal expansion for GaN, at a driving voltage of 10 V is 4×10^{-5} Å. The total measured expansion of GaN (Figs.6.3 and 6.4) is of the order of 0.1 Å. For AlN the difference is even larger. It is apparent that

the contribution of thermal expansion to the measured surface displacement is negligible.

6.7.3 Size of electrostriction for GaN and AlN

The M_{33} coefficient for each film was calculated from the slope of the plot of d_T vs. bias field. All values of the slopes from these plots at different driving voltages with positive bias field were taken into account. The intercept of the d_T vs. bias field plot, which gives the piezoelectric coefficient, was also determined. Table 6.4 collects the M_{33} coefficient and the intercept value for each film. Values of the measured d_{33}, as reported in chapter 4, are included in this table for comparison.

Table 6.4 The M_{33} coefficients (in units of 10^{-18} m^2V^{-2}), the intercept values (in units of pmV^{-1}), and the d_{33} coefficients obtained from chapter 4 (in units of pmV^{-1}) measured for all films used.

Film	M_{33}	Intercept Value	d_{33}
Polycrystalline GaN film	0.9	1.9	2.0
Polycrystalline AlN film	0.2	4.3	4.0
Single-crystal GaN	3.7*	0.1	2.8

* Evaluated from the linear portion of the plots in Fig.6.5b.

From the above table, the measured M_{33} coefficient is highest in the single crystal GaN film. This value is, however, smaller than those of PMN and PVDF (table 6.1). For polycrystalline films, there is no significant difference between the value of d_{33} determined from the intercepts and the values measured directly (chapter 4). For the single crystal GaN film, it seems

that there is an additional crystal field which tends to interact with the applied bias. Therefore, the intercept value is not a reliable measure of the d_{33} coefficient for this film.

6.8 Conclusions

It has been demonstrated that there is a significant quadratic electromechanical response in all three materials; GaN, AlN, and GaAS. Two possible mechanisms, namely Maxwell stress and thermal effects have been shown to be too small to explain the observed response.

Of the materials studied here, the polycrystalline GaN is the only one which adheres reasonably well to the predictions of equation (6.12). The plots of d_T against E_b are reasonably linear, and do not show large variation with driving field. The value of d_{33} obtained from extrapolation also agrees with the measurements of chapter 4. The symmetric form of Fig.6.3 suggests that the internal crystal field does not exert a significant biasing effect on the response. This in turn leads to the conclusion that the response at zero bias is piezoelectric in nature, and not a biased electrostrictive response.

In polycrystalline AlN there there appears to be a threshold effect. For driving voltages up to 10 V there is little evidence of electrostriction (as evident from the lack of variation of displacement with E_b). However a driving voltage of 20 V shows the type of variation expected from a sample exhibiting significant electrostricion. The reason for this threshold effect is not clear, but may be associated with the layer of aluminium oxide on the surface of these samples.

The single crystal GaN shows a non-linear reponse, hence the d_{33} value, obtained by extrapolating an attempted linear fit, is quite inconsistent

with the d_{33} measured in chapter 4. Again the reason for the discrepancy is not apparent.

The most reliable results for GaAs are those obtained with the indium electrodes. Even those show considerable asymmetry. The reason for this is not clear, but may be a consequence of a non-ohmic contact at the sample surface, even though the indium electrodes appeared to be reasonable.

Overall, the conclusions which follow from the results presented here must be regarded as tentative at this stage. However it appears that these materials do have both a piezoelectric response and a significant electrostrictive reponse. The results are significant because of the application of these materials in semiconductor devices. Accurate modelling of such devices will require the inclusion of both effects.

7

Summary and Prognosis

7.1 Main Conclusions

The present work utilizes the inverse piezoelectric effect to measure the piezoelectric coefficients in three III-V compound semiconductors; GaAs, GaN, and AlN. A Michelson interferometer was used to measure the mechanical strains caused by the application of an electric field. The following conclusions arise from the investigation:

(1) The interferometric technique is a useful technique for measuring piezoelectric coefficients, especially in materials where the coefficients are less than 10 pmV^{-1}. Both the magnitude and sign of the coefficient can be determined. In materials in which the sign of the coefficient is defined, the measurement gives a simple method for determining the positive direction of the crystal axes. Measurements of mechanical displacements with a resolution of about 10^{-3} Å can be readily achieved. Limitations in the measurement arise mainly from external mechanical vibrations, although the effects of these can

be minimised by careful design of the mounting of the optical components and the sample.

(2) This is the first time that the interferometric technique has been used to determine the magnitude and sign of the d_{14} coefficient for GaAs. The electrode material and dimensions play a role in the observed piezoelectric response. An electrode consisting of annealed indium, with a thin layer of gold on the top is the most suitable electrode for GaAs. For samples prepared from a commercial [111] oriented wafer, it was found essential to ensure that a large area of the surface was electroded. Such samples gave reliable measurements of the d_{14} coefficient in the frequency range from 1 kHz to 10 kHz. The measured d_{14} coefficient of GaAs determined in this frequency range was found to be (-2.7 ± 0.1) pmV^{-1}.

GaAs has a reasonably high electrical conductivity. The interferometric method uses the inverse effect and avoids problems arising from the conductivity. The results confirm the equality of the measured coefficients for the direct and inverse piezoelectric effect.

(3) The present work represents the first time that the piezoelectric coefficients for AlN and GaN have been measured by interferometry. For GaN this work presents the first reported measurements of the piezoelectric coefficients by any method, apart from a publication by the author (Muensit and Guy, 1998).

The film resistivity was found to be several orders of magnitude higher than that of the substrate. The effects of bending become evident at low frequencies, if the sample is not mounted properly. If the sample is rigidly glued to the holder, the bending effects can be removed from the low frequency measurements. However, some resonance effects are still evident at frequencies above 50 kHz.

The measured values of the d_{33} and d_{31} coefficients for GaN are found to be (3.4 ± 0.1) pmV^{-1} and (–1.7 ± 0.1) pmV^{-1} respectively. Since these values were measured on a single crystal wafer and have been corrected for substrate clamping, the values should be a good measure of the true piezoelectric coefficients of bulk GaN.

For AlN, the measured values of the d_{33} and d_{31} coefficients are found to be (5.1 ± 0.2) pmV^{-1}, and (–2.6 ± 0.1) pmV^{-1} respectively. Since these figures are measured on a polycrystalline sample it is quite probable that the values for bulk AlN would be somewhat higher. If the experience with GaN is taken as a guide, the single crystal values could be up to 30% higher than the values given here.

The piezoelectric measurements indicate that the positive c axis in all of the nitride films points away from the substrate. The piezoelectric measurements provide a simple means for identifying the positive c axis direction.

(4) The interferometric technique has been used to measure the shear piezoelectric coefficient d_{15} for AlN and GaN. This work represents the first application of the technique to measure this particular coefficient. The measured d_{15} for AlN was found to be (–3.6 ± 0.1) pmV^{-1}. The measured d_{15} for GaN was found to be (–3.1 ± 0.1) pmV^{-1}. There are some problems remaining in the application of the technique for the measurements of this coefficient. However the value obtained from the AlN film agrees reasonably well with the only available value in the literature. For GaN, this work presents the only known measurement of this coefficient.

(5) A significant quadratic electromechanical response was observed in all three materials; GaN, AlN, and GaAs. Two possible mechanisms, namely Maxwell stress and thermal effects have been shown to be too small to explain

the observed response. This leads to the conjecture that there is a significant electrostrictive response present.

For the polycrystalline GaN and AlN, the measured displacements agree reasonably well with the theoretical predictions and it is possible to extract reasonable values of the electrostriction coefficients. The measured electrostrictive coefficients M_{33} for the GaN and AlN polycrystalline films were 0.9×10^{-18} and 0.2×10^{-18} m^2V^{-2} respectively. The value for AlN should be treated with suspicion, because of an unexplained threshold effect in the data.

For the commercial single crystal GaN wafers, the response is asymmetric, and although it is possible to extract a value of the electrostrictive coefficient from the data, this must be treated with some suspicion. GaAs data is also asymmetric and the same suspicion must attach to it.

7.2 Prognosis for Future work

The present work represents the first use of the interferometric technique for determining the piezoelectric coefficients of compound semiconductors. There are questions which arose during the course of the project and remain unsolved. These questions and possible directions for future work are drawn as follow:

(1) In measurements of the d_{15} coefficient, some difficulties still remain to be solved in the method. In particular the effects of mirror resonance need to be addressed and a more accurate determination of the field distribution in the film is required.

(2) The measurements of electrostriction leave several questions unanswered. The AlN sample displayed a threshold effect, while the GaN wafer and the GaAs samples both displayed asymmetry in their response. It is possible that factors such as initial stress in the sample or electrode effects

may be involved. Further work is needed to elucidate the factors involved, and the exact amount of the electrostrictive contribution.

(3) A number of notable advances in the growth and application of the three III-V nitrides, GaN, AlN, and InN (indium nitride), have been reported (Strite and Morkoç, 1992). However InN has not received the attention given to GaN and AlN, and remains the least understood of the nitrides. InN has the same crystal symmetry (6*mm*) as well as the same set of piezoelectric coefficients as GaN and AlN. Measurement of piezoelectric coefficients of InN is therefore obvious as an extension of this work.

(4) The present work shows that the interferometric technique can be applied to measuring the small piezoelectric coefficients of compound semiconductors. These materials are currently finding application in strained layer heterostructures such as GaN/AlGaN. It would be of considerable interest to measure the piezoelectric response of such heterostructures.

Appendix

Table A.1 Twenty piezoelectric crystal classes and the *d* coefficients (Nye, 1985, p123). Numbers of the *d* coefficient for each crystal class are given in brackets.

System	International Point Group	Nonzero *d* Coefficients
Triclinic	1	d_{11} , d_{12} , d_{13} , d_{14} , d_{15} , d_{16} , d_{21} , d_{22} , d_{23} ,d_{24} , d_{25} , d_{26} , d_{31} , d_{32} , d_{33} , d_{34} , d_{35} ,d_{36} (18)
Monoclinic	2	d_{14} , d_{16} , d_{21} , d_{22} , d_{23} , d_{25} , d_{34} , d_{36} . (8)
	m	d_{11} ,d_{12} ,d_{13} ,d_{15} ,d_{24} ,d_{26} ,d_{31} ,d_{32} ,d_{33}, d_{35}. (10)
Orthorombic	222	d_{14} ,d_{25} ,d_{36}. (3)
	*mm*2	d_{15} ,d_{24} ,d_{31} ,d_{32} ,d_{33}. (5)
Tetragonal	4	d_{14},d_{15},d_{31},d_{33}. (4)
	$\bar{4}$	d_{14},d_{15},d_{31},d_{36}. (4)
	422	d_{14}. (1)
	4*mm*	d_{15} ,d_{31} ,d_{33}. (3)
	$\bar{4}2\,m$	d_{14} ,d_{36}. (2)
Trigonal	3	d_{11} ,d_{14} ,d_{15} ,d_{16} ,d_{31} ,d_{33}. (6)
	32	d_{11} ,d_{14}. (2)
	3*m*	d_{15} ,d_{16} ,d_{31} ,d_{33}. (4)
Hexagonal	6	d_{14} ,d_{15} ,d_{31} ,d_{33}. (4)
	$\bar{6}$	d_{11} ,d_{16} . (2)
	622	d_{14} . (1)
	6*mm*	d_{15} ,d_{31} ,d_{33}. (3)
	$\bar{6}m2$	d_{11} . (1)
Cubic	23 , $\bar{4}3\,m$	d_{14}. (1)

Table A.2 The electrostrictive coefficients for various classes (Nye, 1985, p250). Numbers of the *M* coefficient for each crystal class are given in brackets.

System	International Point Group	Nonzero *M* Coefficients
Triclinic	1, $\bar{1}$	M_{11}, M_{12}, M_{13}, M_{14}, M_{15}, M_{16}, M_{21}, M_{22}, M_{23}, M_{24}, M_{25}, M_{26}, M_{31}, M_{32}, M_{33}, M_{34}, M_{35}, M_{36}, M_{41}, M_{42}, M_{43}, M_{44}, M_{45}, M_{46}, M_{51}, M_{52}, M_{53}, M_{54}, M_{55}, M_{56}, M_{61}, M_{62}, M_{63}, M_{64}, M_{65}, M_{66}. (36)
Monoclinic	2, *m*	M_{11}, M_{12}, M_{13}, M_{15}, M_{21}, M_{22}, M_{23}, M_{25}, M_{31}, M_{32}, M_{33}, M_{35}, M_{44}, M_{46}, M_{51}, M_{52}, M_{53}, M_{55}, M_{64}, M_{66}. (20)
	2/*m*	M_{11}, M_{12}, M_{13}, M_{16}, M_{21}, M_{22}, M_{23}, M_{26}, M_{31}, M_{32}, M_{33}, M_{36}, M_{44}, M_{45}, M_{54}, M_{55}, M_{61}, M_{62}, M_{63}, M_{66}. (20)
Orthorombic	222, *mm*2, *mmm*	M_{11}, M_{12}, M_{13}, M_{21}, M_{22}, M_{23}, M_{31}, M_{32}, M_{33}, M_{44}, M_{55}, M_{66}. (12)
Tetragonal	4, $\bar{4}$, 4/*m*	M_{11}, M_{12}, M_{13}, M_{16}, M_{31}, M_{33}, M_{44}, M_{45}, M_{61}, M_{66}. (10)
	4*mm*, $\bar{4}2m$, 422, 4/*mmm*	M_{11}, M_{12}, M_{13}, M_{31}, M_{33}, M_{44}, M_{66}. (7)
Trigonal	3, $\bar{3}$	M_{11}, M_{12}, M_{13}, M_{14}, M_{15}, M_{16}, M_{31}, M_{33}, M_{41}, M_{44}, M_{45}, M_{46}. (12)
	3*m*, 32, $\bar{3}m$	M_{11}, M_{12}, M_{13}, M_{14}, M_{31}, M_{33}, M_{41}, M_{44}. (8)
Hexagonal	6, $\bar{6}$, 6/*m*	M_{11}, M_{12}, M_{13}, M_{16}, M_{31}, M_{33}, M_{44}, M_{55} (8)
	$\bar{6}m2$, 6*mm*, 622, 6/*mmm*	M_{11}, M_{12}, M_{13}, M_{31}, M_{33}, M_{44}. (6)
Cubic	23, *m*3	M_{11}, M_{12}, M_{13}, M_{44}. (4)
	$\bar{4}3m$, 432, *m*3*m*	M_{11}, M_{12}, M_{44}. (3)
Isotropic		M_{11}, M_{12}. (2)

References

Adachi,S., J. Appl. Phys. **58** (1985) R1.

Adachi,S., *Physical Properties of III-V Semiconductor Compounds* (John Wiley & Sons, Inc., New York, 1992).

Anderson,R.A., and Kepler,R.G., Ferroelectrics **32** (1981) 13.

Arlt,G., J. Appl. Phys. **36** (1965) 2317.

Arlt,G., and Quadflieg,P., Phys. Stat. Sol. **25** (1968) 323.

Berlincourt Piezo d_{33} Meter, Operating Mannual, 1974.

Berlincourt,D., Jaffe,H., and Shiozawa,L.R., Phys. Rev. **129** (1963) 1009.

Berger,Lev I., *Semiconductor Materials* (CRC Press,Inc., New York, 1997).

Bernardini,F., Fiorentini,V., and Vanderbilt,D., Phys. Rev. B **56** (1997) R10024.

Birman,J.L., Phys. Rev. **111** (1958) 1510.

Blakemore,J.S., J. Appl. Phys. **53** (1982) R123.

Bottom,V.E.,J. Appl. Phys. **41**(1970) 3941, and references therein.

Butcher,K.S.A., Ph.D. thesis , Macquarie University, Sydney, 1997.

Bykovski,A.D., Gelmont,B.L., and Shur,M.S., J. Appl. Phys. **74** (1993) 6734.

Bykovski,A.D., Gelmont,B.L, Shur,M., and Khan,A., J. Appl. Phys. **77** (1995) 1616.

Bykovski,A.D., Gelmont,B.L., and Shur,M.S., J. Appl. Phys. **81** (1997) 6332.

Bykovski,A.D., Kaminski,V.V., Shur,M.S., Chen,Q.C., and Khan,M.A., Appl. Phys. Lett. **68** (1996) 818.

Cady,W.G., *Piezoelectricity* Vol.1 (Dover Publications,Inc., New York, 1964).

Caridi,E.A., Chang,T.Y., Goossen,K.W., and Eastman,L.F., Appl. Phys. Lett. **56** (1990) 659.

Charlson,E.J., and Mott,G., Proc. IEEE **51** (1963) 1239.

Chin,V.W.L., Solid-State Electron. **37** (1994) 1345.

David,J.P.R., Grey,R., Rees,G.J., Pabla,A.S., Sale,T.E., Woodhead,J., Sánchez-Rojas,J.L., Pate,M.A., Hill,G., Robson,P.N., Hogg,R.A., Fisher,T.A., Skolnick,M.S., Whittaker,D.M., Willcox,A.R.K., and Mowbray,D.J., Electron.Mat. **23** (1994) 975.

Detchprohm,T., Kuroda,T, Hiramatsu,K., Sawaki,N., and Goto,H., Inst. Phys. Conf. Ser. **142** (1996) 859.

Devonshire,A.F.,Phil. Mag. Suppl. **3** (1954) 85.

Fisher,T.A., Hogg,R.A., Willcox,R.K., Whittaker,D.M., Skolnick,M.S., Mowbray,D.J., David,J.P.R., Pabla,A.S., Rees,G.J., Sánchez-Rojas,J.L., Woodhead,J., Hill,G., Pate,M.A., and Robson,P.N., Solid-State Electron. **37** (1994) 645.

Gironcoli,S. de, Baroni,S., and Resta,R., Phys. Rev.Lett. **62** (1989) 2853.

Grey,R., David,J.P.R., Hill,G., Pabla,A.S., Pate,M.A., Rees,G.j., Robson.,P.N., Rodriguez-Girones,P.J., Sale,T.E., Woodhead,J., Fisher,T.A., Hogg,R.A., Mowbray, D.J., Skolnick,M.S., Whittaker,D.M.,and Willcox,A.R.K., Microelectron. J.**26** (1995) 811.

Gualtieri,J.G., and Kosinski,J.A., IEEE Trans. Ultroson., Ferroelec., Freq. Contr., **41** (1994) 53.

Hafner,E., Proc. IEEE **57** (1969) 179.

Hambleton,K.G., Phys. Lett. (Netherlands) **16** (1965) 241.

Hariharan,P., *Basics of Interferometry* (Academic Press,Inc.,New York,1992).

Harken,D.R., Huang,X.R., McCallum,D.S., Smirl,A.L., Sánchez-Rojas,J.L., Sacedón, Calleja,E., and Muñoz,E., Appl. Phys. Lett. **66** (1995) 857.

Hickernell,F.S., IEEE Trans. Son. Ultrason. **Su-32** (1985) 621.

Hsu,L., and Walukiewicz,W., Appl. Phys. Lett. **73** (1998) 339.

Hutson,A.R., Phys. Rev. Lett. **4**, (1960) 505.

Hutson,A.R., U.S. Patent, 3 090 876 (May 21, 1963).

Hutson,A.R., and White,D.L., J. Appl. Phys. **33** (1962) 40.

IEEE Standard on Piezoelectricity (ANSI/IEEE Standard 176-1987), (The Institute of Electrical and Electronics Engineers,Inc., New York,1988).

Ikeda,T., *Fundamentals of Piezoelectricity* (Oxford University Press, New York, 1990).

Jaffe,H., Berlincourt,D., Krueger, and Shiozawa,L.R., Proceeding of the 14th Annual Symposium on Frequency Control (Fort Monmount, New Jersey, May 31, 1960).

Kamiya,T., Jpn.J. Appl. Phys. **35** (1996) 4421.

Kholkin,A.L., Wütchrich,Ch., Taylor,D.V.,and Setter,N., Rev. Sci. Instrum. **67** (1996) 1935.

Khurgin,J., J. Appl. Phys. **66** (1989) 994.

Kim,E.S., and Muller,R.S., IEEE Electron. Device Lett. **EDL-7**, (1987) 254.

Kobiakov,I.B., Solid-State Commun. **35** (1980) 305.

Kholkhin,A.I., Colla,E.L., Tugantsev,A.K.,and Taylor,D.V., Appl. Phys. Lett. **8** (1996) 2577.

Kröger,F.A., Phys. Letters **15** (1965) 218.

Kuech,T.F., Collins,R.T., Smith,D.L., and Mailhiot,C.J., J. Appl. Phys. **67** (1990) 2650.

Kuttruff,H., *Ultrasonic : Fundamentals and Applications* (Elsvier Science Publishers , London, 1991).

Kwaaitaal,Th., Luymes, B.J., and van der Pijll,G.A., J. Phys. D: Appl. Phys.**13** (1980) 1005.

Landolt-Börnstein Data Series, Group III, Vol. II *Elastic, Piezoelectric, Pyroelectric, Piezooptic, and Electrooptic Constants* (Springer-Verlag,Berlin, 1979).

Lefki,K., and Dormans,G.J.M., J. Appl. Phys. **76** (1994) 1764.

Li,X, Ph.D thesis, Macquarie University, Sydney (1991).

Li,W., and Ni,W.-X., Appl. Phys. Lett. **68** (1996) 2705.

Li,J.-F.,Viehland,D.D.,Tani,T.,Lakeman,C.D.E.,and Payne,D.A., J. Appl. Phys. **75** (1994) 442.

Li, J.-F., Moses,P., and Viehland,D., Rev. Sci. Instrum. **66** (1995) 215.

Liaw,H.M., and Hickernell,F.S., IEEE Trans. Ultrason. Ferroelec. Freq.Cont. **42** (1995) 404.

Matthes,B., Brozeit,E., Zucker,O., and Gauer,P., Thin Solid Films **226** (1993) 178.

Mason W.P., *Piezoelectric Crystals and Their Application to Ultrasonics* (D.Van Nostrand Co., Inc., New York, 1950).

Mason,W.P., *Physical Acoustics* (Academic Press, New York, 1964).

Mason,W.P., and Jaffe,H., Proc. Inst. Radio Eng.: Methods for Measuring Piezoelectric, Elastic, and Dielectric Coefficients of Crystals and Ceramics, (June, 1954) 921.

Matin,R.M., Phys. Rev.B **6** (1972) 4546.

Melnik,Yu.V., Vassilevski,K.V., Nikitina,I.P., Babanin,A.I., Davydov,V.Yu., and Dmitrive,V.A., J. Nitride Semicond. Res. **2** (1997) 39.

McKitterick,J.B., Phys. Rev.B **28** (1983) 7384.

McNeil,L.E., Grimsditch, M., and French,R.H., J. Am. Ceram. Soc. **76** (1993) 1132.

Meng,Z.Y., and Cross,L.E., J. Appl. Phys. **57** (1985) 488.

Misawa,K., Moritani,A., and Nakai,J., Jpn. J. Appl. Phys. **15** (1976) 2103.

Mizuta,M., Fujieda,S., Matsumoto,Y., and Kawamura,T., Jpn. J. Appl. Phys. **25** (1986) L945.

Morony,R.M.,White,R.M.,and Howe,R.T., Proc. IEEE Ultrason. Symp., Montreal (1989) 745.

Mroz,Jr.,T.J. Ceramic Bulletin **71** (1992).

Muensit,S., and Guy,I.L., Appl. Phys. Lett. **72** (1998) 1896.

Nalwa,H.S., *Ferroelectric Polymers* (Marcel Dekker, Inc., New York, 1995).

Nye,J.F., *Physical Properties of Crystal* (Oxford University Press, New York, 1985).

O'Clock,Jr.,G.D., and Duffy,M.T., Appl. Phys. Lett. **23** (1973) 55.

Okamura,H., and Minowa, J., Elec.Lett. **25** (1989) 395.

Pabla,A.S., Woodhead,J., Grey,R., and Rees,G.J., Electron. Lett. **30** (1994) 1521.

Paisley,M.J., Sitar,Z., Posthill,J.B., and Davis,R.F., J. Vac. Sci. Technol. A **7** (1989) 701.

Pan,W.Y., and Cross,L.E., Rev. Sci. Instrum. **60** (1989) 2701.

Pointon,A.J., IEE Proc. **129** (1982) 285.

Polian,A., Grimsditch,M., and Grzegory,I., J. Appl. Phys. **79** (1996) 3343.

Rees,G.J., Microelectron. J., **28** (1997) 957, and references therein.

Royer,D., and Kmetik,V., Electron. Lett. **28** (1992) 1828.

Ruiz,E., Alvarez,S., and Alemany P., Phys. Rev. B **49** (1994) 5188.

Sánchez-Rojas,J.L., Sacedón,A., Calle,F., Calleja,E., and Muñoz,E., Appl. Phys. Lett. **65** (1994) 2214.

Sheleg,A.U., and Savastenko,V.A., Vesti Akad. Nauk. BSSR Ser. Fiz. Mat. Nauk **3** (1976) 126.

Sheleg,A.U., and Savastenko,V.A., Izv. Akad. Nauk. SSSR, Neorg. Mater. **15** (1979) 1598.

Smith,D.L., Microelectron. J. **28** (1997) 707, and references therein.

Smith,D.L., Solid-State Commun. **57** (1986) 919.

Smith,D.L., and Mailhiot,C., J. Appl. Phys. **63** (1988) 2717.

Strite,S., and Morkoç,H., J. Vac. Sci. Technol. B **10** (1992).

Sundar,V., and Newnham,R.E., Ferroelectrics **135** (1992) 431.

Sundar,V., Gachigi,K.Wa., McCauley,D., Markowski,K.A., and Newnham,R.E., Proc. 9th IEEE Int. Symp. Appl. Ferroelectrics, August 7-10, 1994, PennState University, USA (1995) 353.

Sze, S.M., *Physics of Semiconductor Devices* (John Wiley & Sons, New York, 1969).

Takagi,Y., Ahart,M., Azuhata,T., Sota,T., Suzuki,K., and Nakamura,S., Physica B **219&220** (1996) 547.

Tanaka,K., Kubo,R., Ohwada,K., Umeda,A., Ueda,K., and Usuda,T., Jpn. J. Appl. Phys. **34** (1995) 5230.

Tansley,T.L., personal communication, 1998.

Tsubouchi,K., Sugai,K.,and Mikoshiba,N., Proc. IEEE Ultrason. Symp. (1981).375.

Van Sterkenburg,S.W.P., J. Phys. D: Appl. Phys. **24** (1991) 1853.

Wan,C.F., Luttmer,J.D., List,R.S., and Strong,R.L., J. Electron. Mat. **24** (1995) 1293.

Wang,H., Zhang,L.E., Cross,L.E., Ting,R., Coughlin,C., and Rittenmyer,K., Proc. 9th IEEE Int. Symp. Appl. Ferroelectrics, August 7-10, 1994, PennState University, USA (1995) 182.

Weidner,R.T., and Sells, R;L., *Elementary Classical Physics* V.I (Allyn and Bacon, Inc., Boston, 1965).

Wenzel,S.W., and White,R.M., IEEE Trans. Electron. Device **ED-35** (1988) 735.

Wiederick,H.D., Sherrit,S., Stimpson,R.B., and Mukherjee,B.K., European Meeting on Ferroelectricity, Nijmegen, 1995.

Wright,A.F., J. Appl. Phys. **82** (1997) 2833.

Yim,W.M., and Paff,R.J., J. Appl. Phys. **45** (1974) 1456.

Yu,E.T., Sullivan,G.J., Asbeck,P.M., Wang,C.D., Qiao,D., and Lau,S.S., Appl. Phys. Lett. **71** (1997) 2794.

Zhang,Q.M., Pan,W.Y., and Cross,L.E., J. Appl. Phys. **63** (1988) 2492.

Zerbst,M., and Boroffka,H., Z.Naturf. **18a** (1963) 642.

Zhenyi,M., Scheinbeim,J.I., Lee,J.W.,and Newman,B.A., J. Polym. Sci. B : Polym. Phys. **32** (1994) 2721.

Zhou,B., Ph.D. thesis , Macquarie University, Sydney, 1996.

Publications by the Author:

- S. Muensit, B. Zhou, D. J. Wilson, I. L. Guy, and T. L. Tansley, 'Study of the Piezoelectric Effect in Gallium Nitride Films Using a Modified Michelson Interferometer', Proceeding of the Conference on Optoelectronics and Microelectronic Materials and Devices 1996, 8-11 December, Australian National University, Canberra, Published by IEEE (Piscataway, N.J.), (1997).

- S. Muensit and I. L. Guy, ' The Piezoelectric Coefficient of Gallium Nitride Thin Films', Appl. Phys. Lett., 72 (1998) 1896.

The piezoelectric coefficient of gallium nitride thin films

S. Muensit[a] and I. L. Guy
Physics Department, Semiconductor Science and Technology Laboratories, Macquarie University, NSW 2109, Australia

(Received 17 November 1997; accepted for publication 17 February 1998)

A laser interferometer was used to measure the d_{33} piezoelectric coefficient of wurtzite GaN. The GaN was in the form of 1 μm thick films, grown by chemical vapor deposition and the measurement of the piezoelectric coefficient was made with a spatial resolution of 100 μm. Sample mounting was found to play an important part in the observed response. For rigidly mounted samples, the measured d_{33} was 2.0 ± 0.1 pm V^{-1}. © *1998 American Institute of Physics.* [S0003-6951(98)03915-1]

In recent years, interest in the piezoelectric properties of thin layer materials has increased because of the range of applications of devices, such as microactuators, microsensors, ultrasonic motors, etc., which are based on piezoelectric thin films.[1-3] In the case of compound semiconductors there is added incentive, in that the piezoelectric properties affect the semiconducting properties.[4,5] Indeed the piezoelectric field in strained layers has been used to modify the operating characteristics of devices fabricated from these materials.[6] For GaN films, many physical properties, measured on films of widely varying quality have been reported.[7] However to date there appears to be a limited amount of measured data for piezoelectric coefficients and no data for the d_{33} coefficient measured here.

GaN films are polycrystalline, with a wurtzite structure[8,9] having 6 mm symmetry. The piezoelectricity of this group is characterized by three independent piezoelectric coefficients d_{33}, d_{31} ($=d_{32}$), and d_{15} ($=d_{24}$), two independent dielectric coefficients ϵ_{11} ($=\epsilon_{22}$) and ϵ_{33}, and five independent elastic coefficients c_{11}, c_{12}, c_{13}, c_{33}, and c_{44}.[10]

The GaN films used were grown by chemical vapor deposition on n^+-(100)Si. Details of these films have been reported elsewhere.[11,12] X-ray diffraction confirmed that the films consisted of the wurtzite phase, with the c axis perpendicular to the film surface. The film thickness was around 1 μm. Aluminum was deposited on the top surface of the film to act as an electrical contact, the substrate providing contact to the other face. An electric field, applied via these contacts, produced piezoelectrically induced changes in film thickness. These changes were measured using an optical interferometer. The arrangement thus measures the converse piezoelectric effect, the change in strain resulting from a change in field.

Several configurations of optical interferometer have been used to measure piezoelectric displacements. In the present case the design was based on that developed by the group at PennState University[13-15] (Fig. 1). The arrangement is essentially a Michelson interferometer with the electrode on the sample surface forming the mirror in one arm. A reference mirror, which can be positioned by a piezoelectric driver, is mounted in the other arm. The two mirrors are adjusted so that the center of the interference pattern falls on an optical detector. The reference mirror is positioned such that the quiescent intensity at the detector falls midway between a minimum and maximum of the interference pattern. Movement of the sample surface produces small changes in intensity at the detector. These changes are proportional to the surface movement, provided that the movement is small (i.e., $\ll\lambda$). The changes are measured using a lock-in amplifier connected to the detector. The detector output is also fed back, through a 1 kHz low pass filter, to the positioner attached to the reference mirror. This provides a means for active compensation of slow drifts and low-frequency external vibration. However, it also restricts operation to frequencies above 1 kHz. The arrangement was found to be capable of resolving surface movement on the order of 10^{-3} Å.

The operation of the interferometer was checked by measuring the piezoelectric d_{11} coefficient of quartz. The value obtained was 2.34 pm V^{-1}, which is within 2% of the value found in the literature.[16] This value was found to be independent of the driving field and was constant over the full frequency range from 1 kHz (limited by the low pass filter in the reference mirror control loop) to 100 kHz (the limit of the lock-in amplifier).

When measuring piezoelectric coefficients in an interferometer, the sample mounting is critical in ensuring that only the desired modes of vibration occur. In the present case, where d_{33} was the coefficient of interest, it was important to ensure that only the thickness mode vibration occurred and that the sample did not undergo bending mode vibrations.

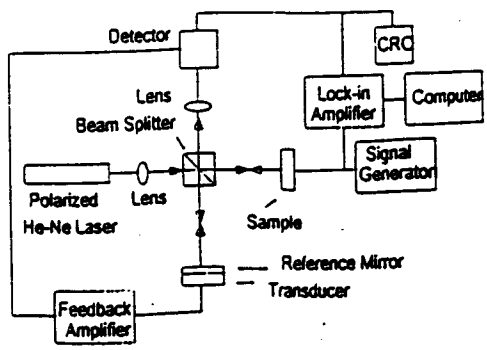

FIG. 1. Schematic diagram of a Michelson He–Ne laser interferometer.

[a]Electronic mail: smuensit@mpce1.mpce.mq.edu.au

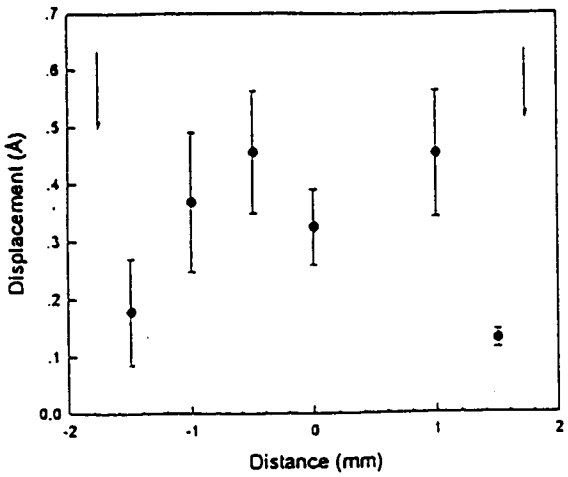

FIG. 2. Variation in the amplitude of piezoelectrically generated vibrations across the surface of an edge mounted GaN sample. The measurement frequency was 2.0 kHz. The arrows indicate the position of the electrode edges.

The GaN samples were glued to a thick brass plate, which was in turn rigidly attached to a substantial optical translation/rotation stage. The probe beam was scanned across the sample surface and the variation in amplitude of vibration was used to ensure that no bending modes were present. Figure 2 shows the variation in motion at various points across the sample surface, for a sample glued on edge to the brass plate. The variation in vibration amplitude across the surface, in particular the larger amplitude towards the center of the sample, indicates bending-mode vibrations.[14] If the sample was mounted by gluing it flat to the brass block, then the surface vibration was as shown in Fig. 3. The uniform vibration amplitude is an indication that the predominant vibration is the thickness mode.

Measurements were normally made at the center of the sample, with the laser beam focused to a spot of about 0.1 mm diameter. The variation of the piezoelectric displacement with driving voltage at 1 kHz is shown in Fig. 4. The piezoelectric response could be measured for driving fields as low as 0.2 kV mm^{-1} and the response was found to be

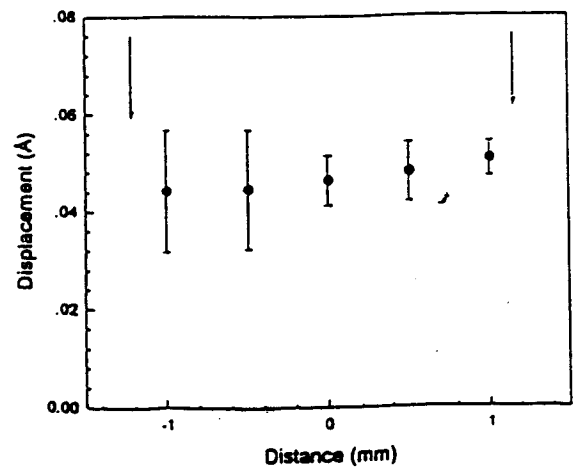

FIG. 3. Variation in the amplitude of piezoelectrically generated vibrations across the surface of a GaN film rigidly glued to the sample holder. The arrows mark the position of the electrode edges.

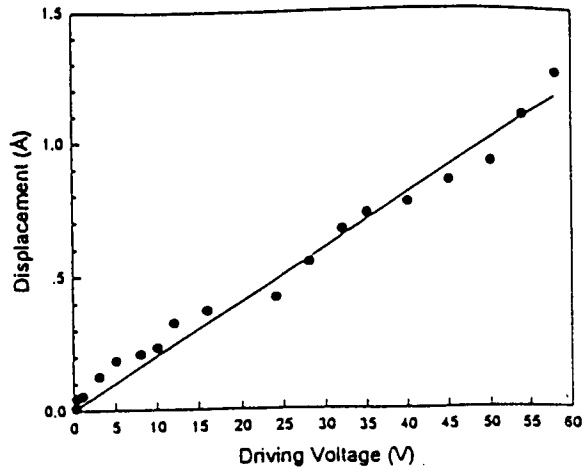

FIG. 4. Variation of vibration amplitude with applied voltage, measured for a 1 μm GaN film at a frequency of 1.0 kHz.

reasonably linear up to the highest fields used, which were about 60 kV mm^{-1}.

Figure 5 shows a plot of measured d_{33} against frequency. It is seen that the value is substantially constant over the full range except at frequencies near 100 kHz, where bending mode vibrations are not totally suppressed. The value of d_{33} in this frequency range was found to be 2.0±0.1 pm V^{-1}.

Since the samples are polycrystalline in nature, it is expected that this value would be lower than the intrinsic value for a single GaN crystal. Several factors act to reduce the piezoelectric coefficient in a film such as those used here. Interfacial stress, defects, and variation in c-axis alignment will all reduce the observed piezoelectric activity. In the present case, the films are known to be dense and have a surface roughness of about 50 nm.[11] Data on the degree of crystal alignment and defect densities are not available. However it is anticipated that the effect of these would be reasonably small. Thus the measured value of d_{33} forms a lower limit for the probable single crystal value.

In summary, the piezoelectric coefficient d_{33} of wurtzite GaN films, grown on (100)Si, has been measured using a Michelson He–Ne laser interferometer. There is evidence of a bending effect in the substrate, even at low frequencies, if the sample is not mounted properly. While the coefficient is much smaller than that exhibited by materials normally used in actuator and sensor applications, the fact that GaN has

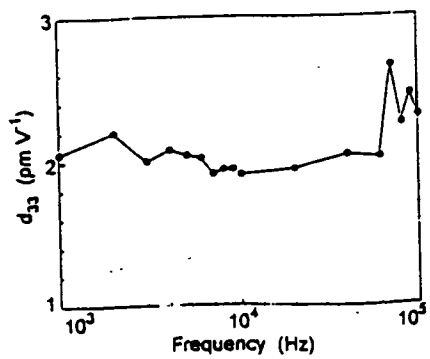

FIG. 5. Plot of the frequency dependence of the measured d_{33} in a GaN film.

interesting potential in the semiconductor area, makes the values of interest. Further investigations of the electrostrictive response of the film are in progress and will be addressed in future work.

This work has been sponsored by the Macquarie University Research Grant Scheme. The authors are grateful to B. Zhou for providing them with the GaN samples and to D. Wilson for assistance with the associated electronics.

[1] E. S. Kim and R. S. Muller, IEEE Electron Device Lett. EDL-7, 254 (1987).
[2] S. W. Wenzel and R. M. White, IEEE Trans. Electron Devices ED-35, 735 (1988).
[3] R. M. Morony, R. M. White, and R. T. Howe, Proceedings of the IEEE Ultrasonics Symposium, Montreal, Canada, 1989, p. 745.
[4] V. W. L. Chin, T. L. Tansley, and T. Osotchan, J. Appl. Phys. 75, 7365 (1994).
[5] A. D. Bykhovski, V. V. Kaminski, M. S. Shur, Q. C. Chen, and M. A. Khan, Appl. Phys. Lett. 68, 818 (1996).
[6] J. L. Sánchez-Rojas, A. Sacedón, F. Calle, E. Calleja, and E. Muñoz, Appl. Phys. Lett. 65, 2214 (1994).
[7] S. Strite and H. Morkoç, J. Vac. Sci. Technol. B 10, 1237 (1992).
[8] P. J. Born and D. S. Robertson, J. Mater. Sci. 15, 3003 (1980).
[9] D. K. Gaskill, N. Bottka, and M. C. Lin, Appl. Phys. Lett. 48, 1449 (1986).
[10] IEEE Standard on Piezoelectricity (ANSI/IEEE Standard 176-1987, 1988).
[11] B. Zhou, X. Li, T. L. Tansley, K. S. A. Butcher, and M. R. Phillips, J. Cryst. Growth 151, 249 (1995).
[12] B. Zhou, Ph.D. thesis, Macquarie University, Sydney, Australia, 1996.
[13] Q. M. Zhang, W. Y. Pan, and L. E. Cross, J. Appl. Phys. 63, 2492 (1988).
[14] A. L. Kholkin, C. Wutchrich, D. V. Taylor, and N. Setter, Rev. Sci. Instrum. 67, 1935 (1996).
[15] J. F. Li, P. Moses, and D. Viehland, Rev. Sci. Instrum. 66, 215 (1995).
[16] Landolt-Börnstein Data Series, Group III, *Elastic, Piezoelectric, Pyroelectric, Piezooptic, and Electrooptic Constants* (Springer, Berlin, 1979), Vol. II.